Université de Montréal

# 3D quantification of osteoclast resorption of equine bone *in vitro*

*Par*

Debora Moreira Grass

Département de sciences cliniques

Faculté de médecine vétérinaire

Mémoire présenté à Faculté de médecine vétérinaire

en vue de l'obtention du grade de *Maîtrise ès sciences* (M. Sc.)

en sciences vétérinaires, option sciences cliniques

Juillet 2023

Département de sciences cliniques, Faculté de médicine vétérinaire

*Ce mémoire intitulé*

**3D quantification of osteoclast resorption of equine bone *in vitro***

*Présenté par*

**Debora Moreira Grass**

*A été évalué par un jury composé des personnes suivantes*

**Guillaume St-Jean**
Président-rapporteur

**Sheila Laverty**
Directrice de recherche

**Natalie Reznikov**
Codirectrice

**Cyrielle Finck**
Membre du jury

# Résumé

Des charges cycliques élevées induisent la formation de microfissures dans l'os, déclenchant un processus de remodelage ciblé, mené par les ostéoclastes et suivi par les ostéoblastes, visant à réparer et à prévenir l'accumulation des dommages. L'os de cheval de course est un modèle idéal pour étudier les effets d'une charge de haute intensité, car il est sujet à une accumulation focale de microfissures et à la résorption qui s'ensuit dans les articulations. Les ostéoclastes équins ont rarement été étudiés in vitro. Le volume de résorption des ostéoclastes est considéré comme un paramètre direct de l'activité des ostéoclastes, mais des méthodes indirectes de quantification en 2D de la résorption osseuse sont plus souvent utilisées. L'objectif de cette étude était de développer une méthode précise, à haut débit et assistée par l'apprentissage profond pour quantifier le volume de résorption des ostéoclastes équins dans les images micro tomodensitométrie (µCT) 3D.

Des ostéoclastes équins ont été cultivés sur des tranches d'os équins, imagés par µCT avant et après la culture. Le volume, le ratio de forme et la profondeur maximale de chaque événement de résorption ont été mesurés dans les images volumétriques de trois tranches d'os. Un convolution neural network (CNN) a ensuite été entraîné à identifier les événements de résorption sur les images µCT post-culture, puis le modèle a été appliqué à des tranches d'os d'archives (n=21), pour lesquelles l'aire de résorption en 2D, et la concentration du biomarqueur de résorption CTX-I étaient connues. Cela a permis d'obtenir des informations 3D sur la résorption des tranches d'os pour lesquels aucune imagerie n'avait été réalisée avant la mise en culture. La valeur modale du volume, la profondeur maximale et le ratio de forme des événements de résorption discrète étaient respectivement de $2,7*10^3 \mu m^3$, 12 µm et 0,18. Le volume de résorption moyen par tranche d'os archivés était de $34155,34*10^3 \mu m^3$. Le volume de résorption mesuré par le CNN était en forte corrélation avec les mesures de CTX-I ($p < 0,001$) et d'aire ($p < 0,001$).

Cette technique de segmentation des images µCT des coupes osseuses assistée par apprentissage profond pour quantifier le volume de résorption osseuse des ostéoclastes équins permettra des recherches futures plus précises et plus approfondies sur l'activité des ostéoclastes. Par exemple, les effets antirésorptifs de médicaments tels que les corticostéroïdes et les bisphosphonates pourront être étudiés à l'avenir.

**Mots-clés :** Ostéoclaste, cheval de course, µCT, résorption osseuse, quantification, volume, apprentissage profond

# Abstract

High cyclic loads induce the formation of microcracks in bone, initiating a process of targeted remodeling, led by osteoclasts, and followed by osteoblasts, aimed at repairing and preventing accumulation of damage. Racehorse bone is an ideal model for studying the effects of high-intensity loading, as it is subject to focal accumulation of microcracks and subsequent resorption within joints. Equine osteoclasts have rarely been investigated *in vitro*. The volume of osteoclast resorption is considered a direct parameter of osteoclast activity, but indirect 2D quantification methods are used more often. The objective of this study was to develop an accurate, high-throughput, deep learning-aided method to quantify equine osteoclast resorption volume in µCT 3D images.

Equine osteoclasts were cultured on equine bone slices, imaged with µCT pre- and post-culture. Volume, aspect ratio (shape factor) and maximum depth of each resorption event were measured in volumetric images of three bone slices. A convolutional neural network (U-Net-like) was then trained to identify resorption events on post-culture µCT images and then the network was applied to archival bone slices (n=21), for which the area of resorption in 2D, and the concentration of a resorption biomarker CTX-I were known. This unlocked the 3D information on resorption for bone slices where no pre-culture imaging was done. The modal volume, maximum depth, and aspect ratio of discrete resorption events were $2.7*10^3 \mu m^3$, 12 µm and 0.18 respectively. The mean resorption volume per bone slice on achieved bone samples was $34155.34*10^3 \mu m^3$. The CNN-labeled resorption volume correlated strongly with both CTX-I ($p < 0.001$) and area measurements ($p < 0.001$).

This technique of deep learning-aided feature segmentation of µCT images of bone slices for quantifying equine osteoclast bone resorption volume allows for more accurate and extensive future investigations on osteoclast activity. For example, the antiresorptive effects of medications like corticosteroids and bisphosphonates can be investigated in the future.

**Keywords:** Osteoclast, racehorse, µCT, bone resorption, quantification, volume, deep learning

# Table of Contents

# List of tables

# List of figures

# List of abbreviations

**BPs:** Bisphosphonates

**c-Fms:** colony-stimulating factor-1 receptor

**CNNs:** Convolutional Neural Networks

**CTX-I:** C-terminal telopeptide of type I collagen

**ECM:** Extracellular Matrix

**ELISA:** Enzyme-linked Immunosorbent Assay

**FDA:** Food and Drug Administration

**HSCs:** Hematopoietic Stem Cells

**M-CSF:** Macrophage colony-stimulating factor

**MPA:** Methylprednisolone Acetate

**MSCs:** Mesenchymal Stem Cells (MSCs)

**NBPs:** Nitrogenous Bisphosphonates

**NFATc1:** Activation of Nuclear Factor of Activated T Cells c1

**Non-NBPs:** Non-nitrogenous Bisphosphonates

**OPG:** Osteoprotegerin

**PBS:** Phosphate Buffered Saline

**POD:** Palmar Osteochondral Disease

**PPi:** Pyrophosphate

**PTOA:** Post-traumatic Osteoarthritis

**RANK:** Receptor Activator of Nuclear Factor Kappa-B

**RANKL:** Receptor Activator of Nuclear Factor Kappa-B Ligand

**SEM:** Scanning Electron Microscopy

**TA:** Triamcinolone Acetonide

**TRACP5b:** Tartrate resistant acid phosphatase isoform 5b

**TRAP:** Tartrate-resistant Acid Phosphatase

# Acknowledgements

I would like to express my utmost appreciation to Dr. Sheila Laverty, my supervisor, for her unwavering support and invaluable guidance throughout the duration of this project. Dr. Laverty's perceptive and feedback have played a pivotal role in shaping my research, motivating me to reach my fullest potential. Her profound expertise in the field and commitment to academic excellence have consistently inspired me.

I am also indebted to my co-supervisor, Dr. Natalie Reznikov, who has not only introduced me to the fascinating world of image analysis and deep learning but has also allowed me to broaden my knowledge and perceive the world from a completely new perspective.

To the jury members, I extend my sincere appreciation for their valuable advice and feedback during the evaluation process. Their expertise and constructive criticism have contributed significantly to the refinement of my work.

I would like to express a special appreciation to Hélène Richard, who deserves sincere recognition for her exceptional support throughout this research endeavor. Beyond her assistance with the laboratory, Hélène went above and beyond to ensure my overall well-being. Her genuine care, constant check-ins, and thoughtful gestures made a significant difference.

In addition, I would like to manifest my heartfelt gratitude to my mother, Erika, who has been my ultimate source of inspiration and courage. Her unwavering belief in me and her constant encouragement to pursue even the most audacious dreams have shaped the person I am today. I am eternally grateful for her love, support, and the example she has set.

I also want to acknowledge my sister, Renata, despite the physical distance between us, for always making herself present and providing unmeasurable support. Her encouragement has been a source of motivation during challenging times.

To my partner, Rommel, I cannot thank him enough for believing in me, even when I doubted myself. His support, understanding, and patience have been my anchor. I am truly grateful for his love, and for being my safe harbor during stormy times.

I cannot forget to acknowledge the incredible emotional support provided by my faithful four-legged companion, Kiara. Throughout the highs and lows, she has been a loyal source of unconditional love and comfort. Her gentle presence, wagging tail, and warm cuddles have brought solace during moments of stress and served as a reminder to take breaks and appreciate the simple joys in life.

Lastly, I would like to extend my appreciation to my dearest friends. With a special mention to Tamara, my closest confidant, who has consistently provided me with support and care. Her genuine concern for mine and Kiara's well-being, ensuring I had enough food and rest, and always bringing laughter into my life have made this experience more enjoyable and memorable. To Maria Sara, our philosophical conversations about life, purpose, and the meaning of our chosen profession during our "pãozinhos" have been both inspiring and thought-provoking. And to my dear friend Hubert for his incredible patience and dedication in making deep learning seem uncomplicated.

To all those mentioned above and to many others who have supported me along the way, whether through their encouragement, advice, or friendship, I am profoundly grateful. Your contributions have played a significant role in the successful completion of this thesis, and I am honored to have had you by my side.

# Introduction

It is well known that microarchitecture of healthy adult bones has the intrinsic ability to undergo constant adaptation in response to biomechanical loads, ensuring optimal performance.[1] This adaptation is orchestrated through synchronized cellular remodeling, or bone multicellular units (BMU), whereby osteoclasts initially resorb the bone by excavating lacunae or cavities and subsequently new bone is deposited by osteoblasts.[2] This intricate process is regulated by a delicate balance between bone resorption and formation, playing a pivotal role in maintaining the structural integrity, mechanical competence, and functional adaptability of bones.[2]

When the bone is subjected to high loads, microcracks occur in its structure, triggering a targeted remodeling response.[3] This physiological response serves the pivotal purpose of repairing localized injury and prevents the cumulative build-up of damage.[4] Mechanotransduction pathways, including the disruption of the lacuno-canalicular network[5] or osteocyte apoptosis at the injury site,[6] play a role in the recruitment and differentiation of osteoclast precursors from the nearby bone marrow into active bone-resorbing osteoclasts by the release of Receptor Activator of Nuclear Factor Kappa-B Ligand (RANKL). RANKL interacts with its receptor (RANK) on the surface of osteoclast precursors, activating signaling pathways that promote the differentiation, activation, and survival of osteoclasts.[7]

Racehorses endure intensive cyclic loading during training and racing regimens, which can lead to microcracks at specific sites of their skeleton. Although microdamage naturally contributes to the skeleton's adaptation to varying biomechanical demands, when there's an imbalance between bone formation and resorption, excessive damage and focal accumulation of bone and calcified cartilage microcracks with associated resorption[8,9] at specific sites undergoing high loads can lead to serious occupational injuries such as joint disease and, in some cases, bone failure (stress fractures) [10-12]. This is particularly evident in the fetlock [8,13-15] and carpus [9,16] of racehorses.

Despite playing an essential role in bone remodelling, equine osteoclasts have seldom been the subject of *in vitro* studies and there are several important questions that remain unanswered, including (1) the precise role of osteoclasts in repairing microdamage, (2) identification of factors that could induce osteoclast differentiation in microdamage sites, and (3) the impact of current intra-articular medications such as corticosteroids and bisphosphonates on osteoclast activity, particularly in areas close to joint surfaces where they may have a role in healing.

Osteoclasts have been differentiated and cultured from post-mortem harvested femoral bone marrow hematopoietic stem cells in the past[17-19] or, more recently, from sternal bone marrow aspirates in standing horses.[20,21] Furthermore, they have been cultured on their natural substrate bone in one report alone.[21] In order to enhance our comprehension of equine osteoclast activity and the factors that affect it, it is crucial to carry out species-specific *in vitro* studies. These investigations would enable us to bridge important knowledge gaps, including the evaluation of how frequently employed medications in athletic horses influence equine osteoclast activity. Analyzing these effects is vital for assessing any potential adverse impacts on skeletal integrity.

Accurately quantifying and characterizing the complex process of bone resorption by osteoclasts poses significant challenges to researchers. The osteoclast resorption activity *in vitro* has traditionally been extrapolated from canonical 2D resorption area measurements of toluidine blue stained bone slices on which osteoclasts had been cultured. [21-35] However, this widely used technique falls short in accurately measuring the volume and 3D morphology of resorption events leading to indirect estimations and oversimplified representations of resorption cavities.[36,37] Moreover, 2D measurements can be misleading and may reflect osteoclast attachment and spreading rather than resorptive activity.[38] Therefore, direct volume measurement of the resorbed tissue is considered to be the ideal parameter to quantify osteoclast bone resorption.[38,39]

Several methods have been implemented in an attempt to measure volume of bone resorption in 3D, including scanning electron microscopy (SEM) stereophotogrammetry, confocal laser microscopy, vertical scanning profilometry, and serial milling. While these techniques have shown promise in providing high-quality images, they often come with certain limitations as they frequently require complex sample preparation, involve destructive methodologies, and are not widely accessible to users.[40] Therefore, the need for continued progress in accurately quantifying the volume of bone resorption is evident. These forthcoming developments should be focused on surmounting the previously mentioned challenges, with the ultimate goal of facilitating effortless and dependable measurement of bone resorption in 3D.

The integration of deep learning techniques has emerged as a widely employed and valuable approach for providing meaningful insights to various tasks related to the segmentation of mineralized tissues using CT scans[41] and µCT. [42,43] By incorporating deep learning, there is a significant potential for improving the accuracy and reliability of the segmentation process, thereby establishing a robust foundation for quantitative analysis and three-dimensional (3D) visualization.[44-46] However, this technique has not yet been implemented for quantifying bone resorption on bone slices *in vitro*.

The central objective of this project was to develop a precise and user-friendly methodology for the evaluation of both the morphological intricacies and volumetric measurement of bone resorption on bone slices *in vitro.*

# Chapter 1 - Literature review

# 1. Bone tissue

Bone tissue is a vital and intricately complex component of the body, providing crucial support, protection, and mobility. Contrary to intuition, bone is a remarkably dynamic tissue that continually adapts to meet mechanical and physiological demands.[2] A comprehensive understanding of the osseous tissue, and more specifically, the role of the orchestrators of bone resorption, the osteoclasts, is essential for unraveling the intricate mechanisms involved in skeletal development, maintenance, and repair. In this review, we will briefly discuss the function, morphology, architecture, composition, as well as the modeling and remodeling cycles of the bone.

## 1.1. Function

Bone tissue encompasses a wide range of functions that extend beyond mechanical support, including biological, metabolic, and recently discovered endocrine roles.[47-52]

### 1.1.1. Mechanical

One of the most well-known functions of bone tissue is its protective role, safeguarding vital organs [47] like the brain (cranial bones) and lungs (ribs). Its architecture allows it to withstand compression, tension, and bending forces (see section 1.2.2). Moreover, bones play a pivotal role in facilitating skeletal movement by serving as levers for muscles and forming joints.[51]

### 1.1.2. Biological

When addressing its biological function, the bone tissue provides a niche for bone marrow hematopoiesis of both myeloid and lymphoid lineages stem cells[47] and serves as a reservoir for mineral and growth factors[47,49] storing 99% of the body's calcium, 85% of phosphorus, 40-60% of magnesium, and sodium in humans.[53]

### 1.1.3. Metabolic

There is a growing hypothesis proposing an endocrine-mediated coordinated regulation between bone mass, energy metabolism, and reproduction function.[54] Notably, osteocalcin, a protein synthesized by osteoblasts (bone forming cells) and stored in the skeletal matrix, has been found to play a crucial role in regulating glucose homeostasis[52,55] and testosterone secretion[52] based on murine research findings.

Additionally, emerging evidence suggests that hormones produced by the hypothalamus, pituitary gland, and adipose tissue may directly influence the maintenance of healthy bone tissue, establishing the bone as an endocrine organ,[56] in addition to their previously known indirect effects through peripheral endocrine organs.

## 1.2. Morphology

When considering morphology, bone can be categorized based on its anatomy and architecture. In the following section, brief explanation of both aspects will be provided.

### 1.2.1. Anatomy

Bones may be classified by their shape e.g., flat, and long bones. Long bones, in particular, can be further divided into three regions: diaphysis, metaphysis, and epiphyses.[50] Its general structure is described as a central marrow space surrounded by bone tissue and periosteum. The diaphysis is a long hollow shaft primarily composed of dense cortical bone and both the metaphysis and epiphyses, at each extremity, are mostly composed of cancellous bone surrounded by a thin cortical shell (Figure 1).[53]

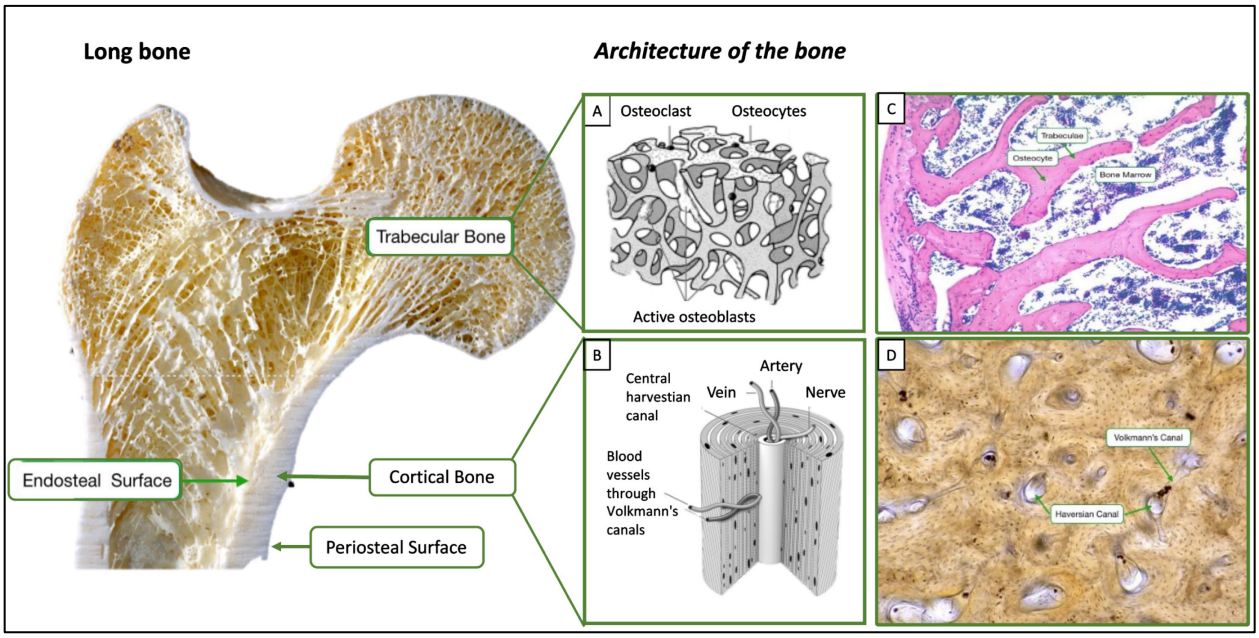


**Figure 1: Anatomy and architecture of the bone**

(A) Trabecular bone; (B) cortical osteon; (C) microscopic image of trabeculae and bone marrow; (D) unstained microscopic image of cortical bone. (Adapted from http://histology.med.yale.edu/bone/bone_reading.php and Buck and Dumanian [51]

## 1.2.2. Architecture

The architecture of the bone pertains to the organization and composition of its internal structure and bone tissues, which can be categorized into two levels: microscopic and macroscopic structure.

### 1.2.2.1. Microscopic structure

Microscopically, bone can be classified into woven and lamellar tissue. Woven tissue represents the immature temporary form of bone that is formed promptly during development or following injury. It is characterized by a highly disorganized type I collagen fiber arrangement.[47,57] Ultimately, this tissue is gradually replaced by lamellar tissue sheets,[57] the mature bone, which is thoroughly organized into parallel laminae.

### 1.2.2.2. Macroscopic structure

In order to accomplish its functions, the skeleton must be strong and rigid enough to protect the soft tissue while simultaneously flexible and elastic to absorb the mechanical forces. This is possible due to the co-existence of the two principal macroscopic osseous tissues: the cortical and trabecular bone which are differentiated by their porosity, location, and function.[47,57]

The type of architecture depends on the region and the bone's function. For example, the vertebrae are mainly composed of trabecular bone that resists compression forces whereas the long bones are predominantly composed of cortical bone to resist torsional forces.[2] Overall, cortical bone represents 80% of the human skeletal weight and trabecular bone is approximately 20%.[2,58]

#### *1.2.2.2.1. Cortical*

Cortical bone, which surrounds the trabecular bone, is characterized as a dense and solid tissue responsible for providing support and protection.[50] It contains an inner endosteal surface, in contact with the trabecular bone, and an outer periosteal surface (Figure 1). This type of bone has a lower turnover rate and a high torsional resistance in healthy adults[2].

Cortical bone microstructure is composed of longitudinal cylinders, called osteons, that are aligned in parallel to the long axis of the bone. This structural unit is formed from concentric layers of bone (lamellae) that surround a central Haversian canal,[53] which are interconnected by Volkmann canals, perpendicular to the axis of the osteon and bone (Figure 1b). Both canals contain the bone's blood vessels and nerve fibers.[53]

#### *1.2.2.2.2. Trabecular*

Trabecular bone, mainly present in the metaphysis and epiphysis of long bones, vertebrae, ribs, and iliac crest, is characterized by a meshwork of bone with interconnecting spaces containing the bone marrow. Its distinctive architecture, characterized by a composition of struts and plates, enables trabecular bone to offer remarkable structural reinforcement, all the while maintaining a lightweight nature and effectively absorbing the stresses related to mechanical impacts.[47,57] This type of bone has a higher turnover rate and a high compression resistance.[2]

## 1.3. Composition

### 1.3.1. Matrix

The bone is composed of an extracellular organic material and mineralized inorganic material. The former is mainly type I collagen, which confers flexibility, resilience, and tensile strength (stretching, twisting and torsion). The latter is principally hydroxyapatite, a crystal formed by calcium and phosphate, contributing to hardness, rigidity, and compressive strength.[2,57]

### 1.3.2. Cells

Bone cells within the bone marrow can be categorized into two lineages: (1) mesenchymal stem cells, a source of osteoblasts and osteocytes and (2) hematopoietic stem cells, a source of osteoclasts (Table 1). In this section, we will briefly describe each one of the bone cells.[57]

Osteoblasts: cuboidal cells responsible for bone formation that occurs in two phases: first the deposition of organic matrix and then its mineralization.[49] Following bone formation, the osteoblasts can (1) remain in the bone matrix as osteocytes, (2) further differentiate into bone lining cells, or (3) undergo apoptosis.[48,59]

Osteocytes: former osteoblasts that became entombed in the bone matrix following the process of bone formation. They have an extensive dendrite network and are part of a syncytium communicating with other bone cells. They are mechanosensory cells and represent 90% of the bone cells. They coordinate the function of osteoblasts and osteoclasts.[59]

Bone Lining Cells: differentiate from osteoblasts by becoming flatter and cover the quiescent bone surfaces e.g., bone marrow cavities.[59] There is conflicting information on their role in bone remodelling and their function is not yet fully understood.

Osteoclasts: large multinucleated cells that differentiate from hematopoietic stem cells and are orchestrators of bone resorption (detailed information provided in section 2).

| | DESCRIPTION | ORIGIN | MAJOR ROLE | LIFESPAN* |
|---|---|---|---|---|
| **OSTEOBLASTS** | Cuboidal cells | Mesenchymal stem cell lineage | Bone formation | ~3 months (active) |
| **OSTEOCYTES** | Stellate shaped | Osteoblasts | Mechanosensory cells/ Coordinate function of osteoblasts and osteoclasts | Long-lived |
| **BONE LINING CELLS** | Flat shaped | Osteoblasts | Unclear | |
| **OSTEOCLASTS** | Large multinucleated | Hematopoietic stem cell lineage | Bone resorption | ~ 2 weeks |

*Lifespan[57]

***Table 1: Bone cells: their origin, major role and lifespan***

## 1.4. Modeling and remodeling cycles

Throughout life, healthy bone undergoes modeling and remodeling whereby the structure and mass of the tissue is altered to respond to the mechanical loads and with the goal of damage prevention and repair. These mechanisms may be influenced by external biophysical forces[60] (ex: mechanical loads, physical activity, lifestyle), genetic components[61] (ex: sex, age, ethnicity) or medication.[62]

### 1.4.1. Modeling

Modeling occurs principally during skeletal development. It consists of the adjustment of the osseous tissue to adapt its shape and size in response to the forces encountered during that period and to ensure both longitudinal and radial bone growth.[2,50,58,63] During this process, bone resorption and formation occur independently as bone matrix is removed from one anatomical region by the activity of osteoclasts, while bone formation occurs at another site primarily through the action of osteoblasts, the latter being the most prevalent and leading to increased bone mass.[2,57]

### 1.4.2. Remodeling

Bone remodeling is a complex and essential process by which the bone tissue is renewed for its own maintenance and to preserve mineral homeostasis of the body.[64]

Unlike the process of bone modeling, remodeling is critically dependent on **the adequate coordinated action between the osteoclasts and osteoblasts in order to maintain a stable bone mass**.[2,50,63] The two cell types, together with the associated blood vessels, form a bone multicellular unit (BMU).

The remodeling cycle is divided into 5 phases: activation, resorption, reversal, formation, and quiescence (resting) (Figure 2) [2,64] and with the first 4 phases estimated to occur over 120 – 200 days depending on anatomical site and level of loading.[2] **The activation phase** begins with the recruitment of osteoclast precursor cells from the bone marrow to the bone surface and its subsequent fusion with other precursors to differentiate into active osteoclasts. Subsequently, the bone-lining cells retract from the bone surface allowing the mature osteoclast to attach to the exposed mineralized matrix, hence initiating **the resorption phase** (detailed explanation provided in section 2). Once resorption is finalized, the bone surface undergoes preparations for the deposition of new bone matrix during **the reversal phase.** Subsequently**, the formation phase**, performed by the osteoblasts, happens in two steps: first, the unmineralized organic matrix (osteoid) is deposited, followed by its mineralization. Finally, in **the quiescence phase** at the end of the remodelling cycle, the bone surface is covered by bone lining cells and the tissue enters the resting mode.[2,64]

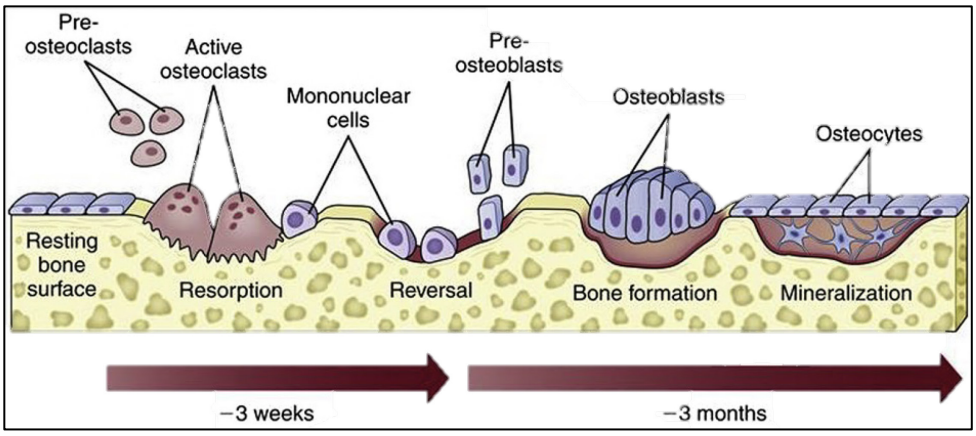


**Figure 2: The remodelling cycle.**

The phases of the remodelling cycle, its associated cells and duration (Adapted from Nandiraju and Ahmed 2019).

# 2. Osteoclast, the "orchestrator" of bone resorption

In the past few decades, knowledge on osteoclast biology has expanded significantly. Rather than simply seen as the "bone resorbing cell", nowadays, they are considered the "orchestrators" of bone resorption.[66,67]

Osteoclasts are large multinucleated cells of hematopoietic origin with unique morphological features that include specialized membrane structures, sealing zones, and ruffled borders that enables the cell to effectively carry out the process of bone resorption (Figure 3).[68,69] Their important metabolic role extends to mineral homeostasis and regulation of osteoblast function[66,67], with emerging evidence also suggesting a potential involvement in hematopoietic stem cell (HSC) maintenance and mobilization[66].

## 2.1. Osteoclast bone resorption

The process of bone resorption involves multiple steps, starting with the attachment of the osteoclast to the bone surface and subsequent changes in its shape and function. During this process, the osteoclast undergoes polarization and reorganization of its cytoskeleton, leading to the formation of four distinct domains: the sealing zone, the ruffled border, the basolateral domain, and the functional secretory domain (Figure 3).[70,71]

The **''sealing zone''**, the domain that separates the resorption cavity, or **"Howship's lacunae",** from the extracellular space[71] is composed of the organelle-free cytoplasmic region called the **''clear zone''** and the membrane facing the bone surface, named the **''sealing membrane''** (Figure 3). The sealing membrane has a circular shape formed by the integrin-based and actin-rich adhesive structural units called **"podosomes"** that develop early in the osteoclast differentiation *in vitro*[70] and create the dynamic structure of the podosomal belt, allowing the osteoclast to tightly attach to the bone surface while migrating (see section 3.5).[66,71]

Alongside the sealing membrane, there is a complex arrangement of membrane extensions that forms the **''ruffled border''** responsible for increasing the contact area of the cell with the bone surface. The ruffled border is the main resorptive organelle, releasing protons (H+), Cl- and lysosomal enzymes (Cathepsin K) into the sealed sub-osteoclastic compartment[71,72]. This process creates an acidic microenvironment (pH of 4.5) that favours the degradation and release of the mineral content from the bone, exposing the organic matrix (mostly type1 collagen) that is principally degraded by the osteoclast collagenase Cathepsin K (Figure 3).[71,72]

The products of bone degradation are eliminated by the **"transcytosis"** mechanism. These products enter the cell by endocytosis and are then transported intracellularly to the opposite basolateral membrane and released into the bloodstream by the **"functional secretory domain"** (Figure 3).[71]

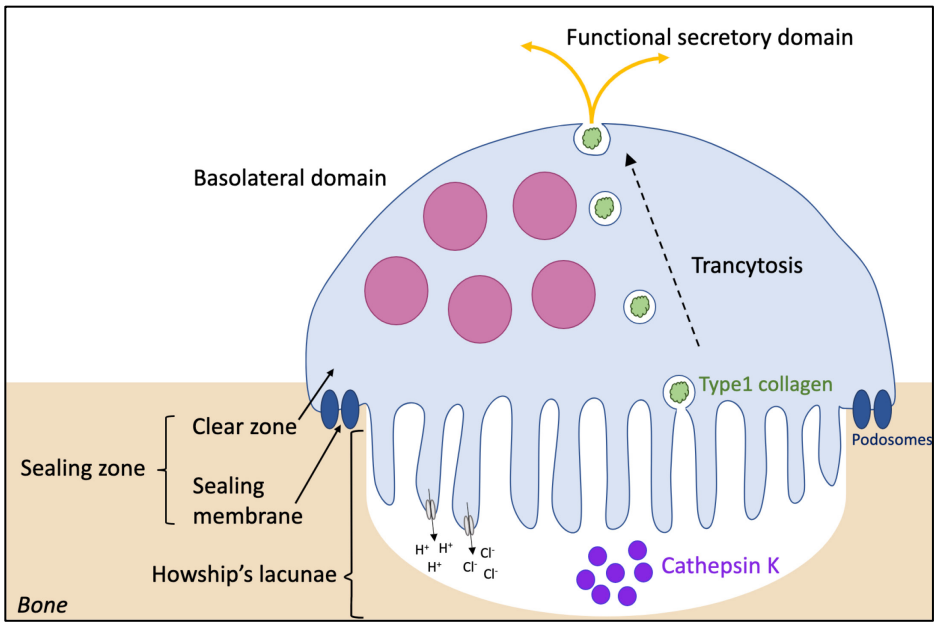


**Figure 3: Schema of the structure organization and morphology of a resorbing osteoclast**

## 2.2. Osteoclastogenesis and osteoclastic differentiation

Osteoclastogenesis is a multi-stage complex process by which the osteoclast is formed by the differentiation of monocyte/macrophage precursors cells from hematopoietic stem cells in the bone marrow spaces (Figure 4).[73,74] It has been suggested that these processes are regulated by a minimum of 24 distinct genes.[74] Some of these genes are involved in the formation and survival of the cell, while others impact the precursor cell's capacity to differentiate.

Osteoblasts are the principal mediators of osteoclastogenesis and osteoclast differentiation by the production of macrophage colony-stimulating factor (M-CSF), receptor activator of NF-kB ligand (RANKL), and osteoprotegerin (OPG), the first two (M-CSF and RANKL) are considered essential molecules of osteoclastogenesis.[75,76] M-CSF binds to the colony-stimulating factor-1 receptor (c-Fms), expressed by osteoclast precursors,[77] stimulating their proliferation, and avoiding their apoptosis (Figure 4).[73,78]

## 2.3. The RANK/RANKL/OPG system

The RANK-RANKL-OPG system regulates the balance between bone resorption and bone formation.[76] RANK binds to its receptor (RANKL), expressed by osteoclast precursors, and triggers a signaling pathway resulting in the induction and activation of nuclear factor of activated T cells c1 (NFATc1), the main transcription regulator of osteoclast differentiation.[75,76,78]

RANKL is also expressed by mature osteoclasts, that are activated by their interaction with RANK to start the process of bone resorption. Furthermore, RANKL is also responsible for inducing the release of the osteoclast enzymes tartrate-resistant acid phosphatase (TRAP) and cathepsin K.[67] OPG, on the other hand, blocks the RANKL-RANK interaction, thus inhibiting osteoclastogenesis (Figure 4).[76,77]

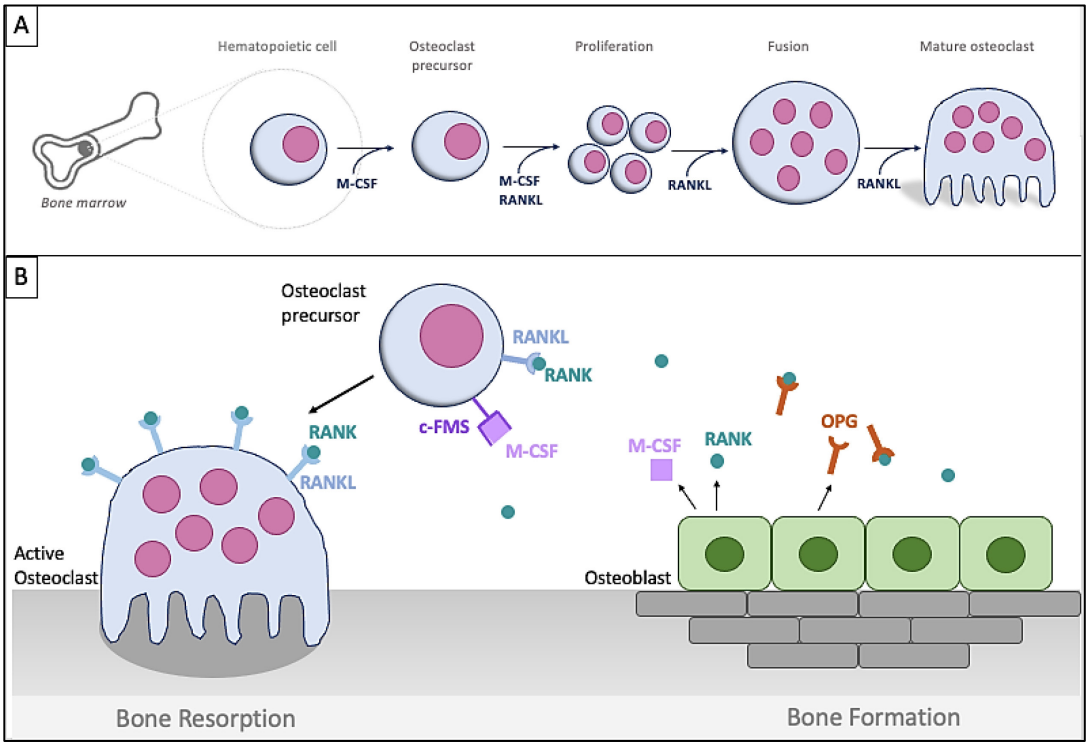


**Figure 4: The RANKL/RANK/OPG cycle.**

(A) Osteoclastogenesis and osteoclast differentiation illustrating the cytokines involved in each phase. (B) The RANKL/RANK/OPG cycle. RANK triggers osteoclast differentiation and activates the process of bone resorption by interacting with its receptor (RANKL). OPG blocks the RANKL-RANK interaction, inhibiting osteoclastogenesis.

## *2.4.* Osteoclast origin, fate, and recycling

Much effort has been put into studying the hematopoietic origin of the osteoclast and the cytokines involved in their differentiation. However, the embryonic origin, lifespan and fate of these cells remain incompletely understood. It is now known that osteoclasts differentiate from embryonic erythro-myeloid progenitors for fetal ossification as the hematopoietic stem cell niche is being developed.[79] Previously, it was believed that osteoclasts had a short lifespan of a few days and up to 6 weeks,[80] however, two recently published studies have shown that erythroid-myeloid progenitor-derived osteoclasts, generated during embryonic development, are still present 6 months after birth in mice[79]. Furthermore, Yahara, et

al. (2020) also found that these long-lasting osteoclasts fuse with the hematopoietic stem cell lineage precursors and contribute to postnatal remodelling in both physiological and pathological conditions.

In respect to osteoclast fate, an additional recent study reported that most osteoclasts undergo fission, breaking down into smaller and more motile cells, once the resorption event is finished, rather than apoptosis as historically accepted. The small post fission cells have been named osteomorphs and they have the ability to fuse with other osteoclast syncytia forming new functional osteoclasts, thus completing osteoclast recycling (Figure 5).[80]

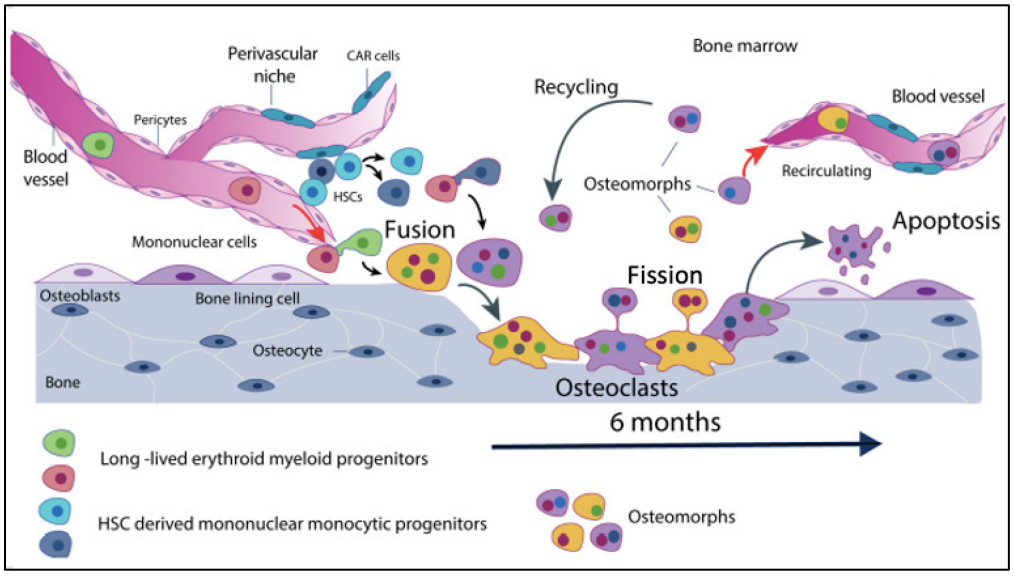


**Figure 5: The osteoclast fate, and recycling.**

Oteomorphs derived from osteoclast fission fuse with osteoclast syncytia forming new functional osteoclasts (Adapted from McDonald, et al. 2021).

# 3. Resorption behaviour

Although most of the studies of *in vitro* osteoclastic bone resorption focussed on pit formation, it has been demonstrated that this is only the beginning of the more complex resorption mechanism.[35,82] Osteoclast bone resorption *in vivo* is characterized by two distinct shapes of cavities: “pits” and “trenches”. Until recently, these two patterns were thought to be the result of the same resorption process with the trenches considered as a series of confluent pits.[83] However, recent time-lapse video recordings of human osteoclasts *in vitro*[82] revealed that the observed cavity patterns are two distinct resorption modes that differ in speed, depth, duration and, consequently, aggressiveness.[30,34,35,82]

Pits are round cavities representing short-time resorption separated by osteoclast migration periods where the cell ceases resorptive activity (intermittent resorption) whereas trenches are characterized as continuous resorption in which the osteoclast migrates while resorbing resulting in a deeper and longer cavity.[30] Soe and Delaissé (2017) observed that 81% of the trenches formed by osteoclasts in osteoclast-bone cultures began as a round pit and subsequently converged into the elongated cavity. Interestingly, they also noted that when the osteoclasts switched from the pit to the trench-mode, the same osteoclast roughly doubled its erosion speed, further confirming that the velocity is associated with the mode itself and not a sub-type of osteoclast.

## 3.1. The modes of resorption

The differentiation between two resorption modes has brought significant changes in the understanding of resorption cavities. In this context, we will discuss the current knowledge regarding the mechanisms underlying these distinct behaviours.

### 3.1.1. Ruffled border's dynamic and orientation

The ruffled border and the sealing zone (see section 2.2) have different dynamics according to the mode of resorption (Figure 6).[84] In the rounded pit-mode, the bone matrix uptake (endocytosis) occurs at the center of the cell and the secretion of enzymes (exocytosis) arises in a concentric fashion at the periphery (Figure 6). In contrast, trench-mode osteoclasts are more crescent shaped where the exocytosis occurs at the leading edge of the moving cell and the endocytosis occurs at the rear-end (Figure 6).[30,35,83,84] In addition, during pit-mode resorption, when the process is interrupted by migration periods, a completely new sealing zone is formed each time.[82]

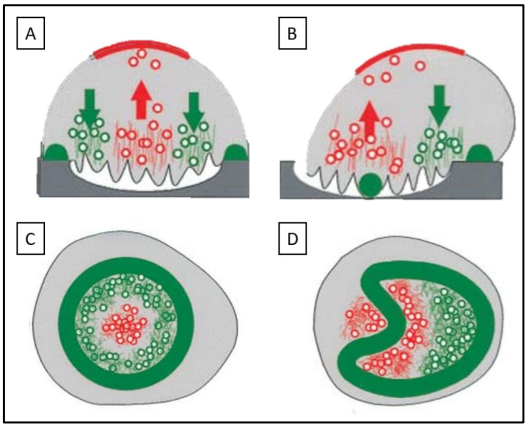


**Figure 6: Image showing the ruffled border's dynamics and organization.**

Green circles represent secretory events (exocytosis) while red circles are the bone matrix uptake (endocytosis). (A-C) Pit-mode osteoclast showing the concentric fashion of endocytosis (at the center) and exocytosis (at the periphery. (B-D) Trench-mode osteoclast showing the crescent shaped organization (Adapted from Mulari, et al. 2003).

Another significant difference between the two modes is the orientation of the ruffled border in relation to the bone surface. While pit-mode osteoclasts are oriented perpendicular to the bone surface, the resorptive activity in trench-mode osteoclasts is parallel to the bone (Figure 7).[28,82]

In addition, the evacuation of bone matrix fragments that undergoes transcytosis (see section 2.2) in the cell following endocytosis occurs opposite the bone surface in pit-mode, but at proximity to the resorption cavity in the trench mode (Figure 7).[35]

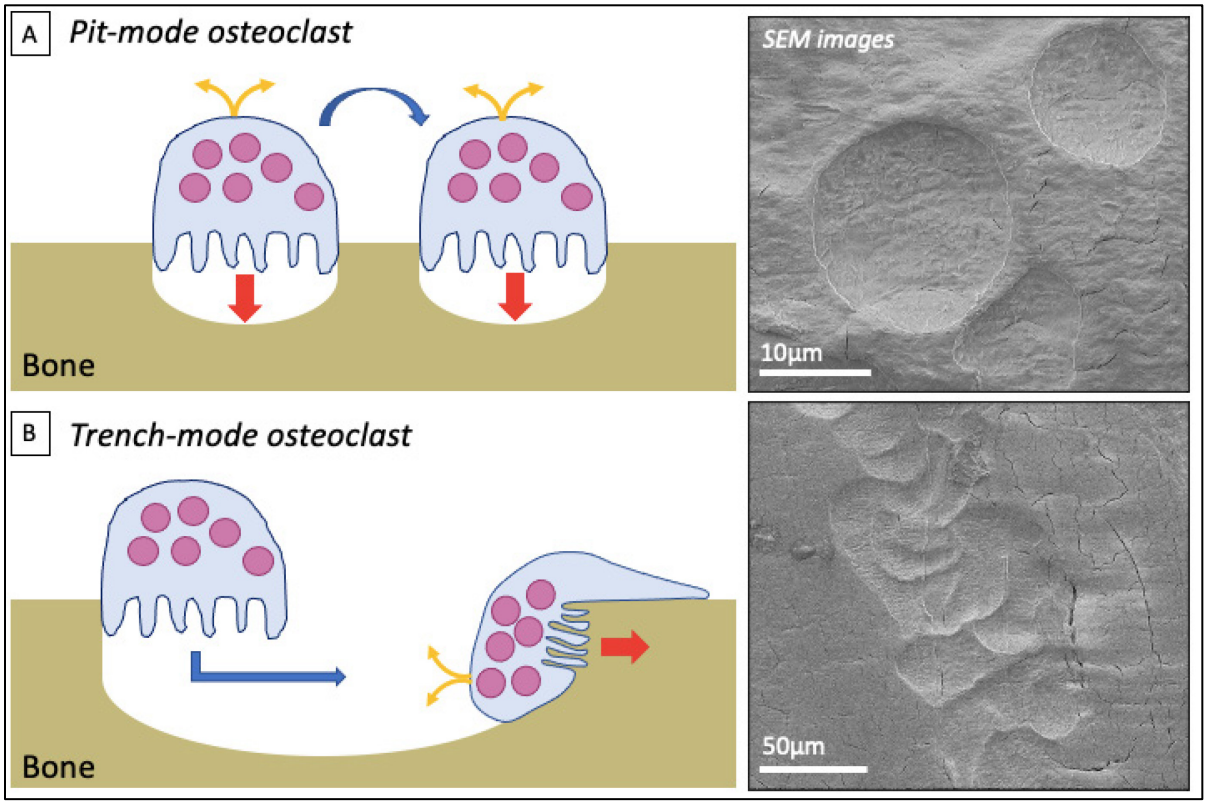


**Figure 7 : Pit versus trench mode resorption.**

(A) Pit-mode osteoclast resorbs the bone perpendicular (red arrow to the surface forming rounded pits. (B) Trench-mode osteoclast showing the parallel orientation of the ruffled border in relation to the bone surface (red arrow). The osteoclast usually starts making a pit and switches to trench-mode changing the axis of ruffle border orientation. Note the location of the function secretory domain (yellow arrows) in close proximity to the bone surface in the trench-mode.

### 3.1.2. Factors that may influence the resorption mode

There are many factors that can influence the behavior of the osteoclasts. Since the discovery of the two distinct modes of resorption, several authors have studied these factors to further understand what exactly determines when an osteoclast will form a round pit or an elongated trench. Unfortunately, there are still many questions to be answered. It is now known that these patterns have great inter-individual variation, and are affected by sex, age, and hormonal status of the donor[30,34] as well as the environment the cell is exposed to.[30]

Merrild, et al. (2015) showed that human osteoclasts differentiated from bone marrow were likely to create a higher proportion of trenches when compared to osteoclasts differentiated from peripheral blood. They also observed that osteoclasts from male donors were more prone to generate trenches rather than pits when compared to female donors. This is in agreement with Jevon, et al. (2002) who observed that cultures of osteoclasts from pre-menopausal females had significantly less resorptive activity than those differentiated from age-matched males. Interestingly, this study also concluded that cultures from post-menopausal females and males of corresponding age had similar resorption activity confirming that the hormonal stage of the donor can also influence the osteoclastic activity. In addition, Moller, et al. (2020)found a correlation between the aggressiveness of bone resorption and both aging and menopause.

### 3.1.3. Trench-mode is a more aggressive resorption process

To resist failure (i.e., fracture), a bone must absorb energy during loading. The quality of the bone tissue matrix, its mineral density and its structural properties will determine the bone's strength[85] and the more aggressive-related trench mode cavity has been associated with greater loss of stiffness of trabecular bone *in vitro* when compared to round pits.[29]

Studies using human osteoclast-bone culture found that while pit-mode osteoclasts resorbs for a median of 13 h,[82] only 13-14% of trench-forming osteoclasts stop their cycle of bone resorption within 72h,[34] indicating that once this process has started, it is unlikely that it will rapidly be interrupted. Soe and Delaissé (2017) (2017) also found that trench-mode osteoclast resorption persisted for longer periods (several days). Furthermore, this group observed that these cells resorbed for significantly longer distances (median length of 76µm) compared with pits (median length of 19µm) and had higher erosion speed (double).

### 3.1.4. Bone resorption pattern is associated with underlying collagen degradation characteristics

Demineralization and collagenolysis are the respective processes of breaking down the mineral and type 1 collagen during bone resorption. The main osteoclast enzymes capable of efficiently degrading the collagen type I fibers that are exposed during demineralization are the collagenase cathepsin K (see section 2.1) [26,28,34] along with matrix metalloproteinases (MMPs).[86]

One of the key challenges of the osteoclast is the synchronization between the demineralization and the collagenolysis, which are, by their nature, processes of distinct velocity.[28,30] When these processes are desynchronized, accumulation of collagen in the excavation cavity can occur, and may interrupt the resorption process.[26,28] In this context, it is important to highlight that collagen and mineral should also be considered as regulators of osteoclast activity rather than simply substrates to be solubilized as osteoclasts exposed to collagen do not develop a sealing zone and are incapable of starting the resorption process.[35]

Scanning Electron Microscopy (SEM) studies have revealed that pit-mode excavations accumulate demineralized collagen at the bottom of the pit but not in trench-mode resorption excavations.[26,28] Delaisse et. al. (2021) also reported that medications such as glucocorticoids (see section 7.2) alters the rate of collagen degradation and the duration of the resorption process.

Furthermore, Soe, et al. (2013) and Borggard, et al. (2020) demonstrated that cathepsin K additionally plays an essential role in the switch from pit to trench mode. The inhibition of cathepsin K collagenolysis results in early cessation of the resorption process and the formation of pits. In contrast, when the degradation of collagen was as efficient as the demineralization, the resorption was longer, with a prevalence of trenches. These findings further support the hypothesis that the effectiveness of the collagenolysis and the synchronization between the latter and demineralization are a prerequisite for the osteoclast to change its resorption mode.[28]

## 3.2. The sealing zones' role in osteoclast migration

It was believed for decades that the resorption and migration of osteoclasts were independent. The sealing zone, as mentioned earlier in section 2.2.3, is composed of an F-actin ring with a superstructure of densely interconnected podosomes that mediates the attachment of the cell to the extracellular matrix.[35,82,83]

Although it is counterintuitive that a sealing structure would permit displacement, an analogy can be made with the tracks of a military tank that allows the osteoclast to move forward while maintaining contact with the ground. The podosomes (see section 2.2.3.1) have a relatively short half-life of about 2-12 min providing a very dynamic nature to this structure[35] where continuous remodeling is necessary. Thus, the coordinated action of formation and disintegration of the podosomes allows the osteoclasts to migrate while maintaining an effective seal in trench-mode.[82,87]

The assembly of new podosomes occurs at the outer rim of the sealing zone (in contact with the bone surface), and the disassembly of older podosomes occurs at the inner rim (in contact with the cavity walls) (Figure 8).[35]

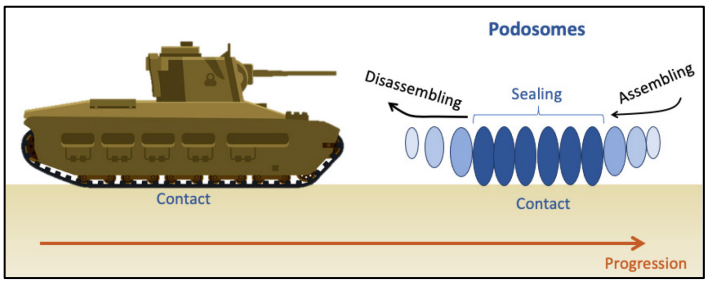


**Figure 8: Osteoclast migration.**

Image showing the analogy between the military tank capable of always maintaining contact with the surface and the assembly and disassembly of podosomes at the sealing zone of the osteoclast (Adapted from Delaissé, et al. 2021).

# 4. Culture of osteoclasts

The ability to culture and study osteoclasts *in vitro* is crucial to understanding the processes of bone remodeling. Historically, *in vitro* culture of osteoclasts was initiated by mature cell harvest from neonatal animals by fragmentation of their bones[88,89] or via co-culturing with osteoblasts.[90] The discovery of RANKL, an essential osteoclastogenic cytokine for the differentiation and activation osteoclasts, transformed the field of osteoclast culture and investigation.[91,92] With this advancement, osteoclast precursor cells (hematopoietic stem cells) are induced to differentiate into osteoclasts *in vitro* by the addition of RANKL and M-CSF. Nowadays, the most common tissue sources for hematopoietic stem cells (HSCs) are bone marrow and peripheral blood.[93]

## 4.1. Osteoclast differentiation from equine bone marrow aspirates

The bone marrow, housed between the bony trabeculae, is composed of a wide variety of cells that include mesenchymal stem cells (MSCs), endothelial cells, red blood cells, leukocytes, and HSCs that include osteoclast precursors. Different methods have been proposed to isolate these subpopulations

including plastic-adhesion, density gradient centrifugation separation techniques, and more recently cell sorting based on cell surface marker expression.[94]

The HSCs population in the bone marrow has been traditionally separated from the MSCs by plastic-adhesion *in vitro*,[95] however, this method is associated with low specificity.[94,96] Thus, in an effort to obtain more refined isolation, the density gradient methods (e.g. Ficoll-Paque or Lymphoprep) have also been employed to separate cells based on density and remove undesired components such as red blood cells, platelets, and granulocytes.[95,97] The drawbacks associated with these methods include their time-consuming nature and challenge in achieving standardization.[98]

A reliable alternative is the red blood cell lysis protocol which has been shown to be effective for isolation of human MSC.[98] Furthermore, this method has been successfully implemented for the isolation and cryopreservation of osteoclast precursors from murine[99] and equine bone marrow.[21]

Gray, et al. (1998) was the first to generate and isolate equine osteoclasts from bone marrow in horses using the plastic-adhesion method and prove that osteoclasts generated from haematopoietic precursors demonstrated identical characteristics to isolated mature equine osteoclasts.[18] However, the bone marrow was harvested from long bones post-mortem. Bone marrow aspiration is employed in the clinics in live horses, and it is also interesting from the research perspective for obtaining tissue. The tuber coxae and the sternum are commonly used for equine bone marrow aspiration,[100] with the sternum preferred due to its thinner bone cortex[101] and recent use in isolating osteoclasts.[21,102]

## 4.2. Bone resorption on equine bone slices - osteoclast on bone cultures

Osteoclasts have been cultured on a wide range of substrates to date including glass, plastic, hydroxyapatite, cortical bone slices (commercially available or handmade) and dentine.[103,104] As it is well known that the extracellular matrix (ECM) in which cells are cultured can influence their proliferation, adhesion, and differentiation,[105] it is surprising that there are some conflicting observations about morphological differences between osteoclasts cultured on different substrates. On the one hand, Kleinhans, et al. (2015) observed a significantly higher cell diameter when human osteoclasts were cultured on bone slices, compared to plastic. On the other hand, Deguchi, et al. (2016) reported that that human osteoclasts cultured on bone substrates were smaller in size and had more irregular shape compared to those grown on glass.

To achieve accurate translation of findings, it is preferable to replicate the *in vivo* conditions as closely as feasible in a laboratory setting. Cultivating osteoclasts on bone serves this purpose effectively. A few studies have cultured different species' osteoclasts on an equine bone substrate. Human[106] and chick

embryo[107] osteoclasts have been grown on equine bone. Malek, et al. (2022) was the first to culture equine osteoclasts differentiated from bone marrow aspirates on equine bone slices to date.

## 4.3. *In vitro* characterization of the osteoclasts and their activity

The characterization of osteoclasts and their activity *in vitro* may be done by staining methods of osteoclast identification, with the tartrate-resistant acid phosphatase (TRAP) being the most commonly utilized, or indirectly by the measurement of bone resorption biomarkers such as C-terminal telopeptide of type I collagen (CTX-I) and tartrate resistant acid phosphatase isoform 5b (TRACP5b) in the culture media from osteoclast on bone cultures.

### 4.3.1. Staining methods for osteoclast identification – osteoclast culture

Multinucleated osteoclasts may be characterized by the expression of the osteoclast-specific enzyme TRAP that is stained and visualized and has been the dominant osteoclast marker employed to date.[17,93,108-111] The number of cells, size and number of nuclei are analysed and cells containing 3 or more TRAP positive nuclei are considerate osteoclasts.[109]

Cathepsin K, an enzyme produced by activated osteoclasts, has also been used to identify osteoclasts by immunohistochemistry in different studies on equine subchondral bone.[16,112,113]

However, both markers have also been identified on multinucleated giant cells[111,114] and are not necessarily osteoclast specific. Thus, ideally, resorption pit assays should be used for a more precise identification and assessment of activity on bone slices (see section 5.1).[114]

### 4.3.2. Indirect measurements methods of osteoclast activity – Bone resorption biomarkers

Osteoclast enzymes, such as cathepsin K, digest type I collagen in the bone matrix, resulting in the release of bone resorption products such as CTX-I, that can be assessed using enzyme-linked immunosorbent assay (ELISA) kits and is a recognized bone resorption marker. [71,72,115,116]CTX-I has been measured in equine osteoclast cultures *in vitro.*[21]

Tartrate-resistant acid phosphatase isoform 5b (TRACP5b) is one of the enzymes produced by osteoclasts and is considered to reflect the number of osteoclasts rather than osteoclast activity.[117-119] Malek, et al. (2022) was the first to measure this enzyme in equine osteoclast cultures. In this *in vitro* study, TRAP5b was shown as an indicator of both bone resorption and osteoclast number.

Although blood biomarkers provide useful indirect indications of osteoclast activity, direct quantification offers a more comprehensive understanding. Furthermore, *in vitro* quantification allows for precise assessment under controlled experimental conditions, enabling manipulation and evaluation of factors that influence bone resorption. This approach facilitates the investigation of the impact of various elements, including drugs, hormones, and disease conditions, on osteoclast activity. In the subsequent section, we will explore the latest techniques employed for quantifying osteoclast activity, highlighting their novelty and significance in advancing our knowledge in this area.

# 5. Quantification of osteoclast activity

The accurate quantification and characterization of osteoclast activity (i.e., bone resorption) remains a challenge in bone research both *in vitro* and *in vivo*. The estimation of the osteoclast resorptive activity *in vitro* is often done to this day by measuring the area of resorption with light microscopy after staining bone or dentine slices with toluidine blue.[38]

The traditional *in vivo* gold standard technique was the transiliac bone biopsy and histomorphometry analysis.[37] In both cases, the three-dimensional properties of osteoclastic resorption are extrapolated from two-dimensional (2D) images, and the representation of osteoclast resorption cavities is limited to indirect estimation of averages and simplified shapes.[36,37] In the forthcoming section, we will delve into various techniques that have been employed to quantify osteoclastic activity both *in vitro* and *in vivo*.

## 5.1. Methods of quantification and imaging techniques - *In vitro*

### 5.1.1. Quantification of bone resorption on bone slices: Light microscopy and resorption-pit assay

The activity of osteoclasts is assessed by their capacity to form bone resorption cavities.[109] In this technique, they are seeded on bone slices and cultured under specific conditions (see section 4). Following the termination of cell culture, the bone slices are washed with phosphate buffered saline to eliminate the cells and fixed with 10% formalin at pH 7.4[21] and then stained with Toluidine Blue staining (1% concentration), which highlights the exposed collagen fibers in resorbed areas[109] that can be visualized in blue with light microscopy.[120] The area of resorption can be quantified with ImageJ software (Figure 9).[21]

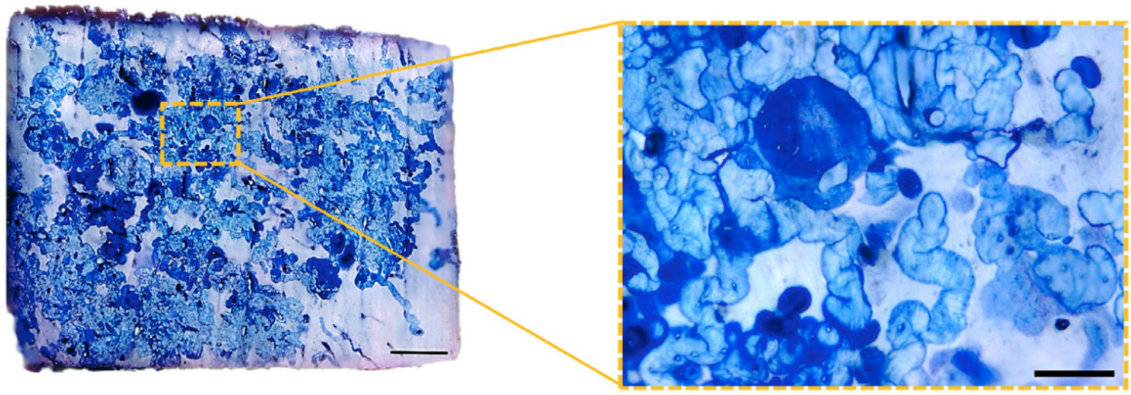

**Figure 9: Equine bone slice stained with toluidine blue.**

Example of a stained bone following osteoclast culture (22 days) showing the areas of resorption in blue.[21]

The area of resorption represents a 2D measurement that may be deceiving since it does not take depth into consideration[121] and as it was discussed in section 3, different types (pit and trench-modes) of resorptions can produce different depths/volumes. For example, an increased area of resorption, if in combination with decreased cavity depth, does not necessarily mean increased resorptive volume.[38,40,122] Furthermore, 2D measurements have been suggested to reflect more osteoclast spreading and attachment instead of resorptive activity.[38-40]

Although the maximum depth of a resorption cavity is a parameter that may be determined with different technologies *in vitro* including reflection light microscopy, scanning electron microscopy (SEM) or SEM stereophotogrammetry to provide supplementary information, it is unlikely that the maximum depth represents the average depth and so it is not considered an accurate measurement,[38] and, therefore, the ideal parameter to quantify osteoclast bone resorption is by the direct measurement of volume of tissue destroyed.[38,39]

### 5.1.2. 3D methods of quantification and imaging techniques

Since the ideal parameter for bone resorption quantification is the volume, it was deemed necessary to develop new approaches over the past few decades to incorporate a more accurate three-dimension (3D) quantification and characterization of the resorption cavities. Here we will address the different imaging techniques proposed for that objective as well as its advantages and disadvantages (Table 2).

| Technique | Measurement | Advantages | Disadvantages | Author |
|---|---|---|---|---|
| **SEM stereophotogrammetry** | Volume of individual resorption cavities | Excellent images | -Expensive technology<br>-Time consuming<br>-Limited to small samples | *Boyde et al. (1984)* |
| **Fluorescence based serial milling** | Volume of individual resorption cavities on cancellous bone | Accurate quantification | -Time consuming | *Tkachenko, et al. (2009)* |
| **Confocal laser microscopy** | Estimation of resorption cavity volume on dentine slices | Provides topographic information | -Limited to a shallow depth of field | *Soysa, et al. (2009)* |
| **Vertical scanning profilometry** | Total resorption volume on dentine slices | Direct and unbiased measurement of the eroded depth and volume | -Requires polished samples | *Pascaretti-Grizon, et al. (2011)* |

***Table 2: Advantages and disadvantages of some of the imaging techniques reported to measure osteoclast resorption volume in vitro.***

**SEM stereophotogrammetry:** SEM is a technique that utilizes focused beam of electrons to obtain high resolution images. When combined with stereophotogrammetry, it is possible to obtain 3D information about a sample's surface by acquiring images from different perspectives or by tilting the sample.[123] This combination was the initial 3D method proposed by Boyde, et al. (1984) to measure depth and volume of individual osteoclast resorption on dentine slices. Since then, several other novel approaches with high-resolution imaging techniques have been shown to be promising for quantifying resorption cavities in a 3D manner.

**Fluorescence-based serial milling**: Serial milling involves systematically trimming a specimen to reveal cross-sections, while collecting a mosaic of images of each newly exposed section, resulting in a high-resolution 3D stack of digital images.[124] Tkachenko, et al. (2009) combined this technique with epifluorescent microscopy where an ultraviolet filter was used to identify bone autofluorescence properties. They were able to obtain 3D sub-micron resolution images (Figure 10) and measure surface area as well as number of resorption cavities on rat lumbar vertebrae cancellous bone samples.

**Confocal Laser microscopy:** This technique employs a laser beam to illuminate a specimen and a pinhole aperture to eliminate out-of-focus light generating high-resolution images with enhanced optical sectioning and decreased background noise.[125] Confocal laser microscopy has been used by Soysa, et al. (2009) to characterize and estimate the volume of resorption pits (Figure 10) on dentine slices.

**Vertical scanning profilometry:** Originally designed for material roughness measurement, this method utilizes optical interferometric analysis to create three-dimensional topography maps of sample surfaces. Pascaretti-Grizon, et al. (2011) applied this technique to measure volume and lacunar resorption depth on dentine slices (Figure 10).

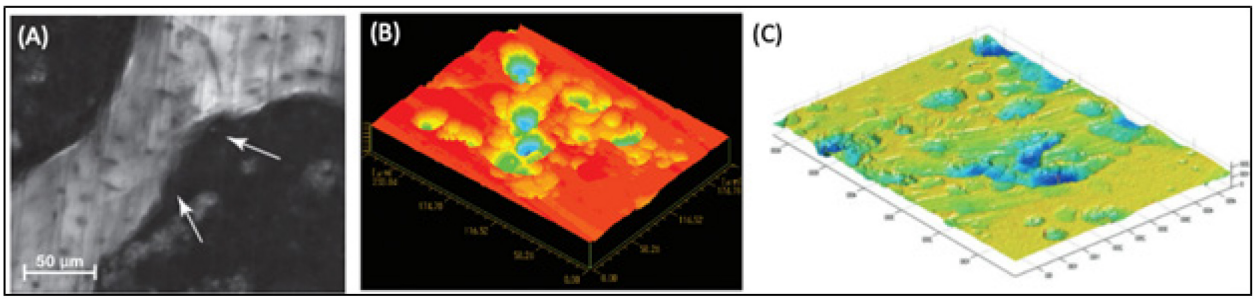


**Figure 10: Images techniques applied for the 3D quantification of resorption cavities.**

(A) Fluorescence based serial milling on rat lumbar vertebrae cancellous bone showing an individual resorption cavity (white arrows)[124] (B) Confocal laser microscopy on dentine slices[40] (C) Vertical scanning profilometry on dentine slices.[39]

Although these methods represent a significant advance towards accurate volumetric measurement of bone resorption, they are very laborious and costly. In addition, they have a destructive nature which limits the techniques to only *in vitro* measurements of relatively small samples. Furthermore, some rather than direct volumetric measurement, produce field topographical images.

## 5.2. Quantification of bone resorption *in vivo*

Traditionally, 2D bone histomorphometry on sections has been implemented as the "gold-standard" method for quantitative evaluation of the microarchitecture, remodelling and metabolism of the skeleton trabecular tissue *in vivo*. The samples are obtained by bone biopsy, usually from the iliac crest, and subsequently the sample is processed, stained, and analysed via microscope. Many parameters may be investigated, including bone area, bone volume and trabecular thickness.[37,126,127] The addition of labeling markers such as calcein or tetracycline at different time points also permits the analysis of time-dependent parameters including bone formation rate. However, it has been a challenge to determinate

bone resorption rate as there is no correspondent dynamic marker capable of doing so. [128,129] Therefore, bone resorption rate is not measured directly, but rather estimated based on the bone formation rate.[130] In addition to the limitations related to extrapolating 3D parameters from 2D measurements, histomorphometry also represents a laborious technique of destructive nature.[129] The introduction of the µCT now allows the direct 3D quantification of *in vivo* bone metabolism in a non-destructive manner preserving the whole sample.

## 5.3. µCT and the bone resorption

µCT was originally designed to evaluate automotive materials[131,132] and first used to image bone in 1983.[133] Since then, µCT has become the new "gold standard" technique to evaluate bone microarchitecture and morphology (Figure 11).[131] This non-destructive 3D imaging technique is known to have a high correlation with histology, and it is now widely used to measure both trabecular and cortical bone microarchitecture allowing the study of relatively large samples.[131,134]

Layton, et al. (1988) were the first to employ µCT to evaluate the subchondral bone architectural changes in a model of osteoarthritis in guinea pigs. It has been employed for several other applications including the correlations between mechanical loading and bone mass in mice;[136,137] the biomechanical effects of resorption cavities in human and canine cancellous bone;[138] as well as the microarchitectural trabecular bone characteristics of dogs treated with bisphosphonates (alendronate) .[139]

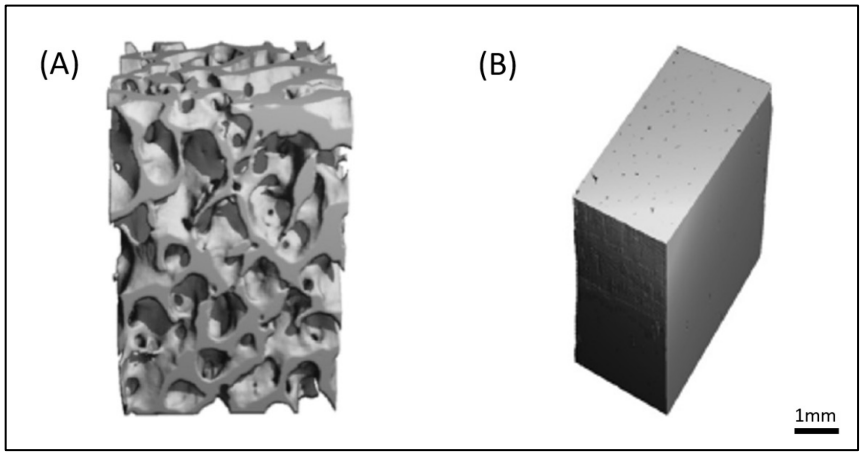


**Figure 11: µCT imaging of bone samples showing the different architectures**

(A) Trabecular bone (B) cortical bone (Adapted from Boerckel, et al. 2014).

Waarsing, et al. (2004) presented a novel method using *in-vivo* µCT to obtain and compare images of scans of the proximal tibia of rats at different time points employing calcein labelling. This advance permitted the quantification of changes in bone architecture in a longitudinal manner. Schulte, et al. (2011) later

described a technique to quantify bone formation and resorption rates with time-lapsed *in vivo* µCT images in mice. These developments were of great importance as they opened a new avenue for quantitative studies of bone between treatment groups.

This non-destructive 3D imaging technique is known to have a high correlation with histology, and it is largely used to measure both trabecular and cortical bone microarchitecture allowing the study of relatively large samples.[131,134]However, to our knowledge, this technique has never been applied for measuring the volume or characterizing osteoclastic resorption cavities *in vitro* on bone slices.

# 6. Osteoclasts and equine bone

In the upcoming section, we will delve into the existing knowledge about osteoclasts and their role in the equine skeleton specifically. Emphasizing the significance of enhancing our understanding of these cells' activity, we will explore how various factors, such as medications that can influence their function and potentially have a significant impact on the development of certain skeletal diseases.

The function of osteoclasts in equine bone, as in humans, is twofold, as they play an essential role in both the development of juvenile horses at the epiphyseal growth cartilage/bone junction and the remodeling of subchondral trabecular bone throughout adult life (subject addressed in section 1.4). This section will focus principally on original research investigations and observations of osteoclast activity in equine skeletal tissues.

## 6.1. Osteoclasts and their role in development and growth

### 6.1.1. Endochondral ossification

Long bones are formed by endochondral ossification, where growth cartilage is replaced by mineralized bone tissue. Osteoclast activity is central for epiphyseal growth, maturation and subsequent subchondral bone and trabecular bone remodelling (see section 1.4.2). Osteoclasts digest and remove the mineralized cartilage in tandem with the penetration of blood vessels and osteogenesis by osteoblasts.[64]

Gilday, et al. (2020) were the first to study the role of osteoclasts *in situ* in histological sections employing Cathepin K immunohistochemistry in equine epiphyseal subchondral bone development in Thoroughbred foals. A higher osteoclast density at the superficial subchondral bone, underlying the articular cartilage of juvenile Thoroughbred horses was found compared to deeper regions, validating their important role in shaping and maturation of the equine athlete's joint.[112] Interestingly, the higher osteoclast density also persisted at this site for up to 24 months of age when compared to that reported for adult horses. Fortin-

Trahan, et al. (2021) subsequently found evidence that the equine osteoclast degrades the deep layer of articular cartilage during subchondral bone maturation at the medial femoral condyle of young juvenile Thoroughbred horses further confirming the active role of the osteoclast digesting the growth cartilage in endochondral ossification and maturation of the joint. [113]

### 6.1.2. Subchondral bone cyst development

Subchondral cystic lesions (SCLs) in the cranial medial femoral condyle of the stifle joint[113] are radiolucent lesions that develop in young horses in the first months of life and may be a serious cause of lameness and develop in young horses in the first months of life.[141] As the lesion is a void in bone tissue, osteoclast bone resorption is believed to have a role in the pathogenesis of the disease; however, the exact origin of the lesions is still uncertain. It has been hypothesized that SCLs may be a form of osteochondrosis[142] that is characterized by focal failure of endochondral ossification due to ischemic necrosis of the ossification center[113,143] or that trauma plays a role in the development of the disease.[113] However, recently, Fortin-Trahan, et al. (2021) failed to find a significant difference in osteoclast density proportion between radiolucent lesions and control sites *in situ* in the medial femoral condyle of juvenile Thoroughbred horses. It is possible that increased osteoclastic activity could have been present in the surrounding lesions due to variations in osteoclast behaviour (see section 3) rather than density.

## 6.2. Adult Racehorse bone remodelling

Osteoclasts not only have an important role in equine skeletal development but also throughout adult life. They are critical for fine tuning bone structure to withstand the loads of athletic activity. Normal bone remodelling events have been described in section 1.4.2.

This section will focus on emerging knowledge of the important role played by the osteoclast in the subchondral bone of equine racehorse joints. There are now an increasing number of sites in the Thoroughbred racehorse's forelimb where osteoclasts are key players in osteochondral pathology in the joints. Varying terminology has been employed for the lesions but the underlying mechanisms to all are similar.

In chronological order, the first identified was in the fetlock (metacarpophalangeal and metatarsophalangeal joints). This condition, now called palmar osteochondral disease (POD)[14,15] was first thought to be a juvenile osteochondrosis[144] and affects the palmar/plantar condyles of the distal third metacarpus and metatarsus. It has been widely studied since then.

Riggs, et al. (1999) evaluated POD lesions using computed tomography (CT) and backscattered electron mode of SEM. Their findings supported the idea that POD lesions, although occasionally found in association with fractures, are improbable to be the cause of such pathology.[13] The disease has been found to be linked with the osteoclastic resorption that happens focally at specific sites of equine's joint subjected to high stress loading of subchondral bone. [8] Additional conditions on the fetlock where osteoclast remodelling is now recognised to play an important part are in fractures of the metacarpus[8] and the sesamoids.[145]

Furthermore, in the carpal joint, a study found that Cathepsin K-stained osteoclast density was increased in the subchondral plate of racehorses with post-traumatic osteoarthritis, immediately under the articular cartilage at focal sites that are prone to fracture , once again underpinning their key role in pathological remodelling of the equine joint surface and skeleton.[9,16]

### 6.2.1. Stress fractures in horses

Stress fractures in racehorses are a consequence of repeated cyclical loading to which the racehorse's skeletons are subjected to during high-intensity exercise.[10,11,146-148] They may lead to complete fractures that occasionally result in euthanasia of the horse. In this situation they have been termed "catastrophic fractures". The latter arise from pre-existing stress fractures that compromise the normal strength of the bones[148] and can occur spontaneously during racing or training, often without any noticeable clinical signs beforehand. [146] The stress fractures in racehorses occurs in specific anatomical locations (table 3) that are subjected to significant biomechanical focal loads.[148]

| Bone/joint | Anatomical location |
|---|---|
| **Scapula** | Distal aspect of the spine |
| **Humerus** | Caudoproximal; craniodistal; medial diaphyseal; caudodistal |
| **Carpus** | Dorsomedial third carpal bone; radial carpal bone; intermediate carpal bone |
| **Third metacarpal** | Mid-diaphyseal and supracondylar; parasagittal groove; proximal palmar; dorsal cortex; distal condyle |
| **Proximal sesamoid** | Palmar flexor region; medial sesamoid abaxial mid-body subchondral bone |
| **Proximal phalanx** | Sagittal groove |
| **Pelvis** | Ilial wing; Pubis |
| **Tibia** | Distomedial; caudoproximal; caudal diaphyseal; proximolateral under the head of the fibula |
| **Tarsus** | Dorsolateral third tarsal bone |
| **Lumbar spine** | L5-L6 vertebral junction |

***Table 3: Predictable sites of stress fractures and stress remodeling (Adapted from Pye and Stover [149], 2022, chapter 3)***

While these fractures can affect multiple bones in the skeleton,[148] there is growing recognition that they can also emerge at joint surfaces.[9,16] It is important to note that the tissue response differs between long bones, which are covered with periosteum, and joint surfaces, composed of cartilage. Load transmission primarily takes place at the joints,[148,150] where bones exhibit a broader surface area at the end for articulation. This architectural feature helps reduce stress on the load-bearing structures, including the subchondral bone.

## 6.2.2. Articular stress fracture in horses

Subchondral bone lies directly under the articular cartilage and comprises a dense outer shell of cortical type bone (subchondral plate) whereas underneath, the looser trabecular bone is made up of struts and rods. The equine subchondral bone, can develop microcracks, also termed microdamage, in its structure because of high-intensity repetitive loads.[8,151] It is a normal feature of wear and tear but can accumulate in situations such as training and racing and eventually lead to bone failure (fracture)[10-12] as described in the fetlock[8,13-15] and carpus,[9] where the biomechanical forces are known to be of higher magnitude.[152]
The body's cells intervene to attempt repair by bone remodelling,[12,151,153] however, when excessive, it can accumulate at specific sites.

Riggs, et al. (1999) were the first to describe a linear defect in the cartilage and underlying subchondral bone at the parasagittal groove of the distal condyles of the third metacarpal/metatarsal bone where fractures arise. Several other authors have performed research supporting the theory that site-specific microcracks are associated with the development of articular stress fractures and defects in the subchondral plate of the condylar grooves due to adaptive failure. Muir, et al. (2006) also found an accumulation of microcracks in the same region using histomorphometry. This is in accordance with the observations by Norrdin and Stover (2006) on the subchondral bone in the distal metacarpal condyle from racehorses with post-traumatic osteoarthritis (PTOA) using SEM (figure 12). The microcracks were identified in sclerotic bone and they also observed osteoclastic resorption lacunae in that region, evidence of a healing response.

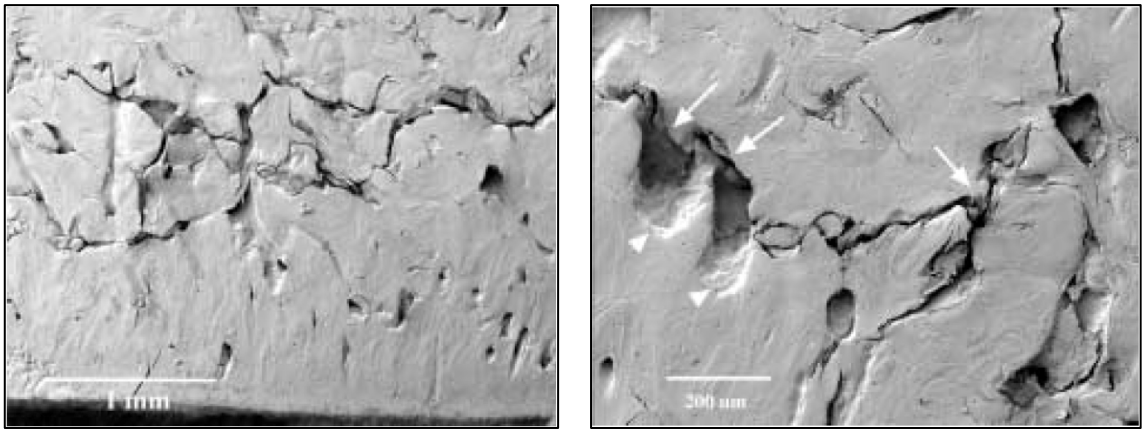


**Figure 12: SEM image of microcracks at the subchondral bone of the fetlock joint.**

Note on image the mismatched surfaces (arrows) and osteoclast resorption sites (white arrows)(Adapted from Norrdin and Stover 2006).

Supporting this theory, it has been shown that there is an increased density of microcracks at the region underlying the parasagittal groove of the metacarpus (Figure 13) of racing horses compared to other region of the joint and non-athletic horses[154] and also that they accumulate with career progression.[151]

More recently, Shaffer, et al. (2021) has also studied fractured proximal sesamoid bone (fetlock joint) of racehorses and found an association between subchondral bone osteopenia and bone failure (Figure 13).

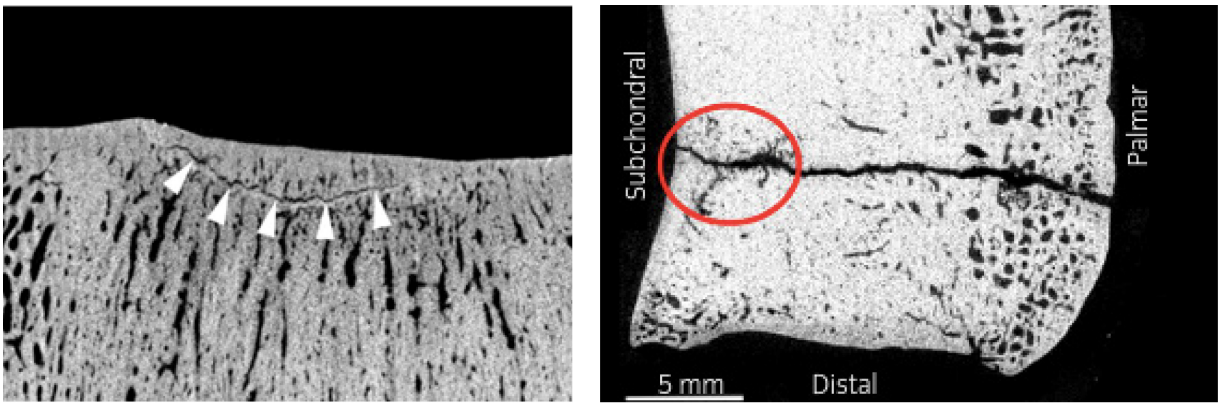


**Figure 13: µCT image illustrating microcracks of the subchondral bone.**

On the left, region underlying parasagittal groove of the III metacarpal bone showing the microcracks (white arrow). On the right, area of focal osteopenia (red circle) associated with fractured proximal sesamoid bone. (Adapted from Whitton, et al. 2018 and Shaffer, et al. 2021).

Finally, in the carpal joint, microstructural changes including the presence of microcracks in the calcified cartilage and subchondral bone, along with areas of resorptive remodeling, have been observed in Standardbred racehorses affected by repetitive trauma osteoarthritis,[9] specifically at the dorsal aspect of the third carpal bone, which is a frequent site for fractures.[155]

### 6.2.3. Osteoclast recruitment and differentiation for targeted remodeling

While the importance of osteoclasts in bone remodeling is well recognized, the mechanisms underlying osteoclast recruitment and differentiation for targeted remodeling are still not fully understood, highlighting a significant gap in our current knowledge.

Osteoclasts precursor recruitment from the local bone marrow and their subsequent differentiation into active bone-resorbing osteoclasts is mediated by multiple mechanotransduction pathways. Osteocytes, well-known for their mechanosensory function, play a crucial role in establishing the lacunar canalicular network, enabling communication between neighboring cells. It is theorized that the disturbance of this network, attributed to microdamage,[5] represents one of the pathways involved in regulating bone remodeling.

Osteocyte apoptosis is also believed to be involved in the signalling mechanism of targeted remodelling[6,156] due to RANKL gradients caused by osteocyte death.[157] However, the specific sites of the equine skeleton predisposed to exercise-induced injury have not consistently shown low osteocyte density.[154,158] The presence of osteoclastogenic cytokine RANKL has only been studied in one paper to

date of post-traumatic osteoarthritis in the carpus and it was shown that there was a significant correlation between the presence of RANKL, osteoclast density and cartilage degeneration focally at the joint surface.[16] It is noteworthy that it was also the site where fractures arose in this bone.

### 6.2.4. The risk factors associated with stress fractures in racehorses

Over the past few decades, much research has been implemented into identifying the risk factors related to stress fractures that lead to complete (catastrophic) fractures in horses as an attempt to predict and minimize its occurrence. One of the biggest challenges lies on the fact that many of those factors have great variability as they depend on the location (different countries and jurisdictions) and type of race[159]. Undeniably, one must take into consideration all the epidemiological risk factors associated with those injuries. In this review, focus is placed on the potential role of the osteoclast and microstructural changes, so factors that may influence equine bone remodelling rate will be addressed.

Withal, Carrier, et al. (1998) found a strong correlation between the risk of humeral fracture and the time since return from lay-up (resting period) in Thoroughbreds racehorses in California. This is in accordance with a more recent study with Thoroughbred racehorses in Florida where the incidence of catastrophic injury was associated with the number of days since last race.[160] The hypothesis behind those findings is that equines reinitiating training or racing subsequent to a prolonged period of reduced exercise could exhibit insufficient bone mass to effectively mitigate exercise-triggered microdamage.[10]

Holmes, et al. (2014) found that racehorses in high intensity training had a lower rate of bone resorption and higher rate of bone formation in areas of elevated mechanical load on the distal metacarpus when compared to horses in rest. In accordance with this finding, Whitton, et al. (2018), observed lower levels of microdamage in the subchondral bone of the distal metacarpus of resting horses. Both studies also showed that the bone damage accumulates with time in training. The hypothesis proposed behind those findings is that, as the resorption phase of the remodelling process is much faster than the formation phase (approximately 2-3 weeks compared to 3 months), there is a window of weakness in the bone tissue when the horse is rested. In other words, when the horse is rested the injured bone is resorbed rapidly by the osteoclasts in the first few weeks but as it takes months for the complete deposition and remodelling of new bone at the repair site. The period between the two is a period where the osteopenic bone may have suboptimal strength at the focally damaged sites undergoing repair and the bone structure is more susceptible to failure.[10,146,159]

### 6.2.5. Silicosis

This review would not be complete without a brief mention of another poorly understood, but rare, equine bone disease that implicates enhanced osteoclastogenesis and resorption. Equine silicosis is a lung disease caused by inhaling cytotoxic silica dioxide crystals and causes osteoporosis, characterized by excessive bone resorption by osteoclasts.[161] Silicates, including the fibrogenic and cytotoxic cristobalite form, are commonly present in soil, with a higher concentration in certain areas of Monterey County, California. The severity of osteoporosis is highly correlated with the presence of cytotoxic crystals in the tracheobronchial lymph nodes, although the underlying mechanism remains unknown.[161,162]

This condition presents with various clinical manifestations, including nonspecific lameness, skeletal deformities such as lordosis, lateral bowing of scapulae and rib cage, and decreased range of motion of the cervical vertebrae which is sometimes associated with neurological signs.[161,163]

The diagnosis of silicosis-induced osteoporosis remains challenging, as indicated by the findings of Arens, et al. (2013), who concluded that the resorption biomarker CTX-I is not a reliable diagnostic tool. Gaining a deeper understanding of osteoclast function and differentiation in the context of silicosis may provide valuable insights not only on the diagnosis of the disease as well as the underlying mechanisms involved in bone damage and remodeling associated with this disease. This knowledge could potentially facilitate the development of targeted therapeutic strategies aimed at alleviating the effects of silicosis and enhancing the overall well-being of affected horses and also humans who also suffer from this condition. Understanding the mechanisms underlying osteoclast function and differentiation in the context of silicosis could shed light on the pathological processes involved in bone damage and remodeling associated with this disease. Such knowledge could pave the way for the development of targeted therapeutic strategies to mitigate the effects of silicosis and improve the well-being of affected horses.

To conclude this section, there is emerging evidence that training and racing are leading to occupational injuries in racehorse's bones and joints that may be catastrophic. The chronological sequence of the pathophysiological events remains incompletely understood. Structural changes in the bones have been more extensively studied than the biological events. As the equine osteoclast is the orchestrator of bone resorption events and bone repair, there is a need to understand its biology. Important unanswered questions are: (1) what is its role in microdamage repair (2) what factors other than RANKL gradients may induce osteoclast differentiation at focally microdamaged sites (3) does excessive focal osteoclast activity at some sites precipitate fracture (4) if osteoclasts are the healers, particularly near the joint surfaces,

what is the impact of current medications frequently employed in equine athletes such as corticosteroids and bisphosphonates on their activity.

# 7. Drugs that target or influence osteoclast function or formation

Various factors have the potential to affect equine osteoclast development, such as commonly used medications like bisphosphonates, corticosteroids, and non-steroidal anti-inflammatory drugs. However, there has been a lack of research conducted to investigate their impact. Consequently, these medications could potentially affect the maturation of joints or the bone's ability to heal. The effects of these medications on osteoclasts in other species, especially humans, have been studied and will be discussed. To maintain brevity, only the two former medications will be addressed.

## 7.1. Bisphosphonates (BPs)

Bisphosphonates (BPs) are widely used in human medicine for the treatment and management of various bone diseases including post-menopausal osteoporosis and Paget's disease.[164-166] BPs are analogues of pyrophosphate (PPi) which is a physiological, inhibitor of mineralization and their main target are the osteoclasts.[167] They are divided into two distinct classes according to the presence or not of a nitrogen atom in their molecular structure that affects their mechanism of action, effect, and potency. They are the non-nitrogenous BPs (non-NBPs) and the nitrogenous BPs (NBPs), the latter being the most recent and more potent class in terms of anti-resorptive affects.[164]

The only veterinary-licensed bisphosphonates are Tiludronate disodium (Tildren, Ceva Animal Health LLC, Lenexa, KS, USA) and Clodronate disodium (Osphos, Dechra, Ltd., Staffordshire, UK), both from the non-NBPs class.[164] The use of both Tildren and Osphos in horses was approved by the Food and Drug Administration (FDA) in 2014 for the treatment of navicular syndrome disease, however, its actual clinical use goes beyond.[168] Various reports have suggested clinical improvement of horses treated with Tildren in different diseases associated with bone remodelling including chronic back pain,[169] distal tarsal osteoarthritis,[170] sesamoiditis,[165] and, more recently, osteoarthritis of the fetlock joint.[171]

### 7.1.1. Mechanism of action and the effects of bisphosphonates on osteoclasts

BPs have high affinity for bone and form complexes with hydroxyapatite crystals, preferentially at areas of active bone resorption. During bone resorption, the BPs that are embedded in the bone can be liberated and once that happens it can either (1) be internalized by the resorbing osteoclast, (2) recirculate locally

and systemically and reattach to bone or (3) be excreted in the urine.[166,172] The BPs that are taken up by the osteoclasts accumulate as non-hydrolysable ATP analogues and induce various morphological changes in the cell, including alteration or loss of the ruffled border and loss of the F-actin ring due to disruption of the cytoskeleton. Eventually, the osteoclast becomes apoptotic and subsequently bone resorption is inhibited.[165,166]

In humans, it has been estimated that BPs could potentially have long lasting residual effects as they can remain bound in bone for periods that range from 1 to 10 years.[166,173] A recent equine study found that clodronate and tiludronate were still present in some bone and tooth samples 4- and 30-days following drug administration, providing evidence that BPs can also reside for long periods in equine bone.[172] Riggs, et al. (2021) also reported that a therapeutic dose of Tildren administered to a horse can be detected in blood and urine for a period of 3 years following administration.

During bone resorption, the BPs that are embedded in the bone can be liberated and once that happens it can either (1) be internalized by the resorbing osteoclast, (2) recirculate locally and systemically and reattach to bone or (3) be excreted in the urine.[166,172] The BPs that are taken up by the osteoclasts accumulate as non-hydrolysable ATP analogues and induce various morphological changes in the cell, including alteration or loss of the ruffled border and loss of the F-actin ring due to disruption of the cytoskeleton. Eventually, the osteoclast becomes apoptotic and subsequently bone resorption is inhibited.[165,166]

### 7.1.2. Bisphosphonates and racehorses

As discussed in section 6 (osteoclasts and equine bone), osteoclasts play a vital role throughout an individual's life in maturation, health, and disease. Anything that adversely affects osteoclastic activity can potentially lead to focal bone fragility because of imbalance between bone formation and bone resorption. As BPs inhibit osteoclasts, the indiscriminate administration of BPs, particularly to young horses, is a significant concern due to their potential negative effects on normal bone and joint maturation and adaptation. Furthermore, the use of BPs in young racehorses affected by microdamage requiring osteoclasts for effective repair, has raised concerns as it has been suggested that it may disrupt the repair process and lead to the advancement of microfractures to catastrophic fractures.[172,174]

Some investigations have explored the impact of bisphosphonate treatment on bone resorption biomarkers in horses with varying outcomes. Horses administered tiludronate intravenously have shown marked reductions in CTX-I concentrations[173] providing indirect evidence of decreased bone resorption.

On the other hand, clodronate intramuscular administration did not produce a similar decrease.[175,176] Although Knych, et al. (2022) found no significant difference in CTX-I concentrations between the control and treatment groups, there was a significant reduction in TRACP5b relative to baseline, suggesting that clodronate may affect osteoclast numbers and thereby activity at label doses.

Because of these concerns, there are currently precise conditions for the use of this drug class in racehorses. Specifically, the International Agreement on Breeding, Racing and Wagering (IABRW) by the International Federation of Horseracing Authorities (IFHA) states that "Any bisphosphonate is not to be administered to a racehorse: "(1) under the age of three years and six months as determined by its recorded date of birth; and (2) on the day of the race or on any of the 30 days before the day of the race in which the horse is declared to run" (https://www.ifhaonline.org/default.asp).

## 7.2. Corticosteroids

Corticosteroids are commonly used intraarticularly in equine medicine to treat osteoarthritis due to their potent anti-inflammatory effects.[177] Osteoporosis leading to fracture is an adverse side effect associated with repeated use of corticosteroids in humans.[178]

### 7.2.1. Mechanism of action and the effects of corticosteroids on osteoclasts

The bone loss associated with the chronic use of corticosteroids in humans *in vivo* is suggested to be biphasic where a rapid increase of bone resorption due to excessive osteoclast activity happens initially, followed by a slower decrease in bone formation due to decreased osteoblast activity[26,178,179]. There is also evidence that corticosteroids increase the expression of the osteoclastogenic cytokine RANKL and decrease the amount of osteoprotegerin (RANK`S decoy receptor) in human osteoclast *in vitro*. This results in stimulation of osteoclast differentiation and maturation[178,180]. However, a consensus regarding the mechanism of action in osteoclast cultures has not yet been reached and the effects of corticosteroids on the differentiation, survival and activity of osteoclasts remains a matter of debate.[26]

Soe and Delaissé (2010) found that although there was no remarkable difference in the resorption area between corticosteroids-treated osteoclast-bone cultures and controls, the morphology of the resorptive cavities was influenced with more trenches formed, rather than pits, revealing a more aggressive resorptive behaviour. This would certainly be a concern if it arises *in vivo* following the use of intraarticular corticosteroids in either humans or horses and merits further study. Various factors may play a role in these contradictory results including interspecies effects and corticosteroids dose variations.

Nowadays, the most commonly used intra-articular corticosteroids in equine medicine are betamethasone esters (Betavet Soluspan), triamcinolone acetonide (TA) (Vetalog) and methylprednisolone acetate (MPA) (Depo-Medrol).[177] A concern is that the concentrations of intraarticular corticosteroids, particularly the slower release preparations (TA and MPA) where the exposure to higher doses is longer (up to 70 days in the case of MPA),[184] may adversely affect the physiological response of osteoclasts that reside in the equine subchondral plate. As described earlier (section 6.1.1), the osteoclasts are present in higher numbers at this site up to 2 years of age when they train and race[112,113] and in osteoarthritic lesions at fracture prone sites.[171] Their role is significant in resorptive lesions like POD and in repairing microdamage of the subchondral plate.[171] Consequently, it is highly likely that osteoclasts are exposed to elevated levels of corticosteroids following intraarticular injections into the joint. This becomes particularly important when joint disease is present and there is a loss of articular surface integrity, such as articular cartilage fibrillations and erosions,[9] which provides access to the subchondral plate. Additionally, it is recognized that there exists a communication mechanism between articular cartilage and subchondral bone, allowing certain molecules to traverse the osteochondral junction.[185] Therefore, the administration of corticosteroids to equine athletes could potentially have detrimental effects on osteoclasts and bone healing process of microdamage.

# 8. Image analysis and deep learning

In this final section, we will delve into the realm of image analysis and deep learning, which have emerged as powerful tools in the field of biological imaging. The application of image analysis techniques, combined with the advancements in deep learning algorithms, has revolutionized the way we extract information from complex biological images. Within the context of osteoclast and bone research, these innovative approaches offer unprecedented opportunities to uncover intricate patterns and quantify various parameters related to osteoclast activity. In recognition of our primary audience being veterinary clinicians, we have included a glossary specifically focused on terms commonly used in the fields of image analysis and deep learning with the goal of facilitating comprehension.

Glossary

**Object:** An object has features that are perceived and identified through natural senses or artificial imaging and detection methods.

**Digital image:** A digital image is an array of numbers that represent the intensity of pixels arranged in a 2D or 3D matrix. Characteristic patterns of pixels can be recognized as the features of objects. By analyzing pixel patterns, it is possible to identify and interpret the objects and features in a digital image.

**Feature:** Measurable distinct and identifiable characteristic or property of an object or pattern. In pattern recognition and categorization, a unique set of features is often used to represent a class of patterns.

**Pattern recognition:** Identification of patterns as proxies of objects

**"Ground truth":** Set of data, usually annotated, or curated by an expert operator, that serves as a reliable and accurate output for evaluating the accuracy and effectiveness of a neural network.

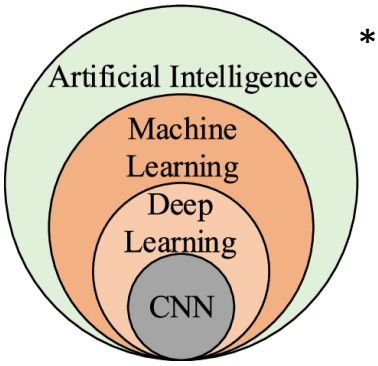

*

**Machine learning**: Machine learning is a subfield of artificial intelligence that focuses on the development of algorithms and models that can enable computers and machines to automatically learn from data and improve their performance on a given task without being explicitly programmed.

**Deep learning:** A subfield of machine learning that employs artificial neural networks with numerous layers to identify and comprehend data patterns. It can process huge volumes of intricate data, such as speech, images, and natural language, and derive significant insights from the data without human interference.

**Output:** Image annotation generated by the network or an expert after processing the input data.

**Input: greyscale image** Data provided to the network as an initial step. This input data is processed through the network's layers of interconnected nodes, also known as artificial neurons, where it is transformed and analyzed.

**Kernel:** Small matrix or filter used for extracting meaningful features from input data. The kernel is typically a square-shaped matrix that slides or convolves over the input data (or patch).

**Patch:** Small region or subset of an input image or data often used as input to the network for feature extraction and analysis.

**Loss function** Function that measures the difference between the predicted output of a neural network and the actual or expected output ("ground truth"). The loss function is used to evaluate how well the artificial neural network is performing on a given task and to provide feedback that allows the network to nudge its weights and biases during the training process to improve its performance (to minimize the loss).

*Zhang, et al. (2022)

## 8.1. Introduction to image analysis

A 2D image often serves as a visual representation of a 3D object but inherently involves a significant loss of information.[187]

Mathematical models are frequently used to represent images. A real image can be defined as a function, denoted as f (x, y), where f represents the amplitude (e.g., intensity of gray level ranging from black to white) of the image at a specific coordinate position (x, y).[188,189] When digitized, a real image can be divided into N rows and M columns, and their intersections correspond to pixels[187,189] where m=0,1,2,…,M-1 and n=0,1,2,…,N-1.[188] Following this logic, the origin of a digital image would be f (0,0), and the next coordinate (first row) would be f (0,1). Similarly, the first column would be represented by f(1,0), and so on (Figure 14). Consequently, a digital image can be represented as a numerical array, such as a matrix, where each element represents a pixel.[188]

$$f(x,y) = \begin{bmatrix} f(0,0) & f(0,1) & \cdots & f(0,\mathcal{N}-1) \\ f(1,0) & f(1,1) & \cdots & f(1,\mathcal{N}-1) \\ \vdots & \vdots & & \vdots \\ f(\mathcal{M}-1,0) & f(\mathcal{M}-1,1) & \cdots & f(\mathcal{M}-1,\mathcal{N}-1) \end{bmatrix}$$

**Figure 14: Representation of an image as a numerical array (matrix).**

(Adapted from Young, et al. 1995, pg 2-6)

## 8.2. Image registration technique

In medical imaging, valuable information can be extracted by comparing multiple images taken at different time points. Radiographic diagnosis often relies on visual inspection and the mental fusion of complementary images.[190]

When it comes to computed tomography (CT) scans taken at different time points, accurately aligning the repeat scans to the exact same coordinates poses a significant challenge. Image registration is the process of determining the spatial alignment of two sets of image data.[190-192]

While manual registration is possible, automatic registration offers more precise results. Over the past few decades, numerous registration algorithms have been developed and are now available in both commercial and open-source software.[190]

If we consider an image as a matrix that maps the coordinates of the image intensity values, the process of image registration involves modifying the matrix representing one image (dataset A, referred to as the moving image) to match the coordinates of another image (dataset B, known as the stationary image) (Figure 15). The moving image is transformed (e.g., rotated and translated) so that the anatomical location

of dataset A aligns with the corresponding anatomical location of dataset B, enabling the quantification of anatomical changes between scans.[190]

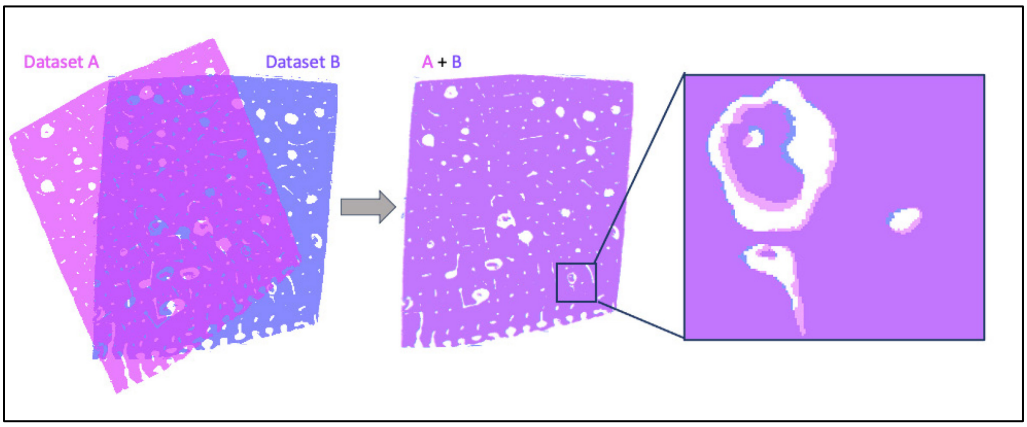


**Figure 15: Image registration.**

Process between two datasets (A and B) and their anatomical differences.

## 8.3. Image segmentation

Image segmentation, a section of digital imaging processing also known as labeling, is the process of subdividing elements of a given image into groups (regions) with common properties using a set criterion (ex: pixel brightness). The objective is to represent the image in a meaningful way, highlighting the regions of interests (ROIs) (Figure 16).[44,193-195]

As medical images contain a significant amount of information, image segmentation provides a clear visualization of the ROIs, removing the unnecessary information in a way that it is convenient for the image to be analyzed.[44,194]

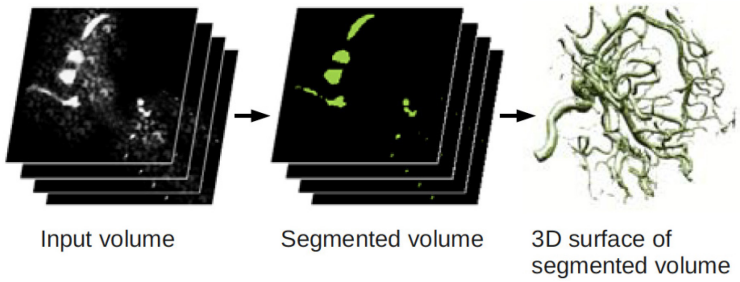


**Figure 16: Image segmentation.**

An example of image segmentation of a computed tomography (CT) scan using threshold to generate a 3D image.[194]

This can be performed manually but is very laborious, time-consuming work.[196] Automatic image segmentation remains a challenge and many deep learning networks have been developed in the last few years aimed at improving image segmentation performance.[193] The accuracy of segmentation is of great importance in image processing as it is a crucial step that influences the accuracy of the results of the analysis.[195]

## 8.3.1. Thresholding

Thresholding is a segmentation technique whereby pixels or voxels (3D pixels) are allocated to different categories, depending on their brightness, with the goal of identifying the part of the image that corresponds to an object in the real world and separating it from the background.[193,197,198] The accuracy of the threshold is of extreme importance as the results of image analysis depend on the technique.[199] A poor-quality segmentation may be associated with consequential issues such as over/under estimating volumes and image noising.[199,200]

## 8.3.2. Automated and unsupervised segmentation

### 8.3.2.1. Deep Learning

Deep learning, a subgroup of machine learning, is a complex multilayer neural network originally inspired by the structure of the human brain that learns by transforming the input (raw data) into different levels of abstractions.[42,44,45,201,202] It has been widely used in medical imaging, especially when a large amount of data needs to be analyzed and some studies have shown superior performance when it comes to lesion detection and classification compared to the methods conventionally used.[44,45] The deep learning network used most frequently when it comes to recognizing patterns in images are the convolutional neural networks (CNNs).[45]

### 8.3.2.2. Convolutional neural network (CNN)

A CNN consists of deep learning algorithm that learns automatically and adaptively how to extract relevant features by adjusting its input weights.[45,203] It is typically composed of different layers where “convolution” and “pooling” are two of the fundamental feature extraction components of the network, operated as a cascade.[203]

#### *8.3.2.2.1. Convolutional operation*

The convolutional operation is the process of feature extraction where a matrix is applied across an input to produce an output.[203,204] This matrix, or array of numbers, is called the kernel. In this process, the kernel is usually of equal and small size, the most used being a 3x3 kernel.[42] In this operation, the product of the multiplication of each element by the kernel is computed and the results are summed up at the end forming a new output (Figure 17).

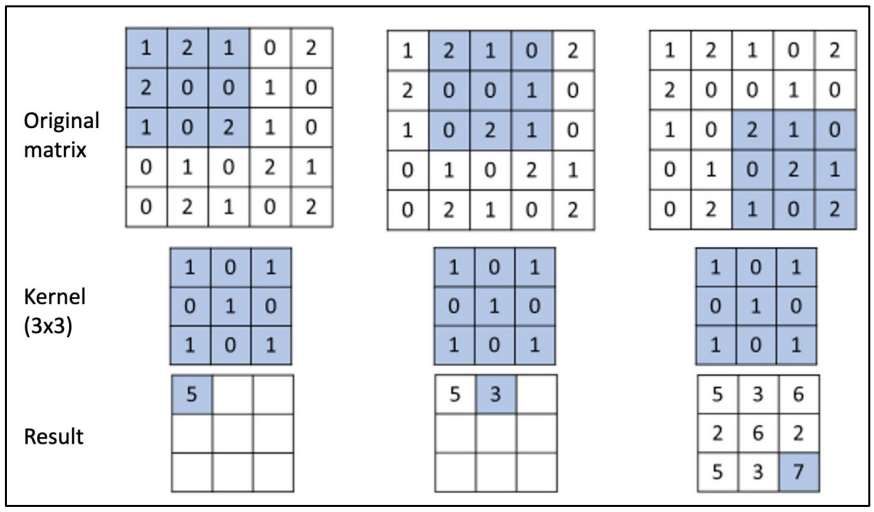


**Figure 17: Convolutional operation.**

Representation of a 3x3 convolutional operation where at each location, the original matrix (input) is multiplied by the kernel. (Adapted from Yamashita, et al. [203] 2018)

### 8.3.2.3. Pooling operation

The pooling operation consists of applying a function to summarize subregions of the output feature map with the purpose of reducing its size.[204] Different functions can be utilized, the most common being the max pooling (Figure 18) that extracts the maximum value of each patch.[203,204]

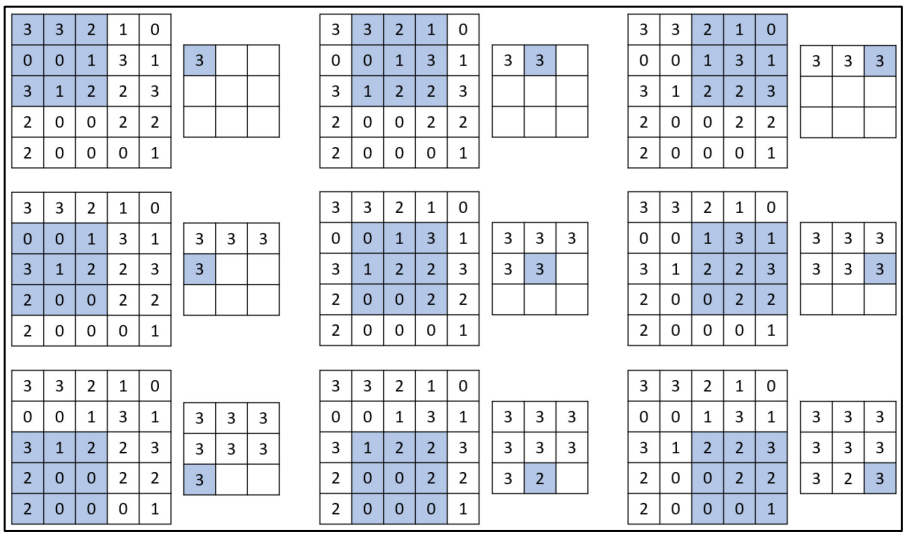

**Figure 18: Pooling operation**.

Representation of a 3x3 max pooling operation (Adapted from Dumoulin and Visin 2016)

#### *8.3.2.3.1. U-NET*

The U-Net is a deep learning training strategy of CNN specifically designed for images.[196,202,205] It utilizes data augmentation to improve efficiency and overcome the challenge of having little training data.[205] Data augmentation consists of modifying the training data through random transformations (flipping, cropping, rotating, etc.) so that instead of having the same exact input for all the training, the model has multiple modified inputs coming from one original input.[203]

The name comes from its U-shaped architecture (Figure 19) that can be divided into two symmetric paths. On the left, the contracting path uses alternating convolutional and pooling layers until further contraction is no longer possible. This is followed by the expansive path, on the right, where up-convolution and convolution are applied.[42,205]

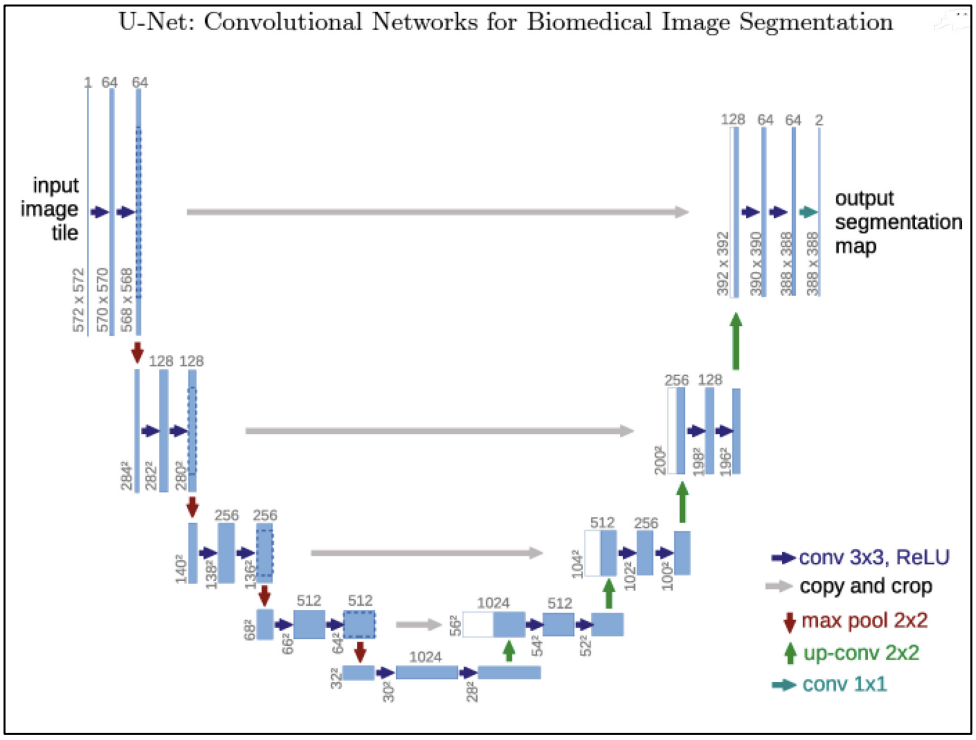


**Figure 19: U-NET.**

Illustration of the U-shape architecture of a U-Net.[205]

#### *8.3.2.3.2. Training a neural network*

Training a neural network means minimizing the distinction between the output predictions by the network and the ground truth (training dataset that has been segmented by an operator).[203] Forward propagation refers to the way the data moves in a neural network from the input layer to the output layer. The reverse route is called back propagation (Figure 20).[206]

To evaluate the quality of the training, a loss index is used to determine how well the model is performing by predicting the error between the prediction and the ground truth.[206] This will depend on the nature of the learning task and the desired behavior of the model. When the loss index is higher than desired, the weights and biases may be adjusted to create a new output (back propagation). This cycle is repeated until the loss index reaches an appropriate minimum value.[206]

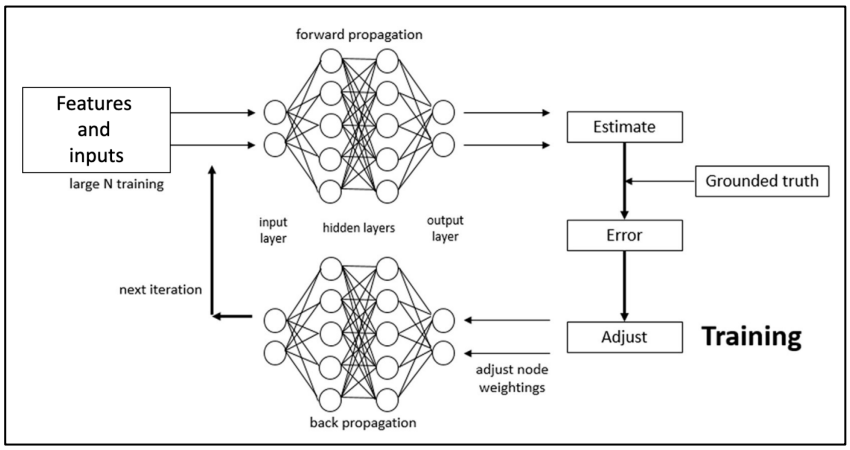


**Figure 20: Network training.**

Image illustrating a neural network training.[206]

In conclusion, deep learning serves as a potent mechanism for identifying patterns, facilitating rapid and meticulous analysis of extensive datasets. This technology in combination with image analysis represents a dynamic synergy that holds immense promise across various scientific disciplines. Furthermore, CNNs, a specialized artificial neural network crafted for image classification and pattern recognition, significantly enhance the precision, reliability, and efficiency of image categorization. The combination of deep learning and µCT imaging holds the promise of equipping us with an innovative tool to investigate the existing knowledge gaps in our comprehension of osteoclast bone resorption.

# Hypothesis and Objectives

Our study aims to evaluate µCT combined with deep learning-aided feature segmentation for detecting and quantifying bone resorption on bone slices *in vitro.* We hypothesize that this novel method will allow the characterization of equine osteoclast resorption on decellularized equine bone slices and the accurate measurement of the resorption volume and depth in a non-destructive manner.

Our first objective was to characterize bone resorption morphology in 3 dimensions (3D) on bone slices that were cultured as a substrate for equine osteoclasts employing µCT and compare findings with selected, site-matched, scanning electron microscopy (SEM) images. Our second objective was to develop an unsupervised method to measure equine osteoclast resorption volume on equine bone slices *in vitro* using a convolutional neural network. A third objective was to test the neural network developed in objective 2 for resorption volume measurement on archived specimens (equine bone slices with osteoclast resorption) and corresponding 2 dimensional (2D) images (standard toluidine blue stain bone resorption area measurements) and biomarker C-terminal telopeptide of type I collagen (CTX-I) in media from a prior *in vitro* study.[21]

# Chapter 2 – Article

**Characterization and quantification of *in-vitro* equine bone resorption in 3D using microcomputed tomography (µCT) and deep learning-aided feature segmentation.**

*Article to be submitted to the Journal of Orthopaedic Surgery and Research*

Grass D[1], Malek G[1], Taieb H[2], Ittah E[2], Richard H[1], Reznikov N[2], Laverty S[1].

[1]Comparative Orthopaedic Research Laboratory, Department of Clinical Sciences, Faculty of Veterinary Medicine, University of Montreal, 3200 Sicotte, St-Hyacinthe, QC, J2S 2M2, Canada

[2]Department of Bioengineering, Faculty of Engineering, McGill University, 3480 University Street, Montreal, Quebec H3A 0E9, Canada.

**Correspondence:** Sheila Laverty, MVB, DACVS, DECVS, FIOR, Department of Clinical Sciences, Faculty of Veterinary Medicine, University of Montreal, 3200 Sicotte, St-Hyacinthe, QC, J2S 2M2, Canada. Email: sheila.laverty@umontreal.ca

**Acknowledgements:** The authors are grateful to The Natural Sciences and Engineering Research Council of Canada (NSERC); the Quebec Cell, Tissue and Gene Therapy Network (ThéCell, a thematic network supported by the Fonds de recherche du Québec-Santé), and the FEMR - Facility for Electron microscopy research at McGill University where Scanning Electron Microscopy (SEM) was performed.

**Data availability statement:** The data that support the findings of this study are available from the corresponding author upon reasonable request.

**Ethical animal research:** The investigation was approved by the Animal Care and Use Committee of the Faculty of Veterinary Medicine of the University of Montreal (protocol #20-Rech-1968).

**ABSTRACT**

**Background:** High cyclic strains induce the formation of microcracks in bone, initiating a process of targeted remodeling, led by osteoclasts and followed by osteoblasts, aimed at repairing and preventing accumulation of damage. Racehorse bone is an ideal model for studying the effects of high-intensity loading, as it is subject to focal accumulation of microcracks and subsequent resorption within joints. Equine osteoclasts have rarely been investigated in *vitro*. The volume of osteoclast resorption is considered a direct parameter of osteoclast activity but indirect 2D methods of quantification of osteoclast resorption are used more often.

**Objectives:** To develop an accurate, high-throughput, deep learning-aided method to quantify equine osteoclast resorption volume in µCT 3D images.

**Methods:** Equine osteoclasts were cultured on equine bone slices, imaged with µCT pre- and post-culture. Volume, aspect ratio (shape factor) and maximum depth of each resorption event were measured in volumetric images of three bone slices. A convolutional neural network (U-Net-like) was then trained to identify resorption events on post-culture µCT images and then the network was applied to archival bone slices (n=21), for which the area of resorption in 2D, and the concentration of a resorption biomarker CTX-I were known. This unlocked the 3D information on resorption for samples where no pre-culture imaging was done.

**Results:** The modal volume, maximum depth, and aspect ratio of individual resorption events using pre- and post-culture µCT images were $2.7*10^3 \mu m^3$, 12 µm and 0.18 respectively. The mean resorption volume per archival bone slice was $34155.34*10^3 \mu m^3$. The CNN-labeled resorption volume correlated strongly with both CTX-I ($p < 0.001$) and area measurements ($p < 0.001$).

**Main limitations:** The neural network occasionally overestimated bone resorption volume, which required a manual touch-up.

**Conclusions:** This technique of deep learning-aided feature segmentation of µCT images of bone slices for quantifying equine osteoclast bone resorption volume allows for more accurate and extensive future investigations on osteoclast activity. For example, the antiresorptive effects of medications like corticosteroids and bisphosphonates can be investigated in the future.

## 1. Introduction

It is well known that the microarchitecture of healthy adult bones is continuously sculpted to adapt to biomechanical loads for optimal performance.[1] In cortical bone, this process is executed by coupled cellular remodeling by bone multicellular units (BMUs) .[2] This is led by osteoclasts, that initially resorb the bone and is followed by the deposition of new bone by osteoblasts.

Under high loads, microcracks in the bone stimulate a targeted remodeling response at the site to repair the focal injury and prevent its accumulation.[3,4] Osteoclast precursor recruitment from the local bone marrow and their differentiation into active bone-resorbing osteoclasts is mediated by mechanotransduction pathways including the disruption of the lacuno-canalicular network[5] and osteocyte apoptosis at the site of injury [6] leading to release of Receptor Activator of Nuclear Factor Kappa-B Ligand (RANKL). RANKL interacts with its receptor (RANK) on the surface of osteoclast precursors promoting differentiation, activation, and survival of osteoclasts.[7]

The racehorse's skeleton serves as an excellent natural model for the study of the effects of cyclic, high intensity loading on cortical and subchondral bone. During both training and racing there is a focal accumulation of microcracks in bone and calcified cartilage, associated with resorption at specific sites subjected to high loads, potentially leading to bone failure or complete fracture.[8,9,13,151,154,207,208] In addition, focal degenerative changes in the subchondral bone plate and overlying articular cartilage have been linked to osteoclast resorption at specific sites prone to fractures in the third carpal bones of racehorses.[9,16]

Despite playing an essential role in bone remodeling, equine osteoclasts have seldom been the subject of *in vitro* studies. They have been differentiated and cultured from post-mortem harvested femoral bone marrow hematopoietic stem cells[17-19] or, more recently, from sternal bone marrow aspirates in standing horses.[20,21] Furthermore, they have been cultured on their natural substrate — bone — in one report alone.[21] Species-specific *in vitro* studies are necessary to learn more about equine osteoclast function and activity and factors that influence it. For example, there is an unmet need to understand the effects of frequently employed medications such as intra-articular corticosteroids[177] or systemically administered bisphosphonates[176] on equine osteoclast activity to determine if they could have any detrimental effects on horse skeletal health. This is particularly important in respect to young equine athletes as it has been recently shown that osteoclasts are present in greater numbers in the subchondral bone plate in younger animals contributing to joint surface and epiphyseal maturation.[112]

Most *in vitro* studies of direct osteoclast resorption activity to date, in all species, measure the surface area of resorption or count pits on bone slices or other substrates that have been incubated with osteoclasts. Osteoclast resorption activity is usually extrapolated from two-dimensional (2D) resorption area measurements of toluidine blue stained bone slices on which osteoclasts have been cultured.[21-24,27,30-32,34,35,38,209-212] However, it has long been acknowledged that the precise quantification of bone resorption requires dependable three-dimensional (3D) measurement techniques for the assessment of volume and depth of resorption events.[38,213,214]

Scanning electron microscopy (SEM) stereophotogrammetry was the initial 3D method proposed to measure the depth and volume of individual osteoclast resorption cavities on dentine[88] and human cortical bone slices.[215,216] The use of confocal laser microscopy later provided topographic information on resorption events,[40,217] but had poor resolution compared with SEM[218] and was limited to a shallow depth of field (~100 µm maximum) .[219] Vertical scanning profilometry, on the other hand, advanced the methodology further by providing a direct measurement of the total eroded volume of entire dentine slices.[39] Drawbacks were that it required polished samples and exhibits high sensitivity to both the surface condition and reflectivity of the specimen. Serial milling 3D has also been employed for quantifying the volume of individual resorption cavities in cancellous bone specimens.[124,220,221] Nonetheless, it is destructive and labor-intensive requiring manual input from a user. Consequently, only a portion of the specimen is often examined. While the numerous reported techniques provided high-quality images, they often require sample preparation, involve a destructive methodology and are not widely available to users.[40]

High-resolution µCT has become increasingly accessible allowing the examination of bone microstructure non-destructively and with minimal preparation[9,151,207,222,223] providing multiplanar, cross-sectional and 3D images for analysis.[224]

Deep learning, a subfield of machine learning, is a powerful tool for detecting patterns,[201] which enables rapid and precise analysis of extensive datasets.[225] Convolutional neural networks (CNNs) are artificial neural networks designed to classify images and image patterns.[226] CNNs improve accuracy, reliability and throughput of image categorization[44,46,227] and have garnered considerable attention in the field of biological imaging, particularly in image segmentatio [228] and the analysis of volumetric data.[229] UNet, a key semantic segmentation approach, based on CNN,[46] effectively addresses the challenge of limited training data availability by applying data augmentation techniques.[205] UNet has been widely used as a

valuable tool for extracting interpretable results in various mineralized tissue segmentation tasks using CT scans[41] and µCT.[42,43]

Our study aims to evaluate µCT combined with deep learning-aided feature segmentation for detecting and quantifying bone resorption on bone slices *in vitro.* We hypothesize that this method will allow the characterization of equine osteoclast resorption on decellularized equine bone slices and the accurate measurement of the resorption volume and depth in a non-destructive manner.

Our first objective was to characterize bone resorption morphology in 3D on bone slices that were cultured as a substrate for equine osteoclasts employing µCT and compare findings with selected, site-matched, SEM images. Our second objective was to train a neural network to measure equine osteoclast resorption volume on equine bone slices *in vitro.* A third objective was to test the neural network developed in objective 2 for resorption volume measurement on archived specimens (equine bone slices with osteoclast resorption) and corresponding 2D images (standard toluidine blue stain bone resorption area measurements) and a bone resorption biomarker C-terminal telopeptide of type I collagen (CTX-I) in media from a prior *in vitro* study.[21]

## 2. Materials and methods

### *2.1 Materials*

Gibco minimum essential medium (αMEM) was purchased from Life Technologies (Carlsbad CA, USA). Penicillin and streptomycin were procured from Gibco Life Technologies (Grand Island, NY, USA). Fetal bovine serum was acquired from Wisent (St-Bruno, CA, USA). Macrophage-colony stimulating factor (M-CSF, 25 ng/mL) was obtained from Peprotech Inc. (NJ, USA) and receptor activator of nuclear factor kappa B ligand (RANKL, 50 ng/mL) from Enzo Life sciences Inc. (Farmingdale, NY, USA). The cryotubes (Cryofreeze® Cryogenic Storage Tubes) were purchased at UltiDent Scientific (St-Laurent, CA, USA). The wells (Nunc® Lab-Tek® II Chamber Slides™; 8 wells (0.7 76 $cm^2$/well), at glass slide) were procured from Thermo Fisher Scientific Inc. (Rochester, NY, USA). The 1.5 mL tubes (Simport Graduated Microtubes with O-Ring Caps) were purchased at UltiDent Scientific (St-Laurent, CA, USA). The monobasic sodium phosphate, toluidine blue (Biopharm, 0.1% in 0.02 M/L monobasic sodium phosphate), red blood cell lysis buffer, dimethylsulfoxide and the Mr. Frosty freezing container (cooling rate of 1°C/min; Nalgene) were all purchased at Sigma–Aldrich (St. Louis, MO, USA). The ELISA immunoassay for CTX-I was obtained from Immunodiagnostic Systems Holdings PLC (IDS).

### *2.2 Methods*

#### *2.2.1 Equine hematopoietic stem cell bank*

The procedure was approved by the Animal Care and Use Committee of the Faculty of Veterinary Medicine of the University of Montreal (protocol #20-Rech-1968). Hematopoietic stem cells were isolated from aspirates of sternal bone marrow harvested from sedated, standing adult horses as described previously (Figure 1).[21] The cells were stored in cryotubes at a concentration of $5.10^6$cells/mL in vapour phase liquid nitrogen in a bank for future investigations.

#### *2.2.2 Equine decellularized bone slices*

Bone slices were prepared from a young horse euthanized at the Faculty of Veterinary Medicine of the University of Montreal for unrelated reasons. Bone slices (4 x 3 x 0.3mm) were cut with a low-speed diamond saw (Isomet Buehler, Lake Bluff, IL, USA) from the distal third of the dorsal metacarpal bone cortex (Figure 2). The slices were washed with 70% ethanol for 12 min and then with PBS for 5 min three times. Bone slices were stored at -20°C in 1.5 mL tubes until cell culture experiments.

### *2.3 Experiment 1: Characterization of equine osteoclast resorption on decellularized equine bone slices in 3D using µCT imaging and deep learning-aided feature segmentation.*

#### *2.3.1 Osteoclast differentiation from hematopoietic stem cells and cell culture experiment with bone slices*

Stored bone slices were thawed and imaged with µCT, prior to cell culture experiments to generate a pre-culture (pre-C) image for the image registration step (section 2.3.3). The bone slices were then washed with 70% ethanol for 12 min followed by PBS for 3.5 min three times in total. One bone slice was added to each well.

Frozen hematopoietic stem cells were selected from the stem cell bank (n=3 donors) and thawed.[21] Culture chambers were first incubated with cell culture medium (supplemented with 10% fetal bocine serum and 1% penicillin-streptomycin) with 5% $CO_2$ at 37°C for a minimum of 1 h. Viable hematopoietic stem cells were then plated at a concentration of $1.10^6$ cells/$cm^2$ in the wells with bone slices and supplemented with M-CSF (50 ng/mL) and RANKL (50 ng/mL).

The cell culture medium was changed the following day (d1), 300µL at 37°C supplemented with M-CSF (50 ng/mL) and RANKL (50 ng/mL), and then every 3 days. On d13, the $CO_2$ level was raised from 5 to 10%

until d21.[27] At the end of the experimental period, the bone slices were collected and stored at -20°C in 1.5 mL tubes until further analysis.

### *2.3.2* µCT *imaging of bone slices*

Images of each bone slice were acquired pre-C and post-culture (post-C) with a XTek HMXST 225 (Nikon, location) at 80kV and with a voxel size of 3µm. All reconstructed µCT scans were then uploaded into Dragonfly 2022-2 software (Object Research System, Montreal, Quebec, Canada) for image processing.

### *2.3.3 Image registration*

Image registration was performed to align the pre-C and post-C scans of the same sample. Pre-C was the fixed image and image registration was done first manually and later refined with the featured-based registration tool.

### *2.2.4 Selection of bone slice surface for analysis*

Retrospective analysis of prior toluidine blue stain bone slice resorption areas from a previous investigation[21] in the laboratory revealed that one side of the bone slice was always substantially more resorbed than the other (Supplementary figure 1). Consequently, for the purposes of this investigation, only the bone slice surface with the most resorption was included for the µCT analysis.

### *2.3.5 Deep learning feature-aided segmentation to separate bone from background.*

A UNet model (depth level: 5; initial filter count: 64) was created using the deep learning segmentation tool available in Dragonfly. The segmentation was binary, with one label being assigned to bone and the remaining to background. The training was performed with two different inputs (pre-C and post-C scans) and their respective binary segmentation (output) in a cascade manner, a technique where the corrected output from one training bout is then used as input for the next step, gradually increasing the amount of training data and refining the neural network's predictions as it goes. The training parameters were the following: patch size was 64, stride-to-input ratio was 1.0, batch size was 32, and the number of epochs was 100.

The same trained neural network was applied to all 3D images, except for one post-C scan for which the Unet model was not sufficiently accurate. A new neural network was trained for that specific bone slice using the same parameters.

### *2.3.6 Image segmentation and denoising*

Following the deep learning-based binary segmentation of bone and background, for each bone slice, pre-C and post-C bone slice images were exported as a region of interest (ROI). The post-C bone ROI was then subtracted from the pre-C bone ROI thereby yielding the total bone resorption volume for each bone slice. The most resorbed surface of one bone slice per donor (n=3) was selected for further analysis. A 6-connected multi-ROI was created (bone resorption multi-ROI). All the labeled voxels that were connected to one of the faces of the neighbor cube (voxel) were considered as part of the same resorption event. For denoising, a minimum volume threshold was conservatively chosen based on previously reported diameter and depth of individual resorption pits when human osteoclasts were cultured on bone slices[30]. The smallest pit was considered to have a hemisphere shape with a 10 µm diameter and 5 µm depth. The volume was calculated by the mathematical formula of hemisphere volume ($\frac{2}{3} \times \pi \times r^3 = \frac{2}{3} \times 3.14 \times 10\ \mu m^3 = 258\ \mu m^3 = 86\ voxel$)[230] and anything with a volume equal or smaller to 258 $\mu m^3$ (86 voxels) was excluded from the bone resorption multi-ROI. Denoising was refined manually for every 2D cross-section.

### *2.3.7 Image analysis: Bone slice resorption volume, aspect ratio and maximum depth*

Each 6-connected ROI was considered as one individual resorption event for the purposes of analysis. The object analysis tool (Dragonfly) was used to characterize the osteoclast resorption events by measuring their volume (µm$^3$) and aspect ratio (0-1). Aspect ratio is the ratio between the height and the width and is used to estimate morphology. An aspect ratio close to 1 will have a rounder shape and closer to 0 an elongated morphology.

Each 3D resorption event (6-connected bone resorption multi-ROI) was isolated using an in-house written code in Matlab (R2022b, v9.13) and the maximum depth of resorption measured on the 2D cross-sectional image. Maximum depth used for analysis was defined as the distance (µm) between the top-most and the bottom-most labeled voxel in a resorption.

### *2.3.8 SEM imaging of bone slices for site-matched comparison*

SEM was performed on the same subset of bone slices (n=3) to compare with the images generated by µCT. The bone slices were washed with 70% ethanol for 30 seconds and then rinsed with PBS three times to remove any possible accumulated debris. Samples were mounted on standard SEM metallic stubs with conductive carbon adhesive and imaged uncoated with a FEI Quanta 450 FEG in high vacuum at 1.5kV

using a standard secondary electron detector at a working distance of 9.3 mm. The site-matched µCT and SEM images were then compared.

### *2.3.9 Area measurements of osteoclast bone slice resorption*

The canonical method for area of bone resorbed by osteoclasts on bone slices in 2D with toluidine blue staining was performed to compare with the µCT volume assessment. Toluidine blue stained images of bone slices were generated as described previously.[21] The slices were digitalized using an optical light microscope (Leica DM4000B Leica Microsystems Inc.) equipped with a camera (Prosilica GT1920C Allied Vision Technologies) and Panoptic software (Meyer Instruments Inc.) at magnification: 10×. The osteoclast resorption patterns were then compared with both µCT and SEM.

## *2.4 Experiment 2: Development and validation of a neural network to measure volume of equine osteoclastic resorption on bone slices in vitro.*

### *2.4.1 Archival specimens and biomarkers*

Archived bone slices (n= 24) from a repository, generated in a prior investigation of equine osteoclastic bone resorption, were available for study.[21] The differentiation of the hematopoietic stem cells on bone slices to osteoclasts was identical to experiment 1 described herein. However, in addition, on d19 the cell culture wells were subjected to inflammatory stimuli (1 or 10 ng/mL of IL-1β or 1000 ng/mL of LPS) for 72 h (n=6 wells for each condition, with M-CSF) and the cell culture was terminated on d22. Cell culture medium for the osteoclast biomarker (CTX-I) assays were collected at d22, at the end of the study. CTX-I ELISA concentrations were immunoassayed on d22 in the harvested cell culture supernatants employing the CrossLaps® for cell culture as previously described.[21] As the results of the investigation revealed no effects of the inflammatory stimuli on the parameters assessed, all the specimens and data (toluidine blue area of resorption and CTX-I) at the end of the experiment were retrieved and combined for comparison and analysis with the current model. Each bone slice had a corresponding measure of resorption area calculated following toluidine blue staining and media levels of the biomarker CTX-I for comparison. Three bone slices were not included in the analyses: one due to breakage and the other two because their CTX-I results exhibited unacceptably high intra-assay coefficients of variation (equal to or greater than 20.0%).

### *2.4.2 µCT imaging of bone slices and deep learning-based segmentation*

µCT projection images of each bone slice were acquired under the same parameters outlined in section 2.3.2. Only post-C specimens were available. A neural network was created using the segmentation wizard

tool in Dragonfly ORS software which allows visual comparison of multiple loss functions and different sets of hyperparameters during validation. The training data were zoomed 2D cross-sectional images of one post-C bone slice (Figure 1- study design). Each image was separated into 4 ROIs (bone, background, bone resorption and vessels). A pre-trained Unet-like neural network with depth level of 4 layers was used for training (Sensor3D pre-trained on ORS500Kv01). The training parameters were the following: patch size was 64, stride-to-input ratio was 0.25, batch size was 64, and the number of epochs was 100. A validation loss function as well as visual inspection was utilized to assess the performance of the segmentation model.

#### *2.4.3 Image segmentation and denoising*

Following deep learning-based segmentation of each bone slice, the bone resorption ROI corresponded to the total volume of resorption was extracted. To avoid resorption overestimation, each specimen was divided into 4 bounding boxes where each box was placed the closest to the resorption surface as possible and the bone resorption ROI was cropped (Supplementary image 2). The results from the 4 bounding boxes were then summed to provide the total bone slice resorption volume. A 6-connected multi-ROI was then created. The same minimum volume threshold as experiment 1 was used (86 voxels) and excluded from the bone resorption multi-ROI.

### 3 Statistical analyses

In experiment 1 as the data was heavily skewed, it was elected to present the mean (± SD), median (25th percentile; 75th percentile) and mode values in the tables to allow meaningful comparisons with prior data reported by other researchers. Statistical significance was determined when the p-value was less than 0.05.

In experiment 2 a mixed linear model was used to assess first whether the inflammatory stimuli influenced the osteoclastic resorption volume. As no significant differences were detected, all sample data were combined. A spearman test correlation was then employed to interrogate the association between equine osteoclastic resorption volume and the release of CTX-I biomarker and area of bone resorption on bone slices. Data was recorded in Microsoft Excel® and analyzed using statistical software (R v. 4.0.3). Statistical significance was determined when the p-value was less than 0.05.

## *4. Results*

### *4.1 Experiment 1: Imaging of equine osteoclast resorption on bone slices using µCT; 3D reconstructions and cross-sectional images.*

A total of 9 bone slices were imaged pre-C and post-C. The pre-C 3D reconstructions of the unresorbed bone slices provided topographical information of both surfaces. The flat unresorbed bone slice surfaces were visibly interrupted by haversian canals, osteons, and vascular canals (Figure 3).

µCT cross-sectional images obtained of the pre-C bone slices revealed a smooth, straight unresorbed surfaces, on each side of the bone slice, traversed by occasional blood vessels (figure3).

Following the 21-day osteoclast culture period, 3D µCT reconstructions of the same bone slice illustrated a topographic map featuring osteoclast bone resorption (Figure 3). Three distinct resorption patterns were observed: round "pit-like", elongated "trench-like", and "resorption events" (Figure 4) that exhibited a wide range of shapes with varying depths and concave bottom surfaces, likely reflecting a mixture of both pit-like and trench-like characteristics. These formations collectively formed a topographical image similar to that of river valleys (Figure 3). µCT cross-sectional images obtained of the post-C bone slices facilitated the clear observation of distinct valleys varying in depth, which corresponded to different resorption events (Figure 3).

The patterns of resorption observed on the site-matched toluidine blue stained surfaces of the bone slices and those observed on the SEM images corresponded well with those observed in the µCT 3D reconstructions (Figure 5).

One specimen was excluded from subsequent measurements because atypical sandpit-like shaped depressions were observed in the post-C imaging 3D reconstructions when compared with images of all other surfaces. (Figure 6). SEM imaging was also subsequently performed on this specimen. The deep aspect of the depressed regions had a different roughness when compared with the resorption cavities on the other specimens suggesting that these represented atypical resorption or potential artefacts rather than another type of resorption cavity.

### *4.2 Bone slice resorption volume, aspect ratio, and maximum depth calculated from µCT cross-sectional images.*

µCT 3D images of the bone slice surfaces from 3 specimens (A, B and C) with mild to severe resorption were then selected for additional measurements to further characterize the type of resorption observed.

The number of resorption events identified and available for further analysis in specimens A, B, and C was 12, 106, and 306 respectively. The volume, maximum depth, and aspect ratio of each osteoclast resorption event was then measured (Figure 4). When the individual resorption cavities were quantified, the distribution of the data was highly skewed. The osteoclast individual resorption event volume, aspect ratio and maximum depth are provided in table 1.

### *4.3 Experiment 2: Automated deep learning-aided feature segmentation to measure equine osteoclastic resorption volume.*

Archival data (µCT images, resorption biomarker in media CTX-I, and area of resorption) were retrieved from a previous study [21] to test the neural network for measurement of resorption volume on post-C bone slice µCT images. A total of 21 bone slice surfaces were included.

In this experiment the trained neural network permitted the 3D visualization of resorption events (Figure 7) as well as volume measurement using only post-C slices in an unbiased way and with a notably reduced amount of manual segmentation required when compared with experiment 1. The deep learning-based segmentation model performed well for the majority of bone slices; however, it was observed that in bone slices with less resorption, the model tended to falsely label some regions as false-positive for resorption. Although overestimation of resorption was a challenge due to the microscopically uneven surfaces of the bone slices created by the diamond bone saw, this was successfully corrected by using cropping boxes (section 2.4.3) (Supplementary figure 2)**.** The loss of the trained neural network, which is used to measure how well the model's predicted output matches the expert-generated output, was 0.02. The segmentation performance was further confirmed by an experienced user (DMG).

The mean (± SD), median (25th percentile; 75th percentile) and minimum-maximum of total volume of resorption, total area of resorption and CTX-I are summarized in table 2. For each bone slice, individual resorption events volume and aspect ratio were also calculated utilizing 6-connected multi-ROI (Figure 7).

### *4.4 Association of the neural network volumetric measurement with biomarker (CTX-I) levels and classical area measurement of resorption*

The CTX-I concentrations in the cell culture experiment media and the area measurements calculated on toluidine blue stained sections from the archived data were retrieved[21].

The statistical interrogation of the associations between the measurements revealed a strong positive strong correlation ($r=0.79$; $p<0.0001$) between automated model volume percentage of resorption per

bone slice and the CTX-I biomarker of resorption levels in the cell culture experiment media at the end of the experiment (figure 8). A strong positive correlation (r=0.95p <0.0001) was also found between the classical area measured on toluidine blue stained bone surfaces of the slices and the volume of osteoclastic resorption calculated by the automated model (figure 8).

**5. Discussion**

This study presents novel tools for enhancing osteoclast research. An accurate technique for the 3D characterization and direct volumetric measurement of discrete osteoclast resorption events on bone slices, integrating µCT imaging and deep learning-aided feature segmentation, has been implemented. In addition, an automated CNN (UNet-like) was also trained for accurate measurement of resorption volumes on bone slices incubated with osteoclasts thereby reducing the need for manual segmentation. The total volumes of resorption measured correlated strongly with the biomarker of bone resorption (CTX-I) concentrations in the culture media of the samples and also the canonical toluidine blue stained resorption area measurements from the same bone slices, underpinning its accuracy. This reported procedure can be useful for more objective future studies of osteoclastic resorption.

Osteoclast activity is often investigated *in vitro* by incubation on their natural substrates, either bone or dentine, to mimic best the *in vivo* environment. The most accessible and frequent metric of their *in vitro* activity, in the past, was the area of toluidine blue stained resorption of bone slices at the end of the osteoclast culture period. However, it has been known for some time that the measurement of the volume of resorption on bone slices is a more accurate parameter of osteoclast activity.[38]

The *in vivo* active phase of osteoclast-mediated bone resorption lasts approximately for a period of 2-3 weeks[2,64,231-233] and is influenced by a variety of factors that include age, mechanical forces, genetics, hormones, inflammation and medication.[64] The *in vitro* culture of equine osteoclasts on bone, conducted for a duration of 3 weeks in the current study, replicates the timeframe observed during natural resorption processes.

Assessing the depth of bone resorption by osteoclasts *in vitro* provides insight into the activity of osteoclasts beyond their basic adherence and spreading behavior.[38] This measurement could potentially play an important role in evaluating the efficacy of therapies targeting osteoclasts and investigating the mechanisms involved in bone remodeling processes as it has been shown that different resorption behaviors are linked to different resorption depth.[30] Resorption cavity depths have been measured using SEM stereophotogrammetry and mean (± SD) maximum depth values varying from 1.96 (± 0.12) to 2.5µm

(± 0.18) were found when chick osteoclasts were grown on dentine slices for 24 hours.[234] Additionally, when murine osteoclasts were cultured on bovine bone for a longer period of 14 days, a similar median (25th percentile; 75th percentile) maximum resorption depth of 1.4µm (1.0; 2.0) was measured applying the same technique.[235] In contrast, vertical scanning profilometry, that allows an assessment of a 3D surface profile of a substrate, detected greater mean resorption depths of 29.7µm (± 4.3) when human osteoclasts were cultured on dentine slices but for longer periods of 21 days.[236] For comparative purposes, the mean maximum depth measured in this study using µCT was 19µm (± 19.59), which aligns with the findings of the previous investigation conducted by Mabilleau, et al. (2012). However, considering the skewed distribution of the data, the median (12µm) and mode values (12µm) were deemed a more accurate depiction of the overall dataset. The apparent discrepancy in the parameter measurements among the aforementioned reports may be explained by variations in culture periods, species, and the substrates investigated.

In order to assess the resemblance of these *in vitro* events to real-life resorption, it is valuable to compare the depth values with those derived from *ex vivo* specimens. Fluorescence-based serial milling of vertebral cancellous bone specimens from healthy elderly humans revealed median maximum resorption depths of 26.3µm and a range of 4.9 to 116.7 µm,[220] a strikingly similar range to the current study (3 – 117µm), underpinning that the *in vitro* model replicates *in vivo* resorption events and measurement techniques. Furthermore, the mean maximum resorption depth of 14.8µm (± 2.56) previously measured in rat vertebrae[237] using the same techniques was similar to the median (12µm) and mode (12µm) recorded in the current study.

While depth measurements are informative of the type of osteoclast activity, the measurement of the resorption volume is the ideal measure of osteoclast activity on bone slices *in vitro* for comparative studies. Although the volume of discrete resorption events on bone or dentine slices has been illustrated in the past by stereophotogrammetric SEM[234,238] and confocal microscopy,[217,239] there is sparse information in the scientific literature on their actual measured volumes. Mean volumes varying from 0.98 up to 4.59 $*10^3 µm^3$ were measured using stereophotogrammetric SEM for osteoclasts from a variety species (rat, chick, and rabbit) grown on dentine slices for 24h.[123] Although a mean resorption event volume of $2.45*10^3 µm^3$ was later measured utilizing confocal microscopy when chick osteoclasts were cultured on dentine slices for 24h,[240] the median volume was lower ($0.85*10^3 µm^3$) when they were cultured on equine metacarpal bone slices for 20h.[107] The mean volume of individual resorption events of human osteoclasts cultured on dentine slices for 21 days was much greater ($57.3 ± 15.6 *10^3 µm^3$) when

measured with vertical scanning profilometry.[236] Despite the fact that the current investigation allowed the measurement of similar mean resorption events volumes (105.55 ± 612.88 *$10^3$µm) to the latter, because of the skewed nature of the data, the median (25th percentile; 75th percentile) value 6.86*$10^3$µm (3.47; 25.28) was again considered to reflect the overall data better. The mean resorption volume (614.16 ± 311.93 *$10^3$µ$m^3$) of natural resorption cavities in cancellous bone from elderly human vertebrae using fluorescence-based serial milling[220] was higher than that measured in the current study (105.55 ± 612.88 *$10^3$µm). On the other hand, the mean resorption cavity volume measured in rat vertebral cancellous bone was 36.50 ± 5. 35 *$10^3$µ$m^3$ using the same technique[237] and closer to that was measured herein.

The measurement of the total volume of resorption of the complete surface of the bone slice is an additional parameter to consider when comparing factors influencing osteoclast activity *in vitro*. However, only a limited number of studies have been able to successfully incorporate this parameter. The bone slices in the present study were approximately uniform in size, but there was variation in mean total volume of resorption per bone slice (34,155.31 ± 23,407.80 *103µm3) indicating a high level of heterogeneity and sensitivity in the resorption experiments.

Previous *in vitro* techniques for measuring the depth and volume of resorption on bone slices have several limitations, such as the requirement for sample preparation, sophisticated equipment, and a researcher's expertise. Additionally, when measuring depth, some of the techniques failed to consider the morphology of the resorption cavities in directions other than the observed plane.[220] This reported approach using µCT imaging of bone slices and deep learning-aided feature segmentation in the current study overcame these limitations. Our method involved minimal sample preparation and generated multiple cross-sectional images that facilitated the visualization and precise measurement of resorption depth and volume using an automated technique and is a user-friendly alternative for measuring the maximum depth of the entire bone slice sample.

In addition to the depth and volume of osteoclast resorption on bone slices, the assessment of the shape and form of the cavities they sculpt in the bone substrate can provide information as to the state of their activity. Recent investigations characterized osteoclast resorption cavity morphology on bone slices[30,34,82] and *ex vivo*[30] by classifying them as being of two distinct types, either "pits" or "trenches", using time-lapse recording in combination with confocal microscopy,[34,82] and SEM.[30] The pit mode are rounded-shaped resorptions characterized by short-term active bone breakdown interrupted by migration periods. The trench mode on the other hand reflects a more aggressive form of resorption combined with osteoclast migration, being deeper,[30] longer, and faster.[82] In the present investigation, although both pits

and trenches were observed, the majority of resorption events could not be easily classified into these 2 discrete categories but were rather combinations of both. This finding also aligns with the observations of Hefti, et al. (2010) when mouse osteoclasts were cultured on bovine bone slices for 14 days and imaged with SEM. In their study, the three different types of resorptions, similar to described here were also observed namely resorption pits, trails and dense areas of resorption where no distinction of pattern was possible. Notably, in their analysis, they also chose to exclude densely resorbed areas from their observations. Herein, it is proposed that resorption cavities should be classified along a spectrum of shapes that more accurately reflect osteoclast activity. It is also possible that different osteoclasts may have resorbed the same region, because of the length of the culture period leading to the creation of pits within trenches and vice versa. Consequently, the term "resorption events" is utilized here rather than "cavities".

The neural network trained in the second arm of the study, provided a practical, user-friendly alternative for calculating resorption volume on bone slices as only post-culture slices were imaged and the amount of manual segmentation required was greatly reduced. The UNet-like CNN, Sensor3D, was initially described for organ segmentation on CT scans.[241] Unlike previous approaches that processed complete sets of tomographic images, it operates on individual slices and considers as few as three sequential image slices, capturing inter-slice dependencies and learning the spatial and temporal relationships between them.[241]

During the process of bone degradation, osteoclastic enzymes, including cathepsin K, digest type I collagen in the bone matrix, causing the release of bone resorption products into the bloodstream including CTX-I, a well-established biomarker of bone resorption.[71,72,115,116] The neural network volume of resorption correlated strongly with the levels of the CTX-I biomarker measured in the media, harvested from the osteoclast on bone cultures, confirming that this new method is accurately measuring resorption.

Although toluidine blue staining of resorption on bone slices post-culture is widely used to assess osteoclast activity, it only captures surface resorption in 2D. The area of resorption measured may be misleading[121] as it may also reflect osteoclast spreading and attachment[38-40] rather than actual resorptive activity. For example, an increased area of resorption, if in combination with decreased cavity depth, does not necessarily mean increased resorptive activity.[38,40,122] Additionally, manual segmentation of area is considered to be time-consuming and prone to bias due to inter-user variations.[196] Therefore, when analyzing bone resorption, it is ideal to consider all three factors: area, depth, and volume[40] that are described in the study herein. The neural network volume measurements of resorption on the bone slices

correlated with the prior canonical area measurements, made with light microscopy on toluidine blue stained bone slices supporting the validity of the 3D measurements. However, the approach is faster and eliminates the labor-intensive aspects associated with manual segmentation enabling a more comprehensive examination of the entire specimen and ensuring a more thorough analysis.

It is acknowledged that this study has several limitations. First, we used a cubic voxel size of 3µm. Previous research by Tkachencko, et al. (2009) reported that images with voxel sizes exceeding 1.4 µm could potentially introduce errors in the detection of smaller resorption cavities in *ex vivo* bone specimens. At the same time, Tkachencko, et al. (2009), employed voxels with an aspect ratio not equal in all dimensions. By using cubic voxels in the current investigation, it allowed reliable detection of resorption cavities at a lower resolution and in cortical bone. Our findings indicate that resorption cavities were clearly visible in the images with a resolution of 3µm cubic voxel. However, it remains plausible that extremely small pits may have gone undetected. An additional potential limitation is that bone slices have physiological structural variations due to the presence of vascular channels and pores. While these variations present a challenge in distinguishing them from resorption cavities during image analysis, the utilization of deep learning enabled the detection and exclusion of these sites from the measurements.

**6. Conclusion**

Deep learning-aided feature segmentation of µCT images of bone slices, following culture with osteoclasts, allows exquisite characterization of osteoclast resorption and accurate measurement of total volume of resorption. For example, we show that thousands of osteoclastic resorption events analyzed here span a broad spectrum of morphologies, rather than fit into two distinct categories. This investigation establishes a foundation for future investigations into equine osteoclast activity and the effects of medications osteoclastic resorption *in vitro*. The accurate measurement of resorption volume may also allow the development of novel species- specific biomarkers of bone resorption.

**7. Tables**

**Table 1. Volume, maximum depth, and aspect ratio of individual resorption events for all bone surfaces from experiment 1 (n=424).**

| | Volume (*$10^3$µm$^3$) | Maximum depth (µm) | Aspect ratio |
|---|---|---|---|
| **Median (25$^{th}$percentile;75$^{th}$ percentile)** | 6.86 (3.47; 25.28) | 12 (6; 21.75) | 0.25 (0.18; 0.35) |
| **Mean (± SD)** | 105.55 (±612.88) | 19.07 (±19.59) | 0.27 (±0.13) |
| **Range** | 2.35 – 9,196.31 | 3 - 117 | 0 – 0.74 |
| **Mode** | *2.7* | *12* | *0.18* |

**Table 2: Volume measured by CNN (Unet-like) model and corresponding archival total area of resorption and CTX-I data.**

| Specimen | Total volume (*$10^3$µm$^3$) | Total area (mm$^2$) * | CTX-I (nM) * |
|---|---|---|---|
| **1** | 16,307.38 | 2.59 | 26 |
| **2** | 7,419.71 | 1.40 | 16.23 |
| **3** | 33,141.74 | 7.49 | 27.29 |
| **4** | 40,461.96 | 5.51 | 25.87 |
| **5** | 2,624.62 | 0.71 | 15.18 |
| **6** | 24,333.45 | 3.21 | 25.38 |
| **7** | 104.19 | 0.30 | 6.43 |
| **8** | 15,200.70 | 2.48 | 14.35 |
| **9** | 1,161.54 | 0.22 | 2.46 |
| **10** | 27,626.02 | 4.86 | 13.01 |
| **11** | 61,428.78 | 9.78 | 43.47 |
| **12** | 18,815.92 | 3.23 | 15.65 |
| **13** | 36,635.49 | 6.88 | 26.57 |
| **14** | 25,999.70 | 4.38 | 10.56 |
| **15** | 34,442.01 | 7.71 | 31.71 |
| **16** | 59,727.11 | 8.47 | 63.81 |
| **17** | 66,978.60 | 9.03 | 32.7 |
| **18** | 48,786.71 | 5.35 | 19.52 |
| **19** | 57,360.10 | 7.87 | 23.39 |
| **20** | 77,423.66 | 7.75 | 28.88 |
| **21** | 61,282.14 | 9.48 | 46.16 |
| **Mean (± SD)** | 34,155.31 (± 23,407.80) | 5.18 (± 3.15) | 24.43 (± 14.56) |
| **Median ($25^{th}$percentile;$75^{th}$ percentile)** | 33,141.74 (16,307.38; 57,360.10) | 5.35 (2.59; 7.75) | 24.39 (15.18; 28.88) |
| **Min-Max** | 104.19 – 77,423.66 | 0.22-9.78 | 2.46 – 63.81 |

*Results reported as part of a previous investigation.[21]

## 8.Figures

**Figure 1: Study design illustrating culture and imaging methods for the µ*CT* characterization and quantification of equine osteoclast resorption on equine bone slices.**

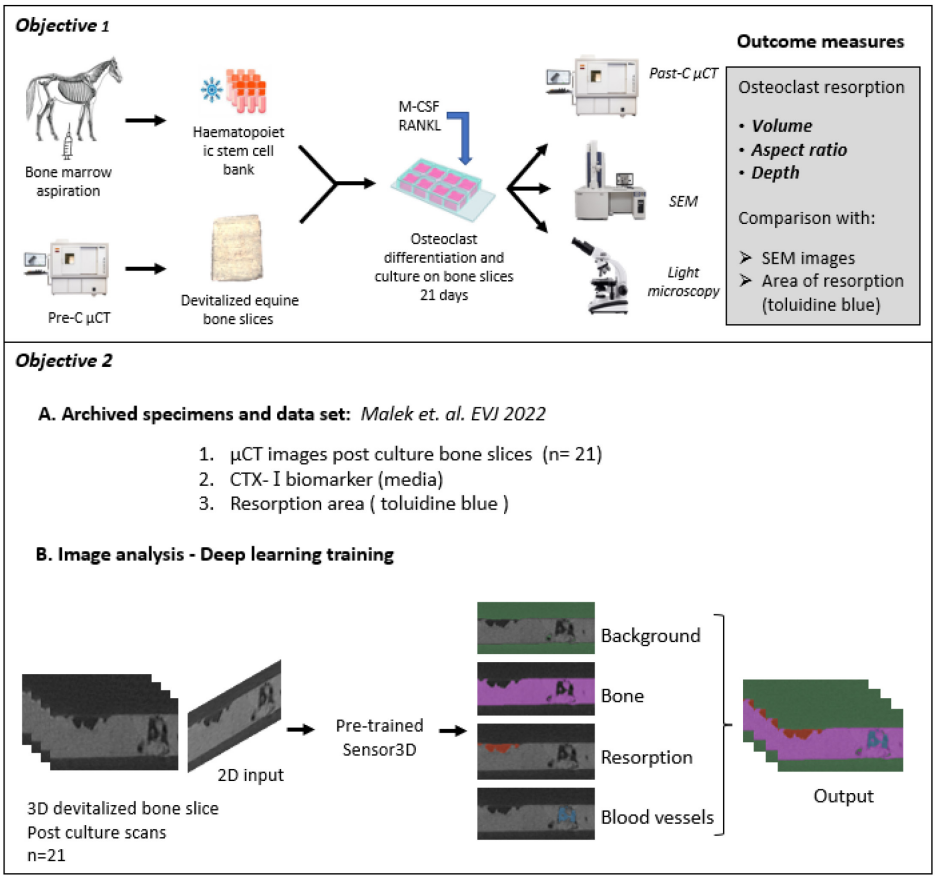


***Experiment 1: Characterization of equine osteoclast resorption on decellularized equine bone slices in 3D employing µ-CT and deep learning-aided feature segmentation.*** Osteoclasts were differentiated from stored hematopoietic stem cells derived from bone marrow aspirates of 3 donors and cultured with bone slices. The bone slices underwent µCT imaging pre and post culture. Site matched SEM images were obtained from selected specimens for comparative purposes. In addition, the bone slices were stained with toluidine blue to reveal resorption area and patterns for comparison. ***Experiment 2: Development and validation of neural network to measure volume of equine osteoclastic resorption on bone slices in vitro.*** (A)Archived data from a previous study was employed (Malek et. al. 2022) for volume quantification with a deep learning model. The most resorbed surfaces from each donor were selected for further imaging processing (n=21). (B) Deep learning model training for volume quantification. Training segmentation was performed with the segmentation wizard tool in Dragonfly ORS software (version 2022.2). The training data were zoomed 2D images of one post-C bone slices. Each 2D was separated into 4 ROIs (bone, background, bone resorption and vessels). A pre-trained Unet-like with depth level of 4 layers was used for training (Sensor3D pre-trained on ORS500Kv01).

**Figure 2: Equine decellularized bone slices.**

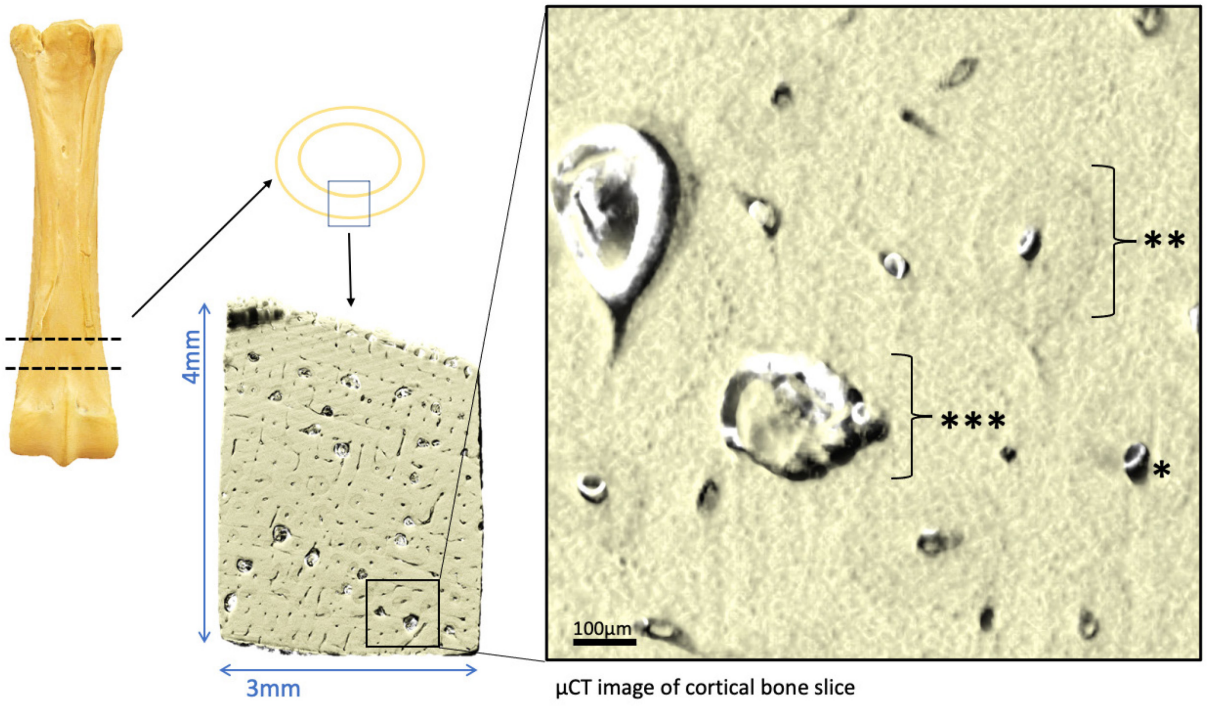


Cortical bone slices were obtained from the distal third metacarpal bone cortex from a young horse at postmortem. Magnification of µCT image (rectangle) shows details of the normal anatomical structures of a cortical bone slice including vascular canals (*). osteons (**) and haversian canals (***).

**Figure 3: Example of pre- and post-culture (with osteoclasts) µCT images of equine bone slices.**

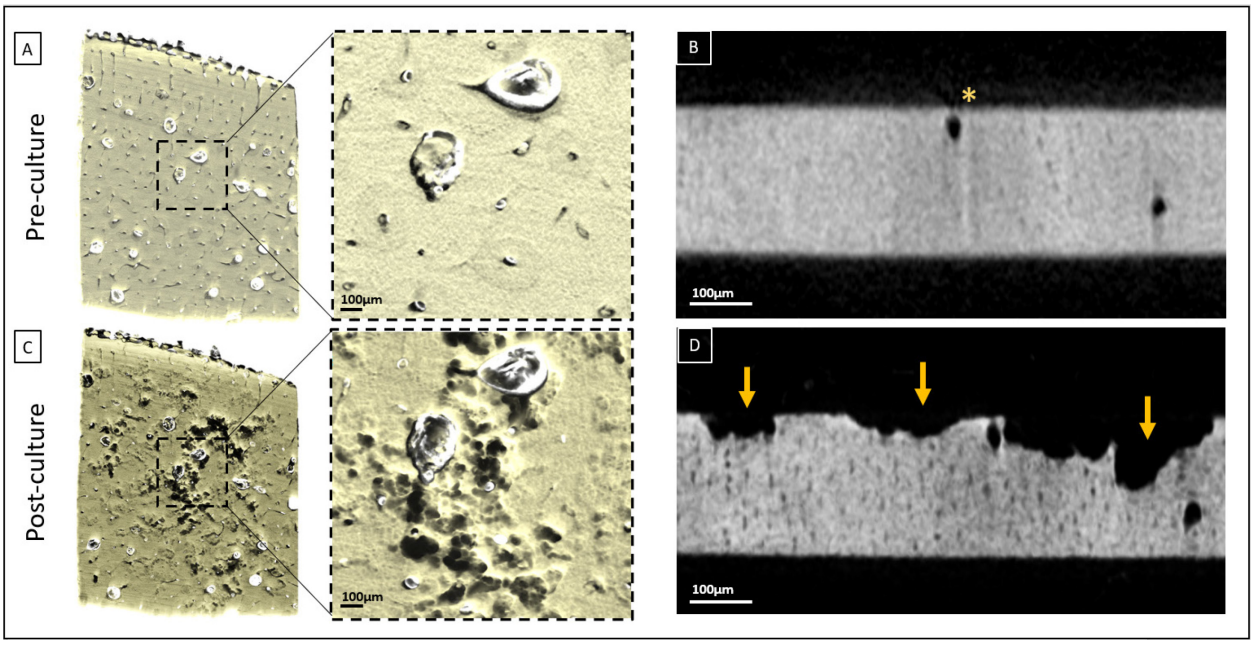


(A) 3D reconstruction of pre-culture unresorbed bone slice. The magnified image (broken rectangle) shows the normal anatomical structures of the bone (B) 2D cross-sectional view showing smooth, straight, unresorbed bone surfaces of the pre-culture bone with blood vessels (asterisk) (C) 3D reconstructions of the same bone slice post-culture with osteoclasts for 21 days. The magnified (broken rectangle) image reveals a topographic map of bone resorption performed by osteoclast cells (D) 2D view at the exact same position as image B with resorption events easily identified (yellow arrows). Note in the post-culture scans the difference in depth between events of resorption.

**Figure 4: 3D representation of resorption events and the measured parameters (volume, aspect ratio and maximum depth) for each specimen (A, B and C) from experiment 1.**

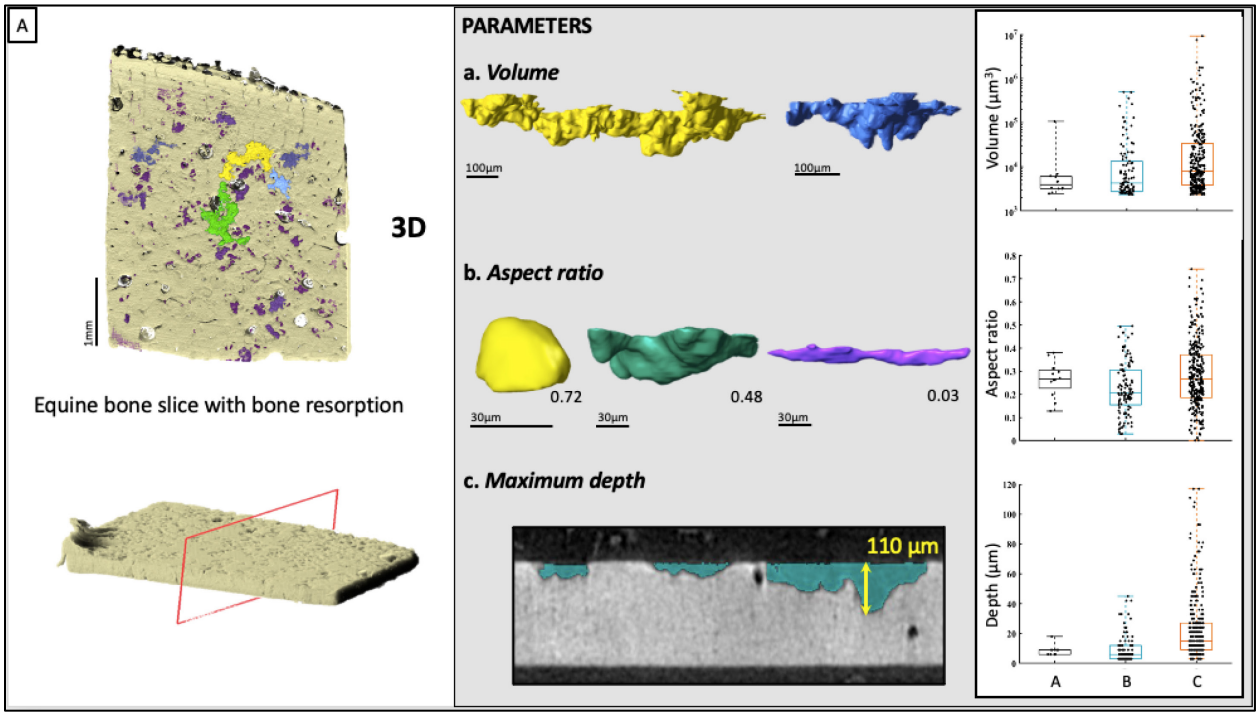


(A) Post osteoclast culture equine bone slice with resorption events extracted from deep learning feature-aided segmentation color coded by volume (a) 3D representation of resorption events showing different volumes (b) 3D representation of aspect ratio and morphology in a segmented 3D µCT image. From left to right; example of a "pit-like" rounded morphology resorption with an aspect ratio of 0.72 (yellow); example of an 0.48 aspect ratio resorption (green); example of a "trench-like" elongated morphology resorption with an aspect ratio of 0.03. (c) 2D cross-section image showing the maximum depth of a resorption event. The total number of resorption events was 12. 106. and 306 for specimen A, B, and C respectively which goes in accordance with the severity of resorption observed (mild, moderate, and severe). For each resorption events the parameters of volume, depth, and aspect ratio were box plotted (graphs on the right).

**Figure 5: Figure showing specimen excluded from the study due to shaped dents that hindered image analysis.**

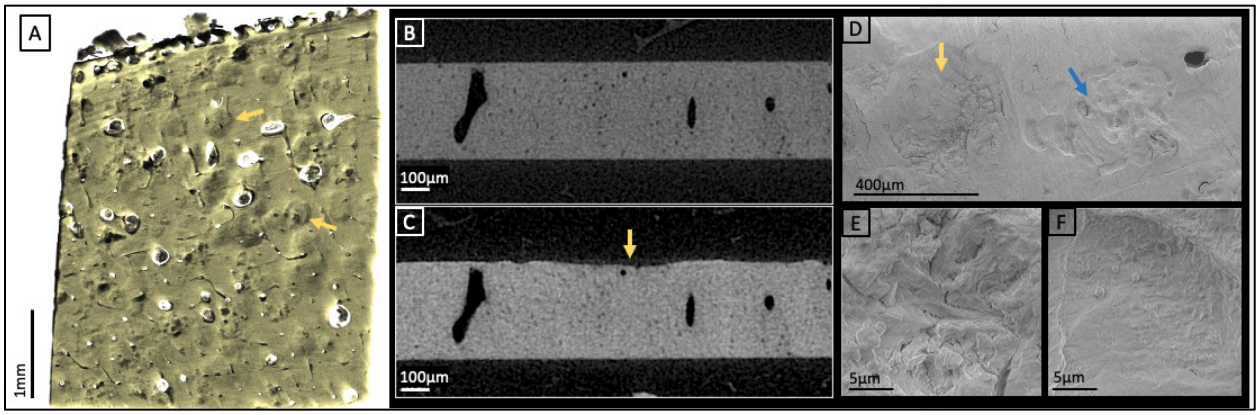


(A) 3D µCT image of the abnormal bone slice showing "pancake-like" dents (yellow arrows); (B) Cross-sectional 2D µCT image of the bone slice pre-culture; (C) Cross-sectional 2D µCT image of the same bone slice showing the dented region (yellow arrow); (D) SEM image of the same bone slice comparing the dented abnormal region (yellow arrow) and a normal resorption cavity (blue arrow); (E) Zoomed SEM image of the bottom surface of the abnormal dented region; (F) Zoomed SEM image of the bottom surface of a normal resorption cavity.

**Figure 6: Comparison between imaging techniques employed at the exact same region.**

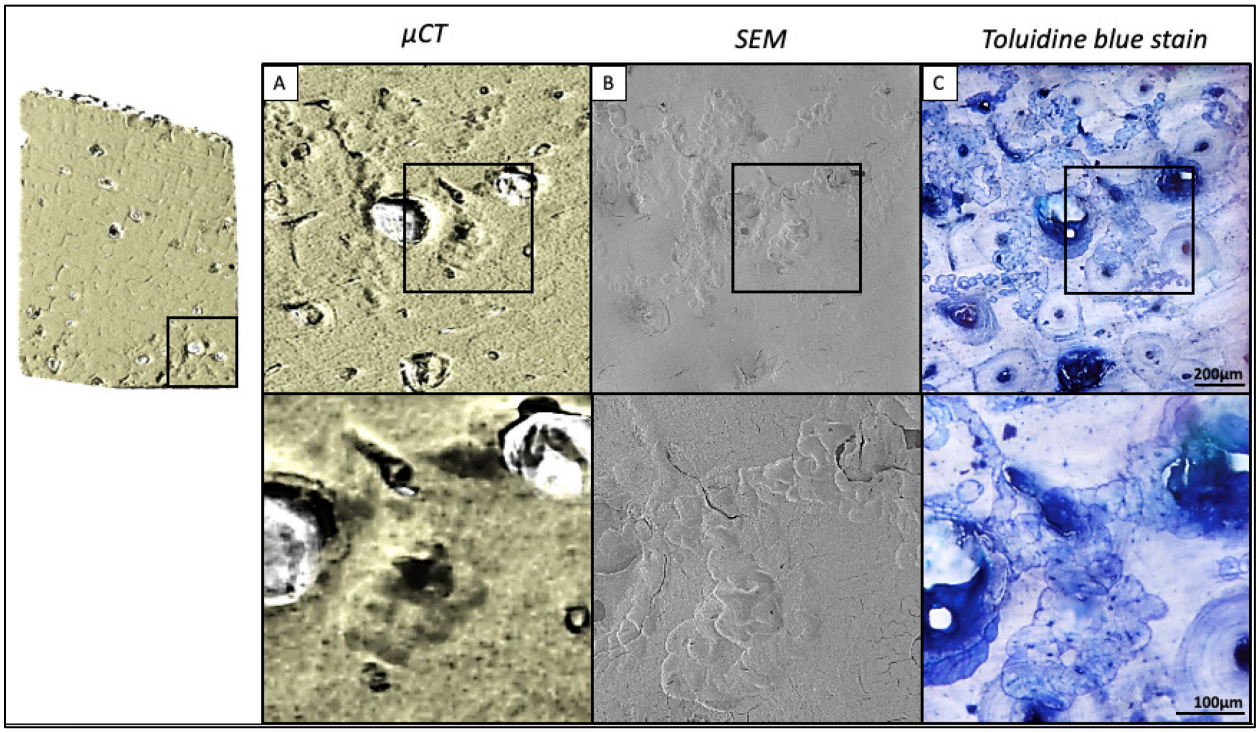


(A) µCT (B) SEM (C) Light microscopy image of a bone slice stained with toluidine blue. Note that although microscopy and SEM showed a better resolution when magnified, those techniques do not give any information on the 3D aspect of resorption cavities. µCT permitted not only a topographic map of osteoclastic bone resorption as well as the extraction of individual events of resorption and morphological characterization.

**Figure 7: Portfolio of resorption events.**

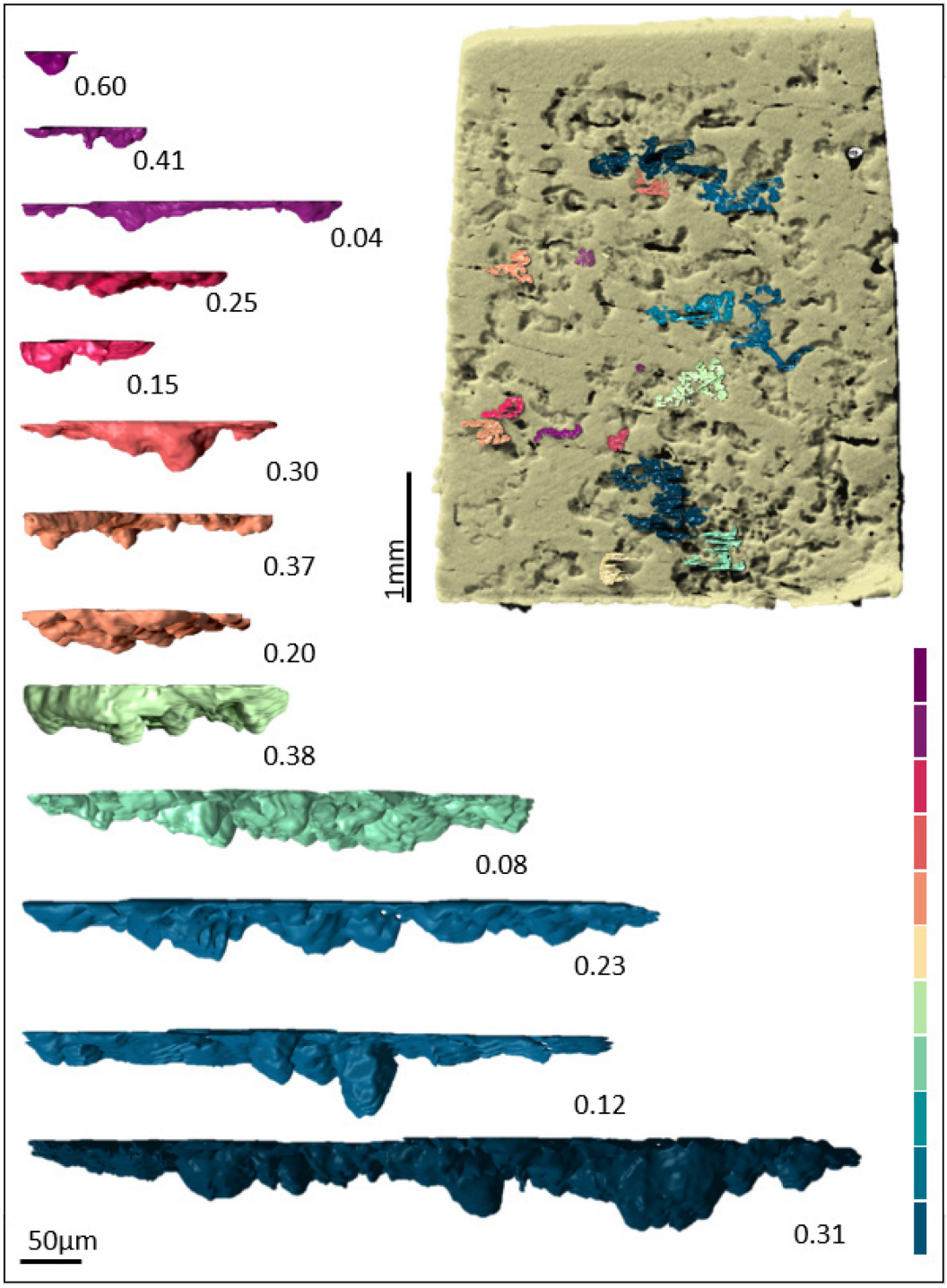


Different resorption events extracted from one of the specimens from experiment 2 illustrating the different morphology and volume. The bone slice shows where each individual resorption event was located. The resorption events are color coded by volume from smallest (purple- $*10^3\mu m^3$) to biggest (dark blue- $*10^3\mu m^3$). The numbers on the right low corner of each resorption events are the aspect ratio.

**Figure 8: Correlation between automated model volume of resorption on bone slices with CTX-I media biomarker and area of resorption.**

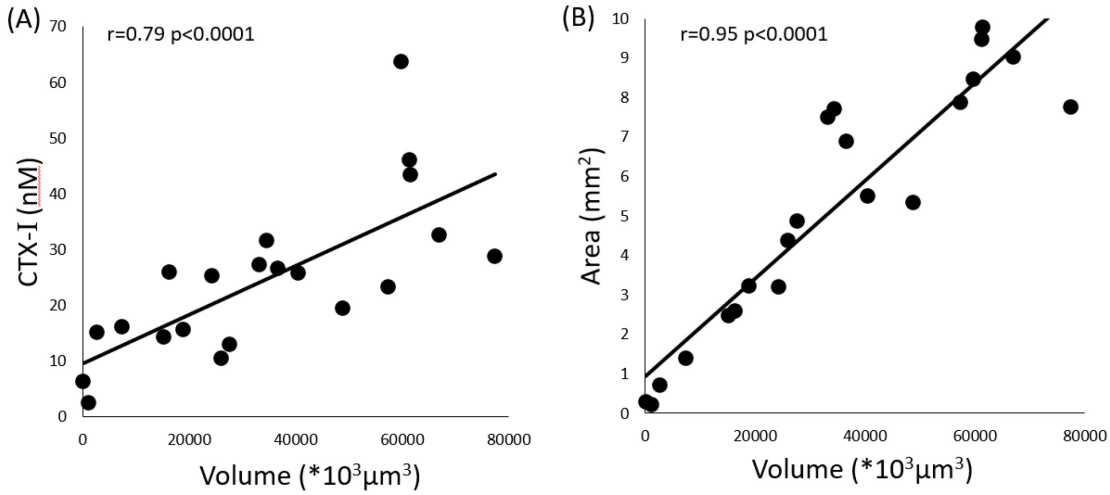


(A) CTX-I concentration per well and volume of resorption were analysed at the end of the culture. There was a strong positive correlation between CTX-I in the media and volume of resorption (r=0.79; p<0.0001). (B) There was a very strong positive correlation between volume of resorption and area of resorption (r=0.95; p<0.0001). Each circle represents a specimen. r, Spearman correlation coefficient.

**Supplementary Figure 1: Retrospective analysis of prior bone slice resorption areas.**

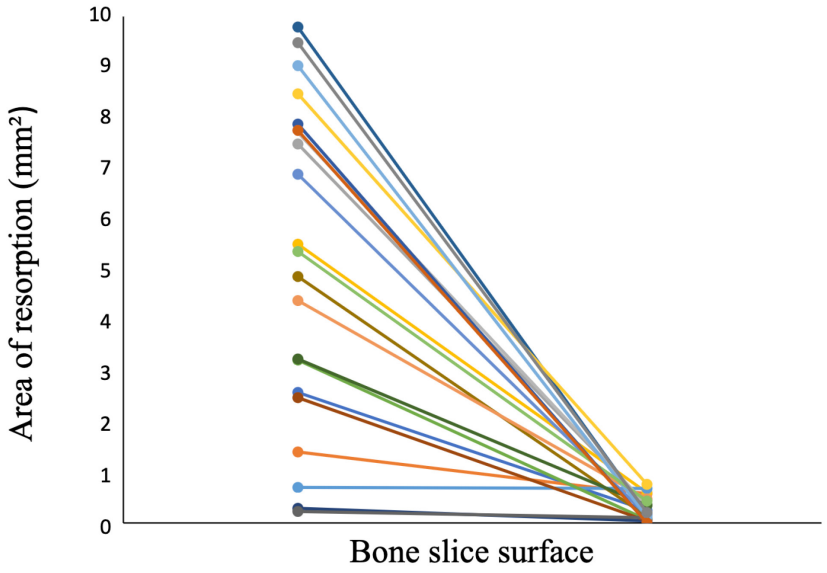


| Specimen | Surface area 1 (mm²) | Surface area 2 (mm²) |
|---|---|---|
| 1 | 2.59 | 0.26 |
| 2 | 1.40 | 0.58 |
| 3 | 7.49 | 0.35 |
| 4 | 5.51 | 0.61 |
| 5 | 0.71 | 0.68 |
| 6 | 3.21 | 0.07 |
| 7 | 0.30 | 0.05 |
| 8 | 2.48 | 0.05 |
| 9 | 0.22 | 0.10 |
| 10 | 4.86 | 0.12 |
| 11 | 9.78 | 0.19 |
| 12 | 3.23 | 0.36 |
| 13 | 6.88 | 0.15 |
| 14 | 4.38 | 0.48 |
| 15 | 7.71 | 0.35 |
| 16 | 8.47 | 0.77 |
| 17 | 9.03 | 0.12 |
| 18 | 5.35 | 0.44 |
| 19 | 7.87 | 0.00 |
| 20 | 7.75 | 0.00 |
| 21 | 9.48 | 0.21 |

Analysis of archival data from previous investigation[21] in the laboratory revealed that one side of the bone slice (surface 1 and 2) was always substantially more resorbed than the other.

**Supplementary Figure 2: Creation of cropping boxes for overestimation correction.**

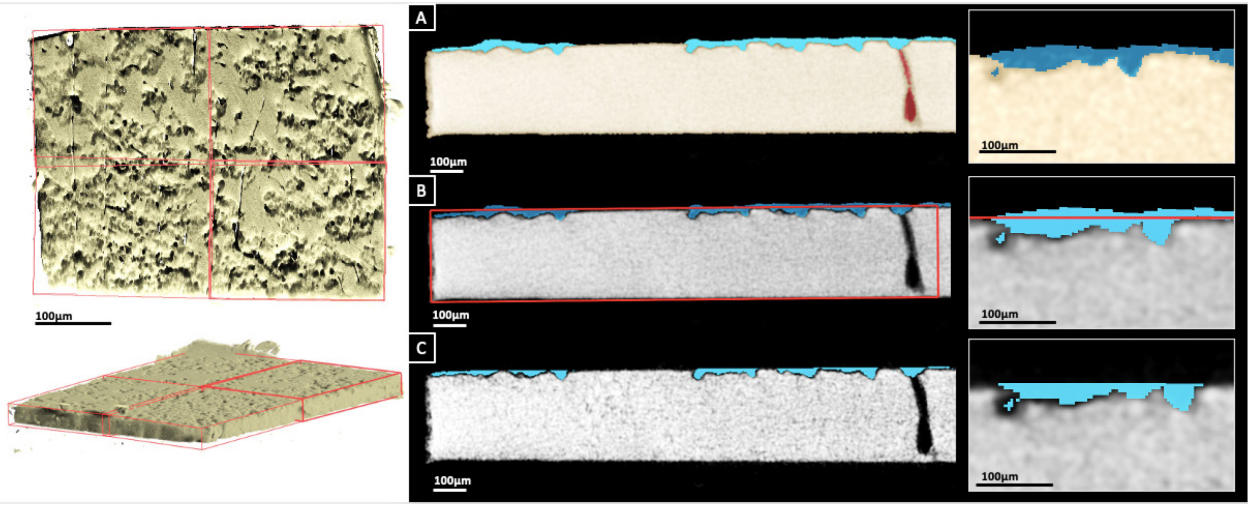


To avoid resorption overestimation, each bone slice was divided into 4 boxes (red rectangles). Each box was placed the closest to the resorption surface as possible (B) and the bone resorption ROI was cropped (C).

# Chapter 3 - General discussion

Several interesting new findings are reported in the present study, providing basis for future research aimed at improving knowledge of the biology of equine osteoclast. An accurate technique integrating µCT imaging and deep learning-aided feature segmentation, has been implemented for the 3D characterization and direct volumetric measurement of discrete osteoclast resorption events on bone slices. In addition, an automated CNN (UNet-like) was trained for accurate measurement of resorption volumes on bone slices incubated with osteoclasts thereby reducing the need for manual segmentation. The total volumes of resorption measured correlated strongly with the biomarker of bone resorption (CTX-I) concentrations in the culture media of the samples and also the canonical toluidine blue stained resorption area measurements from the same bone slices, underpinning its accuracy. This reported procedure can be useful for more objective future studies of osteoclastic resorption.

Osteoclast activity is often investigated in vitro by culturing them on their natural substrates, either bone or dentine, to mimic best the in vivo environment. The most accessible and frequent metric of their *in vitro* activity, in the past, was the area of toluidine blue stained resorption on bone slices at the end of the osteoclast culture period. However, it has been known for some time that the measurement of the volume of resorption on bone slices is a more accurate parameter of osteoclast activity.[38] In the present study, µCT image registration of matching bone slices, pre and post culture with osteoclasts, combined with deep learning-aided feature segmentation facilitated volume measurement and yielded data on both 2D cross-section images and in 3D enabling very detailed characterization of resorption events. Subsequently, a neural network was trained specifically to enable the assessment of resorption volume in post-cultured bone slices alone.

Using Deep Learning helps analyze data quickly and accurately. This becomes even clearer after the network has been trained. Nonetheless, it's noteworthy that the arduous process of establishing an efficient and well-trained network demands substantial effort and diligence. In the present research, two different neural networks were used, and both needed extensive training.

The discovery of new technologies and tools within the Dragonfly software prompted the creation of the second neural network, indicating a departure from the original plan. However, this change resulted in a notably more potent tool, capable of autonomously quantifying bone resorption volume using solely post-culture bone slices.

**Depth of osteoclast resorption**

The assessment of the depth of osteoclast bone resorption by osteoclasts in vitro provides insight into the activity of osteoclasts beyond their basic adherence and spreading behavior that area measurements

capture.[38] The measurement of depth could potentially allow evaluation of the effects of therapies targeting osteoclasts and investigating the mechanisms involved in bone remodeling processes as it has been shown that different resorption behaviours are linked to different resorption depth.[30] Resorption cavity depths have been measured using SEM stereophotogrammetry and mean (± SD) maximum depth values varying from 1.96 (± 0.12) to 2.5µm (± 0.18) were detected when chick osteoclasts were grown on dentine slices for 24 hours.[234] Additionally, when murine osteoclasts were cultured on bovine bone slices for a much longer period of 14 days, a similar median (25th percentile; 75th percentile) maximum resorption depth of 1.4µm (1.0; 2.0) was measured applying the same technique.[235] In contrast, vertical scanning profilometry, that allows an assessment of a 3D surface profile of a substrate, detected greater mean resorption depths of 29.7µm (± 4.3) when human osteoclasts were cultured on dentine slices but for even greater cultures periods of 21 days.[236] For comparative purposes, the mean maximum depth measured in this study using µCT was 19µm (± 19.59), which aligns with the findings of the previous investigation conducted by Mabilleau, et al. (2012). However, in light of the skewed distribution of the data, the median (12µm) and mode values (12µm) were deemed to be a more accurate depiction of the overall dataset. The apparent discrepancy in the parameter measurements among the aforementioned reports may be explained by variations in culture periods, species, and the substrates investigated.

In order to assess the resemblance of these in vitro events to real-life resorption, it is valuable to compare the depth values with those derived from ex vivo specimens. Fluorescence-based serial milling of vertebral cancellous bone specimens from healthy elderly humans revealed median maximum resorption depths of 26.3µm with a range from 4.9 to 116.7 µm,[220] a strikingly similar range to the current study (3 – 117µm), underpinning that the in vitro model replicates in vivo resorption events and measurement techniques. Furthermore, the mean maximum resorption depth of 14.8µm (± 2.56) previously measured in rat vertebrae[237] using the same techniques was similar to the median (12µm) and mode (12µm) recorded in the current study.

**Volume of osteoclast resorption-individual resorption events**

While depth measurements are informative of the type of osteoclast activity, the measurement of the resorption volume is the ideal measure of osteoclast activity on bone slices in vitro for comparative studies. Although the volume of discrete or individual resorption events on bone or dentine slices has been illustrated in the past by stereophotogrammetric SEM[234,238] and confocal microscopy,[217,239] there is sparse information in the scientific literature on their actual measured volumes. Mean volumes varying from 0.98 up to 4.59 $*10^3 \mu m^3$ were measured using stereophotogrammetric SEM for osteoclasts from a

variety species (rat, chick, and rabbit) grown on dentine slices for 24h.[123] Although a mean resorption event volume of 2.45*$10^3$µm$^3$ was also measured using confocal microscopy when chick osteoclasts were cultured on dentine slices for 24h,[240] the median volume was lower (0.85*$10^3$µm$^3$) when they were cultured on equine metacarpal bone slices for 20h.[107] The mean volume of individual resorption events of human osteoclasts cultured on dentine slices for 21 days was much greater (57.3 ± 15.6 *$10^3$µm$^3$) when measured with vertical scanning profilometry.[236] Despite the fact that the current investigation allowed the measurement of similar mean resorption events volumes (105.55 ± 612.88 *$10^3$µm) to the latter, because of the skewed nature of the data, the median (25th percentile; 75th percentile) value 6.86*$10^3$µm (3.47; 25.28) was again considered to reflect the overall data better. The mean resorption volume (614.16 ± 311.93 *$10^3$µm$^3$) of natural resorption cavities in cancellous bone from elderly human vertebrae using fluorescence-based serial milling[220] was higher than that measured in the current study (105.55 ± 612.88 *$10^3$µm). On the other hand, the mean resorption cavity volume measured in rat vertebral cancellous bone was 36.50 ± 5. 35 *$10^3$µm$^3$ using the same technique[237] and closer to that was measured herein.

**Total volume of osteoclast resorption on bone slices**

The measurement of the total volume of resorption of the complete surface of the bone slice is an additional parameter to consider when comparing factors influencing osteoclast activity *in vitro*. However, only a limited number of studies have been able to successfully incorporate this parameter. The bone slices in the present study were approximately uniform in size, but there was a substantial variability in the mean total volume of resorption per bone slice (34,155.31 ± 23,407.80 *$10^3$µm$^3$) indicating a high level of heterogeneity and sensitivity in the resorption experiments.

Previous in vitro techniques for measuring the depth and volume of resorption on bone slices have several limitations, such as the requirement for sample preparation, sophisticated equipment, and a researcher's expertise. Additionally, when measuring depth, some of the techniques failed to consider the morphology of the resorption cavities in directions other than the observed plane.[220] This reported approach using µCT imaging of bone slices and deep learning-aided feature segmentation in the current study overcame these limitations. Our method involved minimal sample preparation and generated multiple cross-sectional images that facilitated the visualization and precise measurement of resorption depth and volume using an automated technique and is a user-friendly alternative for measuring the maximum depth of the entire bone slice sample.

**Analysis of the morphology of individual osteoclast resorption events**

In addition to the depth and volume of osteoclast resorption on bone slices, the assessment of the shape and form of the cavities they sculpt in the bone substrate can provide information as to the state of their activity. Recent investigations characterized osteoclast resorption cavity morphology on bone slices[30,34,82] and ex vivo[30] by classifying them as being of two distinct types, either "pits" or "trenches", using time-lapse recording in combination with confocal microscopy,[34,82] and SEM.[30] The pit mode are rounded-shaped resorptions characterized by short-term active bone breakdown that is interrupted by migration periods. The trench mode on the other hand reflects a more aggressive form of resorption combined with osteoclast migration, being deeper,[30] longer, and faster.[82] In the present investigation, although both pits and trenches were observed, the majority of resorption events could not be easily classified into these 2 discrete categories but were rather combinations of both. This observation is in agreement with Hefti, et al. (2010) who observed three different types of resorption, namely resorption pits, trails and dense areas of resorption where no distinction of patter was possible when mouse osteoclasts were cultured on bovine bone slices for 14 days and imaged with SEM. It is important to note that they elected to exclude these densely resorbed areas from their analysis because of the difficulty of doing so. Herein, it is proposed that resorption cavities should be classified along a spectrum of shapes that more accurately reflect osteoclast activity, rather than simply pits and trenches. It is also possible that different osteoclasts may have resorbed the same region, because of the length of the culture period leading to the creation of pits within trenches and vice versa. Consequently, the term "resorption events" is utilized here rather than "cavities".

**Deep learning segmentation of osteoclast resorption on bone slices**

The neural network trained in the second arm of the study, provided a practical, user-friendly alternative for calculating resorption volume on bone slices as only post-culture slices were imaged and the amount of manual segmentation required was greatly reduced. The UNet-like CNN, Sensor3D, was initially described for organ segmentation on CT scans.[241] Unlike previous approaches that processed complete sets of tomographic images, it operates on individual slices and considers as few as three sequential image slices, capturing inter-slice dependencies and learning the spatial and temporal relationships between them.[241]

**Comparisons of the deep learning segmentation of osteoclast resorption with classical parameters of resorption: CTX-I biomarker and toluidine blue area measurements**

During the process of bone degradation, osteoclastic enzymes, including cathepsin K, digest type I collagen in the bone matrix, causing the release of bone resorption products into the bloodstream including CTX-

I, a well-established biomarker of bone resorption.[71,72,115,116] The neural network volume of resorption correlated strongly with the levels of the CTX-I biomarker measured in the media, harvested from the osteoclast on bone cultures, confirming that this new method is accurately measuring resorption.

Although toluidine blue staining of resorption on bone slices post-culture is widely used to assess osteoclast activity, it only captures surface resorption in 2D. The area of resorption measured may be misleading[121] as it may also reflect osteoclast spreading and attachment rather than actual resorptive activity.[38-40] For example, an increased area of resorption, if in combination with decreased cavity depth, does not necessarily mean increased resorptive activity.[38,40,122] Additionally, manual segmentation of area is considered to be time-consuming and prone to bias due to inter-user variations.[196] Therefore, when analyzing bone resorption, it is ideal to consider all three factors: area, depth, and volume[40] that are described in the study herein. The neural network volume measurements of resorption on the bone slices correlated with the prior canonical area measurements, made with light microscopy on toluidine blue stained bone slices supporting the validity of the 3D measurements. However, the approach is faster and eliminates the labor-intensive aspects associated with manual segmentation enabling a more comprehensive examination of the entire specimen and ensuring a more thorough analysis.

One bone slice had atypical sandpit-like depressions, not described previously to our knowledge. SEM imaging of this specimen revealed that the deep regions of these depressions exhibited a characteristic roughness not observed in the resorption cavities, observed in the majority of specimens. As all specimens were cultured under identical conditions, these atypical depressions are likely indicative of an unusual type of resorption or potential unexplained artifacts.

**Study limitations**

It is acknowledged that this study has several limitations. Firstly, the use of a cubic voxel size of 3µm in µCT imaging may introduce limitations in the detection of smaller resorption cavities. Previous research by Tkachenck, et al. (2009) reported that images with voxel sizes exceeding 1.4 µm could potentially introduce errors in the detection of smaller resorption cavities in ex vivo bone specimens. At the same time, Tkachenko, et al. (2009), employed voxels with an aspect ratio not equal in all dimensions. By using cubic voxels in the current investigation, it allowed reliable detection of resorption cavities in cortical bone indicating that resorption cavities were clearly visible in the images with a resolution of 3µm cubic voxel. However, it remains plausible that extremely small pits may have gone undetected. Another potential limitation of this study is the presence of physiological structural variations in the bone slices, such as vascular channels and pores. These structural variations can pose challenges in accurately distinguishing

them from true resorption cavities during image analysis. However, the implementation of deep learning techniques in the form of feature segmentation enabled the detection and exclusion of these sites from the measurements. It is important to recognize these limitations and consider their potential implications on the results and interpretations of the study. Further investigations could explore the use of smaller voxel sizes to enhance the detection of smaller resorption cavities and improve the resolution of µCT imaging. Additionally, efforts to refine the deep learning model for more accurate discrimination between true resorption cavities and physiological structural variations could enhance the reliability of the measurements.

The findings of this study provide valuable and significant insights into the detection and quantification of osteoclast bone resorption by incorporating µCT imaging and deep learning-aided feature segmentation techniques. This non-destructive approach not only enhances our understanding of osteoclast activity but also lays a strong foundation for numerous future possibilities in osteoclast research.

One promising avenue that will be facilitated by this technique is the evaluation of different medications commonly administered intra-articularly in equine veterinary medicine, such as corticosteroids, allowing researchers to assess their effects on osteoclast activity in vitro at clinically relevant doses and consequently any adverse effects on the equine athlete's skeleton. Furthermore, it provides an opportunity to delve deeper into the volume and three-dimensional aspects of osteoclast bone resorption. These insights and analysis empower researchers to acquire a more comprehensive comprehension of the spatial distribution, patterns, and intricacies involved in bone resorption, as well as factors that influence the delicate equilibrium between bone resorption and bone formation. These discoveries could potentially pave the way for developing innovative tools, including a precise bone resorption biomarker, specifically for horses, aimed at identifying early imbalances in bone health. This preventive approach could enable us to make timely modifications to racehorse training routines, potentially reducing the risk of severe injuries.

# Conclusion

Accurately quantifying and characterizing bone resorption by osteoclasts poses significant challenges. Traditional 2D resorption area measurements have limitations, often providing oversimplified representations. Several 3D methods have been explored; however, they have their own restrictions in terms of resolution, destructive nature, and sample preparation requirements. High-resolution µCT has provided a non-destructive and accessible means of examining bone microstructure, prompting its exploration for the detection and quantification of bone resorption on bone slices.

The application of deep learning-aided feature segmentation on µCT images of bone slices cultured with osteoclasts offers a powerful and precise method for characterizing osteoclast resorption and accurately measuring the total volume of resorption. This study paves the way for more extensive and accurate investigations into factors that influence equine osteoclast resorption *in vitro*, including the effects of medications such as corticosteroids and bisphosphonates. Understanding how these medications impact osteoclast activity can provide valuable insights into their efficacy and potential side effects.

Future investigations are essential to expand our understanding of equine osteoclast activity and the factors that influence it. By accurately measuring the resorption volume using this technique, it becomes possible to further explore species-specific biomarkers of bone resorption. This advancement has significant implications for equine health and welfare, as it aids on the identification of specific biomarkers that can be used to assess osteoclast activity in horses. Such biomarkers may have the potential to serve as early indicators of bone resorption, aiding in the screening and prevention of fatal fractures in racehorses.

# References


1 Wolff, J. in The Law of Bone Remodelling (ed Julius Wolff) 1-1 (Springer Berlin Heidelberg, 1986).

2 Kenkre, J. S. & Bassett, J. The bone remodelling cycle. *Ann Clin Biochem* **55**, 308-327 (2018). https://doi.org:10.1177/0004563218759371

3 Mori, S. & Burr, D. B. Increased intracortical remodeling following fatigue damage. *Bone* **14**, 103-109 (1993). https://doi.org:10.1016/8756-3282(93)90235-3

4 Burr, D. B. Targeted and nontargeted remodeling. *Bone* **30**, 2-4 (2002). https://doi.org:https://doi.org/10.1016/S8756-3282(01)00619-6

5 Li, M. C. M., Chow, S. K. H., Wong, R. M. Y., Qin, L. & Cheung, W. H. The role of osteocytes-specific molecular mechanism in regulation of mechanotransduction - A systematic review. *J Orthop Translat* **29**, 1-9 (2021). https://doi.org:10.1016/j.jot.2021.04.005

6 Verborgt, O., Gibson, G. J. & Schaffler, M. B. Loss of osteocyte integrity in association with microdamage and bone remodeling after fatigue in vivo. *J Bone Miner Res* **15**, 60-67 (2000). https://doi.org:10.1359/jbmr.2000.15.1.60

7 Kitaura, H. *et al.* Osteocyte-Related Cytokines Regulate Osteoclast Formation and Bone Resorption. *Int J Mol Sci* **21** (2020). https://doi.org:10.3390/ijms21145169

8 Norrdin, R. W. & Stover, S. M. Subchondral bone failure in overload arthrosis: a scanning electron microscopic study in horses. *J Musculoskelet Neuronal Interact* **6**, 251-257 (2006).

9 Lacourt, M. *et al.* Relationship between cartilage and subchondral bone lesions in repetitive impact trauma-induced equine osteoarthritis. *Osteoarthritis Cartilage* **20**, 572-583 (2012). https://doi.org:10.1016/j.joca.2012.02.004

10 Carrier, T. K. *et al.* Association between long periods without high-speed workouts and risk of complete humeral or pelvic fracture in thoroughbred racehorses: 54 cases (1991-1994). *J Am Vet Med Assoc* **212**, 1582-1587 (1998).

11 Martig, S., Chen, W., Lee, P. V. & Whitton, R. C. Bone fatigue and its implications for injuries in racehorses. *Equine Vet J* **46**, 408-415 (2014). https://doi.org:10.1111/evj.12241

12 Holmes, J. M., Mirams, M., Mackie, E. J. & Whitton, R. C. Thoroughbred horses in race training have lower levels of subchondral bone remodelling in highly loaded regions of the distal metacarpus compared to horses resting from training. *Vet J* **202**, 443-447 (2014). https://doi.org:10.1016/j.tvjl.2014.09.010

13 Riggs, C. M., Whitehouse, G. H. & Boyde, A. Pathology of the distal condyles of the third metacarpal and third metatarsal bones of the horse. *Equine Vet J* **31**, 140-148 (1999). https://doi.org:10.1111/j.2042-3306.1999.tb03807.x

14 Pinchbeck, G. L., Clegg, P. D., Boyde, A., Barr, E. D. & Riggs, C. M. Horse-, training- and race-level risk factors for palmar/plantar osteochondral disease in the racing Thoroughbred. *Equine Vet J* **45**, 582-586 (2013). https://doi.org:10.1111/evj.12038

15 Bani Hassan, E., Mirams, M., Ghasem-Zadeh, A., Mackie, E. J. & Whitton, R. C. Role of subchondral bone remodelling in collapse of the articular surface of Thoroughbred racehorses with palmar osteochondral disease. *Equine Vet J* **48**, 228-233 (2016). https://doi.org:10.1111/evj.12415

16 Bertuglia, A. *et al.* Osteoclasts are recruited to the subchondral bone in naturally occurring post-traumatic equine carpal osteoarthritis and may contribute to cartilage degradation. *Osteoarthritis Cartilage* **24**, 555-566 (2016). https://doi.org:10.1016/j.joca.2015.10.008

17 Gray, A. W., Davies, M. E. & Jeffcott, L. B. In vitro generation of equine osteoclasts from bone marrow cells using a novel culture system. *Res Vet Sci* **65**, 155-160 (1998). https://doi.org:10.1016/s0034-5288(98)90168-0

18 Gray, A. W., Davies, M. E. & Jeffcott, L. B. Equine osteoclast-like cells generated in vitro demonstrate similar characteristics to directly isolated mature osteoclasts. *Res Vet Sci* **68**, 161-167 (2000). https://doi.org:10.1053/rvsc.1999.0367
19 Gray, A. W., Davies, M. E. & Jeffcott, L. B. Localisation and activity of cathepsins K and B in equine osteoclasts. *Res Vet Sci* **72**, 95-103 (2002). https://doi.org:10.1053/rvsc.2001.0522
20 Hussein, H. *et al.* Cathepsin K Localizes to Equine Bone In Vivo and Inhibits Bone Marrow Stem and Progenitor Cells Differentiation In Vitro. *J Stem Cells Regen Med* **13**, 45-53 (2017). https://doi.org:10.46582/jsrm.1302008
21 Malek, G., Richard, H., Beauchamp, G. & Laverty, S. An in vitro model for discovery of osteoclast specific biomarkers towards identification of racehorses at risk for catastrophic fractures. *Equine Vet J* (2022). https://doi.org:10.1111/evj.13600
22 Solari, F., Flamant, F., Cherel, Y., Wyers, M. & Jurdic, P. The osteoclast generation: an in vitro and in vivo study with a genetically labelled avian monocytic cell line. *J Cell Sci* **109 ( Pt 6)**, 1203-1213 (1996). https://doi.org:10.1242/jcs.109.6.1203
23 Breuil, V. *et al.* Human osteoclast formation and activity in vitro: effects of alendronate. *J Bone Miner Res* **13**, 1721-1729 (1998). https://doi.org:10.1359/jbmr.1998.13.11.1721
24 Malaval, L. *et al.* Bone sialoprotein plays a functional role in bone formation and osteoclastogenesis. *J Exp Med* **205**, 1145-1153 (2008). https://doi.org:10.1084/jem.20071294
25 Søe, K. *et al.* Involvement of human endogenous retroviral syncytin-1 in human osteoclast fusion. *Bone* **48**, 837-846 (2011). https://doi.org:10.1016/j.bone.2010.11.011
26 Søe, K. & Delaissé, J. M. Glucocorticoids maintain human osteoclasts in the active mode of their resorption cycle. *J Bone Miner Res* **25**, 2184-2192 (2010). https://doi.org:10.1002/jbmr.113
27 Durand, M. *et al.* Monocytes from patients with osteoarthritis display increased osteoclastogenesis and bone resorption: the In Vitro Osteoclast Differentiation in Arthritis study. *Arthritis Rheum* **65**, 148-158 (2013). https://doi.org:10.1002/art.37722
28 Søe, K., Merrild, D. M. & Delaissé, J. M. Steering the osteoclast through the demineralization-collagenolysis balance. *Bone* **56**, 191-198 (2013). https://doi.org:10.1016/j.bone.2013.06.007
29 Vanderoost, J., Søe, K., Merrild, D. M., Delaissé, J. M. & van Lenthe, G. H. Glucocorticoid-induced changes in the geometry of osteoclast resorption cavities affect trabecular bone stiffness. *Calcif Tissue Int* **92**, 240-250 (2013). https://doi.org:10.1007/s00223-012-9674-6
30 Merrild, D. M. *et al.* Pit- and trench-forming osteoclasts: a distinction that matters. *Bone Res* **3**, 15032 (2015). https://doi.org:10.1038/boneres.2015.32
31 Panwar, P. *et al.* A novel approach to inhibit bone resorption: exosite inhibitors against cathepsin K. *Br J Pharmacol* **173**, 396-410 (2016). https://doi.org:10.1111/bph.13383
32 Panwar, P. *et al.* An Ectosteric Inhibitor of Cathepsin K Inhibits Bone Resorption in Ovariectomized Mice. *J Bone Miner Res* **34**, 777-778 (2019). https://doi.org:10.1002/jbmr.3687
33 Moller, A. M. J. *et al.* Aging and menopause reprogram osteoclast precursors for aggressive bone resorption. *Bone Res* **8**, 27 (2020). https://doi.org:10.1038/s41413-020-0102-7
34 Borggaard, X. G., Pirapaharan, D. C., Delaisse, J. M. & Soe, K. Osteoclasts' Ability to Generate Trenches Rather Than Pits Depends on High Levels of Active Cathepsin K and Efficient Clearance of Resorption Products. *Int J Mol Sci* **21** (2020). https://doi.org:10.3390/ijms21165924
35 Delaisse, J. M., Søe, K., Andersen, T. L., Rojek, A. M. & Marcussen, N. The Mechanism Switching the Osteoclast From Short to Long Duration Bone Resorption. *Front Cell Dev Biol* **9**, 644503 (2021). https://doi.org:10.3389/fcell.2021.644503
36 Chappard, D., Retailleau-Gaborit, N., Legrand, E., Baslé, M. F. & Audran, M. Comparison insight bone measurements by histomorphometry and microCT. *J Bone Miner Res* **20**, 1177-1184 (2005). https://doi.org:10.1359/jbmr.050205

37 Vanderoost, J. & van Lenthe, G. H. From histology to micro-CT: Measuring and modeling resorption cavities and their relation to bone competence. *World J Radiol* **6**, 643-656 (2014). https://doi.org:10.4329/wjr.v6.i9.643
38 Boyde, A. & Jones, S. J. Pitfalls in pit measurement. *Calcif Tissue Int* **49**, 65-70 (1991). https://doi.org:10.1007/bf02565123
39 Pascaretti-Grizon, F., Mabilleau, G., Basle, M. F. & Chappard, D. Measurement by vertical scanning profilometry of resorption volume and lacunae depth caused by osteoclasts on dentine slices. *J Microsc* **241**, 147-152 (2011). https://doi.org:10.1111/j.1365-2818.2010.03410.x
40 Soysa, N. S., Alles, N., Aoki, K. & Ohya, K. Three-dimensional characterization of osteoclast bone-resorbing activity in the resorption lacunae. *J Med Dent Sci* **56**, 107-112 (2009).
41 Minnema, J. *et al.* A review on the application of deep learning for CT reconstruction, bone segmentation and surgical planning in oral and maxillofacial surgery. *Dentomaxillofacial Radiology* **51**, 20210437 (2022). https://doi.org:10.1259/dmfr.20210437
42 Reznikov, N., Buss, D. J., Provencher, B., McKee, M. D. & Piché, N. Deep learning for 3D imaging and image analysis in biomineralization research. *Journal of Structural Biology* **212**, 107598 (2020). https://doi.org:https://doi.org/10.1016/j.jsb.2020.107598
43 Reznikov, N., Liang, H., McKee, M. D. & Piché, N. Technical note: Mapping of trabecular bone anisotropy and volume fraction in 3D using µCT images of the human calcaneus. *American Journal of Biological Anthropology* **177**, 566-580 (2022). https://doi.org:https://doi.org/10.1002/ajpa.24474
44 Anwar, S. M. *et al.* Medical Image Analysis using Convolutional Neural Networks: A Review. *Journal of Medical Systems* **42**, 226 (2018). https://doi.org:10.1007/s10916-018-1088-1
45 Chan, H. P., Samala, R. K., Hadjiiski, L. M. & Zhou, C. Deep Learning in Medical Image Analysis. *Adv Exp Med Biol* **1213**, 3-21 (2020). https://doi.org:10.1007/978-3-030-33128-3_1
46 Du, G., Cao, X., Liang, J., Chen, X. & Zhan, Y. Medical Image Segmentation based on U-Net: A Review. *Journal of Imaging Science and Technology* **64** (2020). https://doi.org:10.2352/J.ImagingSci.Technol.2020.64.2.020508
47 Burr, D. B. in *Basic and Applied Bone Biology (Second Edition)* (eds David B. Burr & Matthew R. Allen) 3-26 (Academic Press, 2019).
48 Grabowski, P. Physiology of bone. *Endocr Dev* **16**, 32-48 (2009). https://doi.org:10.1159/000223687
49 Florencio-Silva, R., Sasso, G. R., Sasso-Cerri, E., Simões, M. J. & Cerri, P. S. Biology of Bone Tissue: Structure, Function, and Factors That Influence Bone Cells. *Biomed Res Int* **2015**, 421746 (2015). https://doi.org:10.1155/2015/421746
50 Clarke, B. Normal bone anatomy and physiology. *Clin J Am Soc Nephrol* **3 Suppl 3**, S131-139 (2008). https://doi.org:10.2215/cjn.04151206
51 Buck, D. W., 2nd & Dumanian, G. A. Bone biology and physiology: Part I. The fundamentals. *Plast Reconstr Surg* **129**, 1314-1320 (2012). https://doi.org:10.1097/PRS.0b013e31824eca94
52 Guntur, A. R. & Rosen, C. J. Bone as an endocrine organ. *Endocr Pract* **18**, 758-762 (2012). https://doi.org:10.4158/ep12141.Ra
53 Buckwalter, J. A., Glimcher, M. J., Cooper, R. R. & Recker, R. Bone biology. I: Structure, blood supply, cells, matrix, and mineralization. *Instr Course Lect* **45**, 371-386 (1996).
54 Karsenty, G. & Olson, E. N. Bone and Muscle Endocrine Functions: Unexpected Paradigms of Inter-organ Communication. *Cell* **164**, 1248-1256 (2016). https://doi.org:10.1016/j.cell.2016.02.043
55 Zoch, M. L., Clemens, T. L. & Riddle, R. C. New insights into the biology of osteocalcin. *Bone* **82**, 42-49 (2016). https://doi.org:10.1016/j.bone.2015.05.046
56 Niwczyk, O. *et al.* Bones and Hormones: Interaction between Hormones of the Hypothalamus, Pituitary, Adipose Tissue and Bone. *Int J Mol Sci* **24** (2023). https://doi.org:10.3390/ijms24076840

57 Hart, N. H. *et al.* Biological basis of bone strength: anatomy, physiology and measurement. *J Musculoskelet Neuronal Interact* **20**, 347-371 (2020).
58 Chappard, D., Baslé, M. F., Legrand, E. & Audran, M. Trabecular bone microarchitecture: a review. *Morphologie* **92**, 162-170 (2008). https://doi.org:10.1016/j.morpho.2008.10.003
59 Bellido, T., Plotkin, L. I. & Bruzzaniti, A. in *Basic and Applied Bone Biology (Second Edition)* (eds David B. Burr & Matthew R. Allen) 37-55 (Academic Press, 2019).
60 Stoltz, J.-F. *et al.* Influence of mechanical forces on bone: Introduction to mechanobiology and mechanical adaptation concept. *Journal of Cellular Immunotherapy* **4**, 10-12 (2018). https://doi.org:https://doi.org/10.1016/j.jocit.2018.09.003
61 Kelly, P. J., Morrison, N. A., Sambrook, P. N., Nguyen, T. V. & Eisman, J. A. Genetic influences on bone turnover, bone density and fracture. *Eur J Endocrinol* **133**, 265-271 (1995). https://doi.org:10.1530/eje.0.1330265
62 Goodman, S. B., Jiranek, W., Petrow, E. & Yasko, A. W. The Effects of Medications on Bone. *JAAOS - Journal of the American Academy of Orthopaedic Surgeons* **15**, 450-460 (2007).
63 Seeman, E. Bone modeling and remodeling. *Crit Rev Eukaryot Gene Expr* **19**, 219-233 (2009). https://doi.org:10.1615/critreveukargeneexpr.v19.i3.40
64 Allen, M. R. & Burr, D. B. in *Basic and Applied Bone Biology (Second Edition)* (eds David B. Burr & Matthew R. Allen) 85-100 (Academic Press, 2019).
65 Nandiraju, D. & Ahmed, I. Human skeletal physiology and factors affecting its modeling and remodeling. *Fertil Steril* **112**, 775-781 (2019). https://doi.org:10.1016/j.fertnstert.2019.10.005
66 Cappariello, A., Maurizi, A., Veeriah, V. & Teti, A. The Great Beauty of the osteoclast. *Arch Biochem Biophys* **558**, 70-78 (2014). https://doi.org:10.1016/j.abb.2014.06.017
67 Boyce, B. F. & Xing, L. Functions of RANKL/RANK/OPG in bone modeling and remodeling. *Arch Biochem Biophys* **473**, 139-146 (2008). https://doi.org:10.1016/j.abb.2008.03.018
68 Ono, T. & Nakashima, T. Recent advances in osteoclast biology. *Histochem Cell Biol* **149**, 325-341 (2018). https://doi.org:10.1007/s00418-018-1636-2
69 McDonald, M. M., Kim, A. S., Mulholland, B. S. & Rauner, M. New Insights Into Osteoclast Biology. *JBMR Plus* **5**, e10539 (2021). https://doi.org:10.1002/jbm4.10539
70 Georgess, D., Machuca-Gayet, I., Blangy, A. & Jurdic, P. Podosome organization drives osteoclast-mediated bone resorption. *Cell Adh Migr* **8**, 191-204 (2014). https://doi.org:10.4161/cam.27840
71 Soysa, N. S. & Alles, N. Osteoclast function and bone-resorbing activity: An overview. *Biochem Biophys Res Commun* **476**, 115-120 (2016). https://doi.org:10.1016/j.bbrc.2016.05.019
72 Baron, R. Polarity and membrane transport in osteoclasts. *Connect Tissue Res* **20**, 109-120 (1989). https://doi.org:10.3109/03008208909023879
73 Yavropoulou, M. P. & Yovos, J. G. Osteoclastogenesis--current knowledge and future perspectives. *J Musculoskelet Neuronal Interact* **8**, 204-216 (2008).
74 Boyle, W. J., Simonet, W. S. & Lacey, D. L. Osteoclast differentiation and activation. *Nature* **423**, 337-342 (2003). https://doi.org:10.1038/nature01658
75 Takayanagi, H. RANKL as the master regulator of osteoclast differentiation. *J Bone Miner Metab* **39**, 13-18 (2021). https://doi.org:10.1007/s00774-020-01191-1
76 Udagawa, N. *et al.* Osteoclast differentiation by RANKL and OPG signaling pathways. *J Bone Miner Metab* **39**, 19-26 (2021). https://doi.org:10.1007/s00774-020-01162-6
77 Yasuda, H. Discovery of the RANKL/RANK/OPG system. *J Bone Miner Metab* **39**, 2-11 (2021). https://doi.org:10.1007/s00774-020-01175-1
78 Kim, J. H. & Kim, N. Regulation of NFATc1 in Osteoclast Differentiation. *J Bone Metab* **21**, 233-241 (2014). https://doi.org:10.11005/jbm.2014.21.4.233
79 Jacome-Galarza, C. E. *et al.* Developmental origin, functional maintenance and genetic rescue of osteoclasts. *Nature* **568**, 541-545 (2019). https://doi.org:10.1038/s41586-019-1105-7

80 McDonald, M. M. *et al.* Osteoclasts recycle via osteomorphs during RANKL-stimulated bone resorption. *Cell* **184**, 1330-1347.e1313 (2021). https://doi.org:10.1016/j.cell.2021.02.002
81 Yahara, Y. *et al.* Erythromyeloid progenitors give rise to a population of osteoclasts that contribute to bone homeostasis and repair. *Nat Cell Biol* **22**, 49-59 (2020). https://doi.org:10.1038/s41556-019-0437-8
82 Søe, K. & Delaissé, J. M. Time-lapse reveals that osteoclasts can move across the bone surface while resorbing. *J Cell Sci* **130**, 2026-2035 (2017). https://doi.org:10.1242/jcs.202036
83 Rumpler, M. *et al.* Osteoclasts on bone and dentin in vitro: mechanism of trail formation and comparison of resorption behavior. *Calcif Tissue Int* **93**, 526-539 (2013). https://doi.org:10.1007/s00223-013-9786-7
84 Mulari, M. T., Zhao, H., Lakkakorpi, P. T. & Väänänen, H. K. Osteoclast ruffled border has distinct subdomains for secretion and degraded matrix uptake. *Traffic* **4**, 113-125 (2003). https://doi.org:10.1034/j.1600-0854.2003.40206.x
85 Chavassieux, P., Seeman, E. & Delmas, P. D. Insights into material and structural basis of bone fragility from diseases associated with fractures: how determinants of the biomechanical properties of bone are compromised by disease. *Endocr Rev* **28**, 151-164 (2007). https://doi.org:10.1210/er.2006-0029
86 Nagase, H. & Woessner, J. F., Jr. Matrix metalloproteinases. *J Biol Chem* **274**, 21491-21494 (1999). https://doi.org:10.1074/jbc.274.31.21491
87 Batsir, S., Geiger, B. & Kam, Z. Dynamics of the sealing zone in cultured osteoclasts. *Cytoskeleton (Hoboken)* **74**, 72-81 (2017). https://doi.org:10.1002/cm.21350
88 Boyde, A., Ali, N. N. & Jones, S. J. Resorption of dentine by isolated osteoclasts in vitro. *Br Dent J* **156**, 216-220 (1984). https://doi.org:10.1038/sj.bdj.4805313
89 Arnett, T. R. & Dempster, D. W. A comparative study of disaggregated chick and rat osteoclasts in vitro: effects of calcitonin and prostaglandins. *Endocrinology* **120**, 602-608 (1987). https://doi.org:10.1210/endo-120-2-602
90 Takahashi, N. *et al.* Osteoblastic cells are involved in osteoclast formation. *Endocrinology* **123**, 2600-2602 (1988). https://doi.org:10.1210/endo-123-5-2600
91 Yasuda, H. *et al.* Osteoclast differentiation factor is a ligand for osteoprotegerin/osteoclastogenesis-inhibitory factor and is identical to TRANCE/RANKL. *Proc Natl Acad Sci U S A* **95**, 3597-3602 (1998). https://doi.org:10.1073/pnas.95.7.3597
92 Lacey, D. L. *et al.* Osteoprotegerin ligand is a cytokine that regulates osteoclast differentiation and activation. *Cell* **93**, 165-176 (1998). https://doi.org:10.1016/s0092-8674(00)81569-x
93 Ansari, S., Ito, K. & Hofmann, S. Cell Sources for Human In vitro Bone Models. *Curr Osteoporos Rep* **19**, 88-100 (2021). https://doi.org:10.1007/s11914-020-00648-6
94 Li, H., Ghazanfari, R., Zacharaki, D., Lim, H. C. & Scheding, S. Isolation and characterization of primary bone marrow mesenchymal stromal cells. *Ann N Y Acad Sci* **1370**, 109-118 (2016). https://doi.org:10.1111/nyas.13102
95 Bourzac, C. *et al.* Isolation of equine bone marrow-derived mesenchymal stem cells: a comparison between three protocols. *Equine Vet J* **42**, 519-527 (2010). https://doi.org:10.1111/j.2042-3306.2010.00098.x
96 Chu, D. T. *et al.* An Update on the Progress of Isolation, Culture, Storage, and Clinical Application of Human Bone Marrow Mesenchymal Stem/Stromal Cells. *Int J Mol Sci* **21** (2020). https://doi.org:10.3390/ijms21030708
97 Yeo, C. *et al.* Ficoll-Paque versus Lymphoprep: a comparative study of two density gradient media for therapeutic bone marrow mononuclear cell preparations. *Regen Med* **4**, 689-696 (2009). https://doi.org:10.2217/rme.09.44

98 Horn, P. *et al.* Isolation of human mesenchymal stromal cells is more efficient by red blood cell lysis. *Cytotherapy* **10**, 676-685 (2008). https://doi.org:https://doi.org/10.1080/14653240802398845

99 Boraschi-Diaz, I. & Komarova, S. V. The protocol for the isolation and cryopreservation of osteoclast precursors from mouse bone marrow and spleen. *Cytotechnology* **68**, 105-114 (2016). https://doi.org:10.1007/s10616-014-9759-3

100 Al Naem, M., Bourebaba, L., Kucharczyk, K., Rocken, M. & Marycz, K. Therapeutic mesenchymal stromal stem cells: Isolation, characterization and role in equine regenerative medicine and metabolic disorders. *Stem Cell Rev Rep* **16**, 301-322 (2020). https://doi.org:10.1007/s12015-019-09932-0

101 Bienzle, D. Bone Marrow Examination: Why, How, and What to Expect from the Pathologist. *Vet Clin North Am Equine Pract* **36**, 35-52 (2020). https://doi.org:10.1016/j.cveq.2019.11.002

102 Hussein, H., Boyaka, P., Dulin, J. & Bertone, A. Cathepsin K inhibition renders equine bone marrow nucleated cells hypo-responsive to LPS and unmethylated CpG stimulation in vitro. *Comp Immunol Microbiol Infect Dis* **45**, 40-47 (2016). https://doi.org:10.1016/j.cimid.2016.02.005

103 Deguchi, T. *et al.* In vitro model of bone to facilitate measurement of adhesion forces and super-resolution imaging of osteoclasts. *Sci Rep* **6**, 22585 (2016). https://doi.org:10.1038/srep22585

104 Saltel, F., Destaing, O., Bard, F., Eichert, D. & Jurdic, P. Apatite-mediated actin dynamics in resorbing osteoclasts. *Mol Biol Cell* **15**, 5231-5241 (2004). https://doi.org:10.1091/mbc.e04-06-0522

105 Kleinhans, C., Schmid, F. F., Schmid, F. V. & Kluger, P. J. Comparison of osteoclastogenesis and resorption activity of human osteoclasts on tissue culture polystyrene and on natural extracellular bone matrix in 2D and 3D. *J Biotechnol* **205**, 101-110 (2015). https://doi.org:10.1016/j.jbiotec.2014.11.039

106 Perrotti, V., Nicholls, B. M. & Piattelli, A. Human osteoclast formation and activity on an equine spongy bone substitute. *Clin Oral Implants Res* **20**, 17-23 (2009). https://doi.org:10.1111/j.1600-0501.2008.01608.x

107 Kingsmill, V. J., Gray, C. & Boyde, A. Osteoclastic resorption of equine cranial and postcranial bone in vitro. *J Bone Miner Metab* **18**, 148-152 (2000). https://doi.org:10.1007/s007740050105

108 Ab Kadir, R., Zainal Ariffin, S. H., Megat Abdul Wahab, R., Kermani, S. & Senafi, S. Characterization of mononucleated human peripheral blood cells. *ScientificWorldJournal* **2012**, 843843 (2012). https://doi.org:10.1100/2012/843843

109 Marino, S., Logan, J. G., Mellis, D. & Capulli, M. Generation and culture of osteoclasts. *Bonekey Rep* **3**, 570 (2014). https://doi.org:10.1038/bonekey.2014.65

110 Kong, L., Smith, W. & Hao, D. Overview of RAW264.7 for osteoclastogensis study: Phenotype and stimuli. *J Cell Mol Med* **23**, 3077-3087 (2019). https://doi.org:10.1111/jcmm.14277

111 Remmers, S. J. A., van der Heijden, F. C., Ito, K. & Hofmann, S. The effects of seeding density and osteoclastic supplement concentration on osteoclastic differentiation and resorption. *Bone Rep* **18**, 101651 (2023). https://doi.org:10.1016/j.bonr.2022.101651

112 Gilday, R., Richard, H., Beauchamp, G., Fogarty, U. & Laverty, S. Abundant osteoclasts in the subchondral bone of the juvenile Thoroughbred metacarpus suggest an important role in joint maturation. *Equine Vet J* **52**, 733-742 (2020). https://doi.org:10.1111/evj.13235

113 Fortin-Trahan, R. *et al.* Osteoclast density is not increased in bone adjacent to radiolucencies (cysts) in juvenile equine medial femoral condyles. *Equine Vet J* (2021). https://doi.org:10.1111/evj.13530

114 Hou, J. M., Lin, J. L., Wen, J. P., Jin, L. & Tang, F. Q. Immunohistochemical identification of osteoclasts and multinucleated macrophages. *Cell Immunol* **292**, 53-56 (2014). https://doi.org:10.1016/j.cellimm.2014.09.002

115 Garnero, P. *et al.* The collagenolytic activity of cathepsin K is unique among mammalian proteinases. *J Biol Chem* **273**, 32347-32352 (1998). https://doi.org:10.1074/jbc.273.48.32347
116 Garnero, P. *et al.* The type I collagen fragments ICTP and CTX reveal distinct enzymatic pathways of bone collagen degradation. *J Bone Miner Res* **18**, 859-867 (2003). https://doi.org:10.1359/jbmr.2003.18.5.859
117 Szulc, P. Bone turnover: Biology and assessment tools. *Best Pract Res Clin Endocrinol Metab* **32**, 725-738 (2018). https://doi.org:10.1016/j.beem.2018.05.003
118 Eastell, R. & Szulc, P. Use of bone turnover markers in postmenopausal osteoporosis. *The Lancet Diabetes & Endocrinology* **5**, 908-923 (2017). https://doi.org:10.1016/s2213-8587(17)30184-5
119 Chavassieux, P., Portero-Muzy, N., Roux, J. P., Garnero, P. & Chapurlat, R. Are Biochemical Markers of Bone Turnover Representative of Bone Histomorphometry in 370 Postmenopausal Women? *J Clin Endocrinol Metab* **100**, 4662-4668 (2015). https://doi.org:10.1210/jc.2015-2957
120 Vesprey, A. & Yang, W. Pit Assay to Measure the Bone Resorptive Activity of Bone Marrow-derived Osteoclasts. *Bio Protoc* **6** (2016). https://doi.org:10.21769/BioProtoc.1836
121 Jansen, I. D. C., van Velzen, T., de Vries, T. J., Szulcek, R. & van Loon, J. Real-time quantification of osteoclastic resorptive activity by electric cell-substrate impedance sensing. *Front Cell Dev Biol* **10**, 921066 (2022). https://doi.org:10.3389/fcell.2022.921066
122 Goldberg, S. R., Georgiou, J., Glogauer, M. & Grynpas, M. D. A 3D scanning confocal imaging method measures pit volume and captures the role of Rac in osteoclast function. *Bone* **51**, 145-152 (2012). https://doi.org:https://doi.org/10.1016/j.bone.2012.04.018
123 Jones, S. J., Boyde, A., Ali, N. N. & Maconnachie, E. Variation in the sizes of resorption lacunae made in vitro. *Scan Electron Microsc*, 1571-1580 (1986).
124 Tkachenko, E. V. *et al.* Voxel size and measures of individual resorption cavities in three-dimensional images of cancellous bone. *Bone* **45**, 487-492 (2009). https://doi.org:10.1016/j.bone.2009.05.019
125 Paddock, S. W. in *Confocal Microscopy Methods and Protocols* (ed Stephen W. Paddock) 1-34 (Humana Press, 1999).
126 Parfitt, A. M. *et al.* Bone histomorphometry: standardization of nomenclature, symbols, and units. Report of the ASBMR Histomorphometry Nomenclature Committee. *J Bone Miner Res* **2**, 595-610 (1987). https://doi.org:10.1002/jbmr.5650020617
127 Vidal, B. *et al.* Bone histomorphometry revisited. *Acta Reumatol Port* **37**, 294-300 (2012).
128 Roux, J. P., Arlot, M. E., Gineyts, E., Meunier, P. J. & Delmas, P. D. Automatic-interactive measurement of resorption cavities in transiliac bone biopsies and correlation with deoxypyridinoline. *Bone* **17**, 153-156 (1995). https://doi.org:10.1016/s8756-3282(95)00174-3
129 Schulte, F. A., Lambers, F. M., Kuhn, G. & Müller, R. In vivo micro-computed tomography allows direct three-dimensional quantification of both bone formation and bone resorption parameters using time-lapsed imaging. *Bone* **48**, 433-442 (2011). https://doi.org:10.1016/j.bone.2010.10.007
130 Dempster, D. W. *et al.* Standardized nomenclature, symbols, and units for bone histomorphometry: a 2012 update of the report of the ASBMR Histomorphometry Nomenclature Committee. *J Bone Miner Res* **28**, 2-17 (2013). https://doi.org:10.1002/jbmr.1805
131 Bouxsein, M. L. *et al.* Guidelines for assessment of bone microstructure in rodents using micro-computed tomography. *J Bone Miner Res* **25**, 1468-1486 (2010). https://doi.org:10.1002/jbmr.141
132 Boerckel, J. D., Mason, D. E., McDermott, A. M. & Alsberg, E. Microcomputed tomography: approaches and applications in bioengineering. *Stem Cell Res Ther* **5**, 144 (2014). https://doi.org:10.1186/scrt534
133 Feldkamp LA, K. M., Kress JW ,Freeling R, H.E.Mathews C and Parfitt AM. in *Fifth Annual Scientific Meeting of the American Society for Bone and Mineral Research.* (ed Calcif Tissue Int).

134 Palacio-Mancheno, P. E., Larriera, A. I., Doty, S. B., Cardoso, L. & Fritton, S. P. 3D assessment of cortical bone porosity and tissue mineral density using high-resolution μCT: effects of resolution and threshold method. *J Bone Miner Res* **29**, 142-150 (2014). https://doi.org:10.1002/jbmr.2012
135 Layton, M. W. *et al.* Examination of subchondral bone architecture in experimental osteoarthritis by microscopic computed axial tomography. *Arthritis Rheum* **31**, 1400-1405 (1988). https://doi.org:10.1002/art.1780311109
136 Christiansen, B. A. & Silva, M. J. The effect of varying magnitudes of whole-body vibration on several skeletal sites in mice. *Ann Biomed Eng* **34**, 1149-1156 (2006). https://doi.org:10.1007/s10439-006-9133-5
137 Liphardt, A. M. *et al.* Changes in mechanical loading affect arthritis-induced bone loss in mice. *Bone* **131**, 115149 (2020). https://doi.org:10.1016/j.bone.2019.115149
138 Easley, S. K., Chang, M. T., Shindich, D., Hernandez, C. J. & Keaveny, T. M. Biomechanical effects of simulated resorption cavities in cancellous bone across a wide range of bone volume fractions. *J Bone Miner Res* **27**, 1927-1935 (2012). https://doi.org:10.1002/jbmr.1657
139 O'Neal, J. M. *et al.* One year of alendronate treatment lowers microstructural stresses associated with trabecular microdamage initiation. *Bone* **47**, 241-247 (2010). https://doi.org:10.1016/j.bone.2010.05.016
140 Waarsing, J. H. *et al.* Detecting and tracking local changes in the tibiae of individual rats: a novel method to analyse longitudinal in vivo micro-CT data. *Bone* **34**, 163-169 (2004). https://doi.org:10.1016/j.bone.2003.08.012
141 Lemirre, T. *et al.* Microstructural features of subchondral radiolucent lesions in the medial femoral condyle of juvenile Thoroughbreds: A microcomputed tomography and histological analysis. *Equine Vet J* **54**, 601-613 (2022). https://doi.org:10.1111/evj.13486
142 Trotter, G. W. & McIlwraith, C. W. Osteochondritis dissecans and subchondral cystic lesions and their relationship to osteochondrosis in the horse. *Journal of Equine Veterinary Science* **1**, 157-162 (1981). https://doi.org:https://doi.org/10.1016/S0737-0806(81)80029-9
143 Bourebaba, L., Röcken, M. & Marycz, K. Osteochondritis dissecans (OCD) in Horses - Molecular Background of its Pathogenesis and Perspectives for Progenitor Stem Cell Therapy. *Stem Cell Rev Rep* **15**, 374-390 (2019). https://doi.org:10.1007/s12015-019-09875-6
144 Hornof, W. J., O'brien, T. R. & Pool, R. R. OSTEOCHONDRITIS DISSECANS OF THE DISTAL METACARPUS IN THE ADULT RACING THOROUGHBRED HORSE. *Veterinary Radiology & Ultrasound* **22**, 98-106 (1981).
145 Shaffer, S. K. *et al.* Subchondral focal osteopenia associated with proximal sesamoid bone fracture in Thoroughbred racehorses. *Equine Vet J* **53**, 294-305 (2021). https://doi.org:10.1111/evj.13291
146 Riggs, C. M. Fractures-a preventable hazard of racing thoroughbreds? *Vet J* **163**, 19-29 (2002). https://doi.org:10.1053/tvjl.2001.0610
147 Diab, S. S. *et al.* Diagnostic approach to catastrophic musculoskeletal injuries in racehorses. *J Vet Diagn Invest* **29**, 405-413 (2017). https://doi.org:10.1177/1040638716685598
148 Stover, S. M. Nomenclature, classification, and documentation of catastrophic fractures and associated preexisting injuries in racehorses. *J Vet Diagn Invest* **29**, 396-404 (2017). https://doi.org:10.1177/1040638717692846
149 Pye, J. L. & Stover, S. M. in *Fractures in the Horse* 29-53 (2022).
150 Riggs, C. M. & Goodship, A. E. in *Fractures in the Horse* 11-27 (2022).
151 Whitton, R. C., Ayodele, B. A., Hitchens, P. L. & Mackie, E. J. Subchondral bone microdamage accumulation in distal metacarpus of Thoroughbred racehorses. *Equine Vet J* **50**, 766-773 (2018). https://doi.org:10.1111/evj.12948

152 Harrison, S. M., Whitton, R. C., Kawcak, C. E., Stover, S. M. & Pandy, M. G. Relationship between muscle forces, joint loading and utilization of elastic strain energy in equine locomotion. *J Exp Biol* **213**, 3998-4009 (2010). https://doi.org:10.1242/jeb.044545

153 Currey, J. D. The many adaptations of bone. *J Biomech* **36**, 1487-1495 (2003). https://doi.org:10.1016/s0021-9290(03)00124-6

154 Muir, P. *et al.* Exercise-induced metacarpophalangeal joint adaptation in the Thoroughbred racehorse. *J Anat* **213**, 706-717 (2008). https://doi.org:10.1111/j.1469-7580.2008.00996.x

155 Palmer, S. E. Prevalence of carpal fractures in thoroughbred and standardbred racehorses. *J Am Vet Med Assoc* **188**, 1171-1173 (1986).

156 Noble, B. S., Stevens, H., Loveridge, N. & Reeve, J. Identification of apoptotic changes in osteocytes in normal and pathological human bone. *Bone* **20**, 273-282 (1997). https://doi.org:10.1016/s8756-3282(96)00365-1

157 Xiong, J. *et al.* Matrix-embedded cells control osteoclast formation. *Nat Med* **17**, 1235-1241 (2011). https://doi.org:10.1038/nm.2448

158 Da Costa Gómez, T. M. *et al.* Up-regulation of site-specific remodeling without accumulation of microcracking and loss of osteocytes. *Bone* **37**, 16-24 (2005). https://doi.org:10.1016/j.bone.2004.12.016

159 Parkin, T. D. Epidemiology of racetrack injuries in racehorses. *Vet Clin North Am Equine Pract* **24**, 1-19 (2008). https://doi.org:10.1016/j.cveq.2007.11.003

160 Hernandez, J., Hawkins, D. L. & Scollay, M. C. Race-start characteristics and risk of catastrophic musculoskeletal injury in Thoroughbred racehorses. *J Am Vet Med Assoc* **218**, 83-86 (2001). https://doi.org:10.2460/javma.2001.218.83

161 Arens, A. M. *et al.* Osteoporosis associated with pulmonary silicosis in an equine bone fragility syndrome. *Vet Pathol* **48**, 593-615 (2011). https://doi.org:10.1177/0300985810385151

162 Zavodovskaya, R. *et al.* Multifocal discrete osteolysis in a horse with silicate associated osteoporosis. *Equine Vet Educ* **31**, 517-522 (2019). https://doi.org:10.1111/eve.12899

163 Anderson, J. D. *et al.* Clinical and scintigraphic findings in horses with a bone fragility disorder: 16 cases (1980-2006). *J Am Vet Med Assoc* **232**, 1694-1699 (2008). https://doi.org:10.2460/javma.232.11.1694

164 Markell, R., Saviola, G., Barker, E. A., Conway, J. D. & Dujardin, C. What Do We Know About Clodronate Now? A Medical and Veterinary Perspective. *J Equine Vet Sci* **88**, 102874 (2020). https://doi.org:10.1016/j.jevs.2019.102874

165 Suva, L. J. *et al.* Bisphosphonates in veterinary medicine: The new horizon for use. *Bone* **142**, 115711 (2021). https://doi.org:10.1016/j.bone.2020.115711

166 Roelofs, A. J., Thompson, K., Ebetino, F. H., Rogers, M. J. & Coxon, F. P. Bisphosphonates: molecular mechanisms of action and effects on bone cells, monocytes and macrophages. *Curr Pharm Des* **16**, 2950-2960 (2010). https://doi.org:10.2174/138161210793563635

167 Reznikov, N. *et al.* Biological stenciling of mineralization in the skeleton: Local enzymatic removal of inhibitors in the extracellular matrix. *Bone* **138**, 115447 (2020). https://doi.org:10.1016/j.bone.2020.115447

168 Yocom, A., Contino, E. & Kawcak, C. Review of the Mechanism of Action and Use of Bisphosphonates in Horses. *J Equine Vet Sci*, 104503 (2023). https://doi.org:10.1016/j.jevs.2023.104503

169 Coudry, V. *et al.* Efficacy of tiludronate in the treatment of horses with signs of pain associated with osteoarthritic lesions of the thoracolumbar vertebral column. *Am J Vet Res* **68**, 329-337 (2007). https://doi.org:10.2460/ajvr.68.3.329

170 Gough, M. R., Thibaud, D. & Smith, R. K. Tiludronate infusion in the treatment of bone spavin: a double blind placebo-controlled trial. *Equine Vet J* **42**, 381-387 (2010). https://doi.org:10.1111/j.2042-3306.2010.00120.x
171 Bertuglia, A. *et al.* Effect of intravenous tiludronate disodium administration on the radiographic progression of osteoarthritis of the fetlock joint in Standardbred racehorses. *J Am Vet Med Assoc* **259**, 651-661 (2021). https://doi.org:10.2460/javma.259.6.651
172 Knych, H. K. *et al.* Detection and residence time of bisphosphonates in bone of horses. *J Vet Diagn Invest* **34**, 23-27 (2022). https://doi.org:10.1177/10406387211050049
173 Delguste, C. *et al.* Comparative pharmacokinetics of two intravenous administration regimens of tiludronate in healthy adult horses and effects on the bone resorption marker CTX-1. *J Vet Pharmacol Ther* **31**, 108-116 (2008). https://doi.org:10.1111/j.1365-2885.2007.00936.x
174 Riggs, C. M. *et al.* Tiludronic acid can be detected in blood and urine samples from Thoroughbred racehorses over 3 years after last administration. *Equine Vet J* **53**, 1287-1295 (2021). https://doi.org:10.1111/evj.13395
175 Mitchell, A. *et al.* Clodronate improves lameness in horses without changing bone turnover markers. *Equine Vet J* **51**, 356-363 (2019). https://doi.org:10.1111/evj.13011
176 Knych, H. K. *et al.* Clodronate detection and effects on markers of bone resorption are prolonged following a single administration to horses. *Equine Vet J* (2022). https://doi.org:10.1111/evj.13866
177 McIlwraith, C. W. The use of intra-articular corticosteroids in the horse: what is known on a scientific basis? *Equine Vet J* **42**, 563-571 (2010). https://doi.org:10.1111/j.2042-3306.2010.00095.x
178 Kobza, A. O., Herman, D., Papaioannou, A., Lau, A. N. & Adachi, J. D. Understanding and Managing Corticosteroid-Induced Osteoporosis. *Open Access Rheumatol* **13**, 177-190 (2021). https://doi.org:10.2147/OARRR.S282606
179 Conaway, H. H., Henning, P., Lie, A., Tuckermann, J. & Lerner, U. H. Activation of dimeric glucocorticoid receptors in osteoclast progenitors potentiates RANKL induced mature osteoclast bone resorbing activity. *Bone* **93**, 43-54 (2016). https://doi.org:10.1016/j.bone.2016.08.024
180 Hirayama, T., Sabokbar, A. & Athanasou, N. A. Effect of corticosteroids on human osteoclast formation and activity. *J Endocrinol* **175**, 155-163 (2002). https://doi.org:10.1677/joe.0.1750155
181 Tobias, J. & Chambers, T. J. Glucocorticoids impair bone resorptive activity and viability of osteoclasts disaggregated from neonatal rat long bones. *Endocrinology* **125**, 1290-1295 (1989). https://doi.org:10.1210/endo-125-3-1290
182 Dempster, D. W., Moonga, B. S., Stein, L. S., Horbert, W. R. & Antakly, T. Glucocorticoids inhibit bone resorption by isolated rat osteoclasts by enhancing apoptosis. *J Endocrinol* **154**, 397-406 (1997). https://doi.org:10.1677/joe.0.1540397
183 Sivagurunathan, S., Muir, M. M., Brennan, T. C., Seale, J. P. & Mason, R. S. Influence of glucocorticoids on human osteoclast generation and activity. *J Bone Miner Res* **20**, 390-398 (2005). https://doi.org:10.1359/JBMR.041233
184 Knych, H. K., Harrison, L. M., Casbeer, H. C. & McKemie, D. S. Disposition of methylprednisolone acetate in plasma, urine, and synovial fluid following intra-articular administration to exercised thoroughbred horses. *J Vet Pharmacol Ther* **37**, 125-132 (2014). https://doi.org:10.1111/jvp.12070
185 Pouran, B. *et al.* Topographic features of nano-pores within the osteochondral interface and their effects on transport properties -a 3D imaging and modeling study. *J Biomech* **123**, 110504 (2021). https://doi.org:10.1016/j.jbiomech.2021.110504
186 Zhang, Y.-D., Jiang, X. & Wang, S.-H. Fingerspelling Recognition by 12-Layer CNN with Stochastic Pooling. *Mobile Networks and Applications* (2022). https://doi.org:10.1007/s11036-021-01900-8

187 Sonka, M., Hlavac, V. & Boyle, R. in *Image Processing, Analysis, and*

*Machine Vision* (eds Milan Sonka, Vaclav Hlavac, & Roger Boyle) Ch. 2, 11-48 (Cengage Learning, 2015).
188 Young, I. T., Gerbrands, J. J., van Vliet, L. J. & TU Delft, F. d. T. N. in *Fundamentals of Image Processing* Ch. 2, 2-6 (Delft University of Technology, 1995).
189 Gonzalez , R. C. W., Richard E. . in *Digital Image Processing* Ch. 1, 23-56 (Pearson, 2007).
190 Teuwen, J., Gouw, Z. A. R. & Sonke, J. J. Artificial Intelligence for Image Registration in Radiation Oncology. *Semin Radiat Oncol* **32**, 330-342 (2022). https://doi.org:10.1016/j.semradonc.2022.06.003
191 Fischer, B. & Modersitzki, J. Ill-posed medicine—an introduction to image registration. *Inverse Problems* **24**, 034008 (2008). https://doi.org:10.1088/0266-5611/24/3/034008
192 Brock, K. K., Mutic, S., McNutt, T. R., Li, H. & Kessler, M. L. Use of image registration and fusion algorithms and techniques in radiotherapy: Report of the AAPM Radiation Therapy Committee Task Group No. 132. *Med Phys* **44**, e43-e76 (2017). https://doi.org:10.1002/mp.12256
193 Malhotra, P., Gupta, S., Koundal, D., Zaguia, A. & Enbeyle, W. Deep Neural Networks for Medical Image Segmentation. *J Healthc Eng* **2022**, 9580991 (2022). https://doi.org:10.1155/2022/9580991
194 Smistad, E., Falch, T. L., Bozorgi, M., Elster, A. C. & Lindseth, F. Medical image segmentation on GPUs--a comprehensive review. *Med Image Anal* **20**, 1-18 (2015). https://doi.org:10.1016/j.media.2014.10.012
195 Gonzalez , R. C. W., Richard E. . in *Digital Image Processing* Ch. 10, 711-809 (Pearson, 2007).
196 Yin, X.-X., Sun, L., Fu, Y., Lu, R. & Zhang, Y. U-Net-Based Medical Image Segmentation. *Journal of Healthcare Engineering* **2022**, 4189781 (2022). https://doi.org:10.1155/2022/4189781
197 Sonka, M., Hlavac, V. & Boyle, R. in *Image Processing, Analysis, and*

*Machine Vision* (eds Milan Sonka, Vaclav Hlavac, & Roger Boyle) Ch. 6, 178-248 (Cengage Learning, 2015).
198 Zhang, J., Yan, C. H., Chui, C. K. & Ong, S. H. Fast segmentation of bone in CT images using 3D adaptive thresholding. *Comput Biol Med* **40**, 231-236 (2010). https://doi.org:10.1016/j.compbiomed.2009.11.020
199 Guldberg, R. E., Lin, A. S., Coleman, R., Robertson, G. & Duvall, C. Microcomputed tomography imaging of skeletal development and growth. *Birth Defects Res C Embryo Today* **72**, 250-259 (2004). https://doi.org:10.1002/bdrc.20016
200 Waarsing, J. H., Day, J. S. & Weinans, H. An improved segmentation method for in vivo microCT imaging. *J Bone Miner Res* **19**, 1640-1650 (2004). https://doi.org:10.1359/jbmr.040705
201 LeCun, Y., Bengio, Y. & Hinton, G. Deep learning. *Nature* **521**, 436-444 (2015). https://doi.org:10.1038/nature14539
202 Hosny, A., Parmar, C., Quackenbush, J., Schwartz, L. H. & Aerts, H. Artificial intelligence in radiology. *Nat Rev Cancer* **18**, 500-510 (2018). https://doi.org:10.1038/s41568-018-0016-5
203 Yamashita, R., Nishio, M., Do, R. K. G. & Togashi, K. Convolutional neural networks: an overview and application in radiology. *Insights Imaging* **9**, 611-629 (2018). https://doi.org:10.1007/s13244-018-0639-9
204 Dumoulin, V. & Visin, F. A guide to convolution arithmetic for deep learning. arXiv:1603.07285 (2016). <https://ui.adsabs.harvard.edu/abs/2016arXiv160307285D>.
205 Ronneberger, O., Fischer, P. & Brox, T. *U-Net: Convolutional Networks for Biomedical Image Segmentation*. Vol. 9351 (2015).
206 Currie, G., Hawk, K. E., Rohren, E., Vial, A. & Klein, R. Machine Learning and Deep Learning in Medical Imaging: Intelligent Imaging. *J Med Imaging Radiat Sci* **50**, 477-487 (2019). https://doi.org:10.1016/j.jmir.2019.09.005

207 Laverty, S., Lacourt, M., Gao, C., Henderson, J. E. & Boyde, A. High density infill in cracks and protrusions from the articular calcified cartilage in osteoarthritis in standardbred horse carpal bones. *Int J Mol Sci* **16**, 9600-9611 (2015). https://doi.org:10.3390/ijms16059600

208 Muir, P. *et al.* Role of endochondral ossification of articular cartilage and functional adaptation of the subchondral plate in the development of fatigue microcracking of joints. *Bone* **38**, 342-349 (2006). https://doi.org:10.1016/j.bone.2005.08.020

209 Møller, A. M. J. *et al.* Zoledronic Acid Is Not Equally Potent on Osteoclasts Generated From Different Individuals. *JBMR Plus* **4**, e10412 (2020). https://doi.org:10.1002/jbm4.10412

210 Møller, A. M. J. *et al.* Septins are critical regulators of osteoclastic bone resorption. *Sci Rep* **8**, 13016 (2018). https://doi.org:10.1038/s41598-018-31159-1

211 Stephens, E. *et al.* Osteoclast signaling-targeting miR-146a-3p and miR-155-5p are downregulated in Paget's disease of bone. *Biochimica et Biophysica Acta (BBA) - Molecular Basis of Disease* **1866**, 165852 (2020). https://doi.org:https://doi.org/10.1016/j.bbadis.2020.165852

212 Allard-Chamard, H. *et al.* Osteoclasts and their circulating precursors in rheumatoid arthritis: Relationships with disease activity and bone erosions. *Bone Rep* **12**, 100282 (2020). https://doi.org:10.1016/j.bonr.2020.100282

213 Boyde, A. & Jones, S. J. Early scanning electron microscopic studies of hard tissue resorption: their relation to current concepts reviewed. *Scanning Microsc* **1**, 369-381 (1987).

214 Piper, K., Boyde, A. & Jones, S. J. The relationship between the number of nuclei of an osteoclast and its resorptive capability in vitro. *Anat Embryol (Berl)* **186**, 291-299 (1992). https://doi.org:10.1007/bf00185977

215 Athanasou, N. A. *et al.* Stereophotogrammetric observations on bone resorption by isolated rabbit osteoclasts. *Micron and Microscopica Acta* **15**, 47-53 (1984). https://doi.org:https://doi.org/10.1016/0739-6260(84)90030-3

216 Chambers, T. J., Revell, P. A., Fuller, K. & Athanasou, N. A. Resorption of bone by isolated rabbit osteoclasts. *J Cell Sci* **66**, 383-399 (1984). https://doi.org:10.1242/jcs.66.1.383

217 Boyde, A., Dillon, C. E. & Jones, S. J. Measurement of osteoclastic resorption pits with a tandem scanning microscope. *J Microsc* **158**, 261-265 (1990). https://doi.org:10.1111/j.1365-2818.1990.tb02999.x

218 Fuller, K., Thong, J. T. L., Breton, B. C. & Chambers, T. J. Automated three-dimensional characterization of osteoclastic resorption lacunae by stereoscopic scanning electron microscopy. *Journal of Bone and Mineral Research* **9**, 17-23 (1994). https://doi.org:https://doi.org/10.1002/jbmr.5650090104

219 Slyfield, C. R., Jr. *et al.* Three-dimensional surface texture visualization of bone tissue through epifluorescence-based serial block face imaging. *J Microsc* **236**, 52-59 (2009). https://doi.org:10.1111/j.1365-2818.2009.03204.x

220 Goff, M. G. *et al.* Three-dimensional characterization of resorption cavity size and location in human vertebral trabecular bone. *Bone* **51**, 28-37 (2012). https://doi.org:https://doi.org/10.1016/j.bone.2012.03.028

221 Slyfield, C. R., Tkachenko, E. V., Wilson, D. L. & Hernandez, C. J. Three-dimensional dynamic bone histomorphometry. *J Bone Miner Res* **27**, 486-495 (2012). https://doi.org:10.1002/jbmr.553

222 Lemirre, T. *et al.* Maturation of the equine medial femoral condyle osteochondral unit. *Osteoarthr Cartil Open* **2**, 100029 (2020). https://doi.org:10.1016/j.ocarto.2020.100029

223 Symons, J. E. *et al.* Mechanical and morphological properties of trabecular bone samples obtained from third metacarpal bones of cadavers of horses with a bone fragility syndrome and horses unaffected by that syndrome. *Am J Vet Res* **73**, 1742-1751 (2012). https://doi.org:10.2460/ajvr.73.11.1742

224 Ritman, E. L. Current Status of Developments and Applications of Micro-CT. *Annual Review of Biomedical Engineering* **13**, 531-552 (2011). https://doi.org:10.1146/annurev-bioeng-071910-124717
225 Wainberg, M., Merico, D., Delong, A. & Frey, B. J. Deep learning in biomedicine. *Nature Biotechnology* **36**, 829-838 (2018). https://doi.org:10.1038/nbt.4233
226 Nielsen, M. A. *Neural Networks and Deep Learning*. (Determination Press, 2015).
227 Chan, H.-P., Samala, R. K., Hadjiiski, L. M. & Zhou, C. in *Deep Learning in Medical Image Analysis : Challenges and Applications* (eds Gobert Lee & Hiroshi Fujita) 3-21 (Springer International Publishing, 2020).
228 Cirean, D., Giusti, A., Gambardella, L. M. & Schmidhuber. Deep Neural Networks Segment Neuronal Membranes in Electron Microscopy Images. *Proceedings of Neural Information Processing Systems* **25** (2012).
229 Cheng, H. C. *et al.* Deep-Learning-Assisted Volume Visualization. *IEEE Trans Vis Comput Graph* **25**, 1378-1391 (2019). https://doi.org:10.1109/tvcg.2018.2796085
230 Alexander, D. C. & Koeberlein, G. M. *Elementary Geometry for College Students*. (Cengage Learning, 2010).
231 I., H. D. J. A. I. Bone Remodeling. *Annals of the New York Academy of Sciences* **1092**, 385-396 (2006). https://doi.org:https://doi.org/10.1196/annals.1365.035
232 Sims, N. A. & Martin, T. J. Coupling the activities of bone formation and resorption: a multitude of signals within the basic multicellular unit. *Bonekey Rep* **3**, 481 (2014). https://doi.org:10.1038/bonekey.2013.215
233 Teitelbaum, S. L. Bone resorption by osteoclasts. *Science* **289**, 1504-1508 (2000). https://doi.org:10.1126/science.289.5484.1504
234 Taylor, M. L., Maconnachie, E., Frank, K., Boyde, A. & Jones, S. J. The effect of fluoride on the resorption of dentine by osteoclasts In Vitro. *Journal of Bone and Mineral Research* **5**, S121-S130 (1990). https://doi.org:https://doi.org/10.1002/jbmr.5650051391
235 Hefti, T., Frischherz, M., Spencer, N. D., Hall, H. & Schlottig, F. A comparison of osteoclast resorption pits on bone with titanium and zirconia surfaces. *Biomaterials* **31**, 7321-7331 (2010). https://doi.org:10.1016/j.biomaterials.2010.06.009
236 Mabilleau, G., Pascaretti-Grizon, F., Baslé, M. F. & Chappard, D. Depth and volume of resorption induced by osteoclasts generated in the presence of RANKL, TNF-alpha/IL-1 or LIGHT. *Cytokine* **57**, 294-299 (2012). https://doi.org:10.1016/j.cyto.2011.11.014
237 Slyfield, C. R., Tkachenko, E. V., Wilson, D. L. & Hernandez, C. J. Three-dimensional dynamic bone histomorphometry. *Journal of Bone and Mineral Research* **27**, 486-495 (2012). https://doi.org:https://doi.org/10.1002/jbmr.553
238 Delaisse, J. M. *et al.* The effects of inhibitors of cysteine-proteinases and collagenase on the resorptive activity of isolated osteoclasts. *Bone* **8**, 305-313 (1987). https://doi.org:10.1016/8756-3282(87)90007-x
239 Goldberg, S. R., Georgiou, J., Glogauer, M. & Grynpas, M. D. A 3D scanning confocal imaging method measures pit volume and captures the role of Rac in osteoclast function. *Bone* **51**, 145-152 (2012). https://doi.org:10.1016/j.bone.2012.04.018
240 Cheung, R. C., Gray, C., Boyde, A. & Jones, S. J. Effects of ethanol on bone cells in vitro resulting in increased resorption. *Bone* **16**, 143-147 (1995).
241 Novikov, A. A., Major, D., Wimmer, M., Lenis, D. & Buhler, K. Deep Sequential Segmentation of Organs in Volumetric Medical Scans. *IEEE Trans Med Imaging* **38**, 1207-1215 (2019). https://doi.org:10.1109/tmi.2018.2881678